

Energetic and Hemodynamic Characteristics of Paravalvular Leak Following Transcatheter Aortic Valve Replacement

Azadeh Saeedi

A Thesis
in the Department of
Mechanical and Industrial Engineering

Presented in Partial Fulfillment of the Requirements
for the Degree Master of Applied Science (Mechanical Engineering)
Concordia University
Montreal, Quebec, Canada

June 2015

© Azadeh Saeedi, 2015

CONCORDIA UNIVERSITY

School of Graduate Studies

This is to certify that the thesis prepared,

By: **Azadeh Saeedi**

Entitled: **“Energetic and Hemodynamic Characteristics of Paravalvular Leak Following Transcatheter Aortic Valve Replacement”**

and submitted in partial fulfillment of the requirements for the degree of

Master of Applied Science (Mechanical Engineering)

Complies with the regulations of the University and meets the accepted standards with respect to originality and quality.

Signed by the Final Examining Committee:

_____	Chair
Dr. A. Dolatabadi	
_____	Examiner
Dr. H.D. Ng	
_____	Examiner
Dr. N. Bouguila	CIISE External
_____	Supervisor
Dr. L. Kadem	

Approved by:

Dr. S. Narayanswamy, MASc Program Director
Department of Mechanical and Industrial Engineering

Dean Amir Asif
Faculty of Engineering and Computer Science

Date: _____

To my beloved parents: Simin and Mohammad,

for their endless love, support and encouragement.

ABSTRACT

Energetic and Hemodynamic Characteristics of Paravalvular Leak Following Transcatheter Aortic Valve Replacement

Azadeh Saeedi

Transcatheter aortic valve replacement (TAVR) has emerged as an alternative treatment for inoperable and high risk patients with severe symptomatic aortic stenosis. TAVR short and medium term results are very promising, however paravalvular leak (PVL) post-TAVR still represents a significant complication. PVL post-TAVR is shown to be an independent predictor of short-term and long-term mortality. Despite, its importance and prevalence, with a wide range of reported incidences, only few studies addressed the PVL after TAVR.

In the present study, first, the mathematical lumped parameter model is used to model the simplified circulatory system in presence of PVL and to evaluate the performance of TAVR by computing the variation of the left ventricle stroke work (LVS_W) under several pre-TAVR and post-TAVR conditions. Results show that in a large majority of cases, TAVR significantly reduced LVS_W. However, in cases with pre-existing aortic stenosis conditions with trace/mild aortic regurgitation, it did not significantly reduce LVS_W or even led to an increase.

Second, a three-dimensional (3D) computational fluid dynamics (CFD) simulation is performed in order to investigate the effect of PVL on the diastolic flow-field characteristics post-TAVR. Results show that PVL leads to significant disturbances in blood flow, which characterized by high speed jets, coherent structures and markedly elevated shear stress on both sides of the implanted aortic leaflets, which could promote a more rapid degeneration of the valve leaflets.

Results could be useful in understating the hemodynamics of PVL post-TAVR and estimating some important parameters, which could not be obtained during the medical assessment (e.g. wall shear stress). Also, they could be a help in the process of choosing the appropriate valve for TAVR procedure, based on comparing the pre and post TAVR different scenarios.

ACKNOWLEDGEMENT

Foremost, I would like to express my sincere gratitude to my supervisor Dr. Lyes Kadem, for the continuous support of my master study and research, for his patience, motivation, enthusiasm, and immense knowledge. His guidance helped me in all the time of research and writing of this thesis.

In addition, I am deeply grateful to Dr. Zahra Keshavarz-Motamed and Dr. Abdelghani Djebbari, for their guidance and invaluable advice. This work would not have been possible without their help and knowledge. I must also acknowledge Dr. Philippe Pibarot and Dr. Nagib Dahdah for the long discussions, insightful comments and constructive criticisms at different stages of my research that helped me sort out the technical details of my work.

My sincere thanks goes to my thesis committee; Dr. H.D. Ng, Dr. N. Bouguila and Dr. A. Dolatabadi, who reviewed this manuscript and helped me to improve its content and presentation.

I thank my fellow labmates at LCFD; Hani Abulkhair, Giuseppe Di Labbio, Emilia Benevento and Alexandre Belanger for reviewing my reports, giving me productive comments, exchanging knowledge and skills and all the good time that we have had together.

I am also very grateful to my family for the support that they have provided me through my entire life. In particular, I owe my parents without whose love, encouragement and support, I would not have finished this thesis.

Finally, I appreciate the financial support that I received from Concordia University, which facilitated my research and life.

Azadeh Saeedi

June, 2015

TABLE OF CONTENT

LIST OF FIGURES	ix
LIST OF TABLES	xii
SYMBOLS.....	.xiii
ABBREVIATIONS	xv
CHAPTER 1: Introduction	1
1.1. Overview.....	1
1.2. Human Body Circulatory System	2
1.3. Heart Valves.....	4
1.4. Aortic Valve.....	5
1.5. Aortic Valve Stenosis	7
1.6. Aortic Valve Replacement.....	8
1.6.1. Surgical Aortic Valve Replacement (SAVR)	9
1.6.2. Transcatheter Aortic Valve Replacement (TAVR).....	13
1.7. Paravalvular Aortic Leak Following TAVR	18
1.7.1. Definition and Causes	19
1.7.2. Presentations and Symptoms.....	19
1.7.3. Assessments and Classifications	20
1.8 Objective and Outline of This Study.....	22
CHAPTER 2: Literature Review	23

2.1.	Introduction	23
2.2.	Numerical Lumped Parameter Modeling	24
2.3.	Computational Mechanics Modeling	25
	2.3.1. Computational Mechanics Modeling in Heart Valves	26
	2.3.2. Computational Mechanics Modeling in Prosthetic Heart Valves	27
	2.3.3. Computational Mechanics Modeling in Transcatheter Aortic Valves	28
2.4.	Engineering Studies in Prosthetic Aortic Valve Regurgitation.....	30
CHAPTER 3:	On the Determination of the Performance of Transcatheter Aortic Valve Implantation: Mathematical Modeling and Clinical Implications	31
3.1.	Introduction	32
3.2.	Method	33
	3.2.1. Heart-Arterial Model	35
	3.2.2. Aortic Stenosis Model.....	35
	3.2.3. Aortic Regurgitation Model.....	36
	3.2.4. Simulated conditions.....	36
	3.2.5. Transcatheter aortic valve replacement performance index (TAVR PI)	38
3.3.	Result.....	39
3.4.	Discussion	43
3.5.	Limitation	46
3.6.	Conclusion.....	46

CHAPTER 4: Fluid Dynamics of Transcatheter Aortic Valve in the Presence of Paravalvular Leak.....	48
4.1. Introduction	49
4.2. Method	50
4.2.1. Geometrical Model.....	50
4.2.2. Numerical Model.....	51
4.2.3. Boundary Conditions and Model Properties	53
4.3. Result.....	54
4.4. Discussion	60
4.5. Limitation	62
4.6. Conclusion.....	63
4.7. Additional Results and Discussions	63
CHAPTER 5: Conclusion and Summary.....	66
REFERENCES.....	68
APPENDIX A.....	83
APPENDIX B.....	84
APPENDIX C.....	86

LIST OF FIGURES

Figure 1-1: Humans circulatory system	3
Figure 1-2: Complete cardiac cycle	4
Figure 1-3: Anatomy of the heart valves	5
Figure 1-4: Aortic valve and heart skeleton.....	6
Figure 1-5: Anatomy of the aortic valve.....	6
Figure 1-6: Stenotic aortic valve vs. normal aortic valve	7
Figure 1-7: Surgical aortic valve replacement (SAVR) procedure.....	9
Figure 1-8: Different types of mechanical heart valves: a) caged-ball valve; b) mono-leaflet tilting valve; c) bileaflet valve.....	10
Figure 1-9: Some types of biological heart valves: a) Stented pericardial bovine bioprosthetic valves, Edwards. PREMOUNT magna, b) Stented porcine aortic valve bioprostheses, Biocore, c) Stentless bioprosthetic valve, TORONTO SPV.....	11
Figure 1-10: Stented trileaflet heart valve scaffold (a) View from aortic side, (b) view from ventricular side, (c, d) After 4 weeks of culturing	12
Figure 1-11: Transcatheter aortic valve replacement procedure (TAVR)	14
Figure 1-12: Different type of transcatheter heart valves: a) SAPIEN (Edwards Lifesciences, Irvine, CA, USA), b) CoreValve™ (Medtronic, Minneapolis, MN, USA), c) Lotus valve (Boston Scientific Inc., Natick, Massachusetts), d) Direct Flow valve (Direct Flow Medical Inc., Santa Rosa, California), e) Acurate (Symetis Inc., Ecublens, Switzerland), f) Portico (St. Jude Medical Inc., St. Paul, Minnesota), g) HLT (Bracco Inc., Princeton, New Jersey), h) JenaClip (JenaValve Inc., Munich, Germany)	15
Figure 3-1: Schematic diagrams: a) schematic representation of the lumped parameter model used to simulate aortic stenosis with/without aortic regurgitation and transcatheter aortic valve with/without paravalvular leak; b) electrical representation of the model. $E_{IV}(t)$: normalized time-varying elastance. R_{AV} and $R_{AR/PLV}$ represent aortic valve stenosis resistance and aortic valve paravalvular leak or regurgitation resistance, respectively.	

L_{AV} and $L_{AR/PLV}$ represent aortic valve stenosis inductance and aortic valve paravalvular leak or regurgitation inductance, respectively. See Table 1 for details. 34

Figure 3-2: Examples of flow, pressure and left ventricle stroke work waveforms obtained using the model for; a) aortic stenosis with EOA of 0.80 cm^2 , with no aortic regurgitation ($R_f=0\%$); b) transcatheter aortic valve with an EOA of 1.60 cm^2 and no paravalvular leak ($R_f=0\%$); c) transcatheter aortic valve with EOA of 1.60 cm^2 but with mild-to-moderate paravalvular leak ($R_f=17\%$); d) corresponding pressure-volume loops and left ventricle stroke work (LVSU)..... 40

Figure 3-3: Correlation between the Performance Index (PI) computed from (Eq. 7) and estimated using equation (8). SEE: standard error of estimate. 43

Figure 4-1: Geometry considered for numerical simulations. (a) Simulation domain; (b) Transcatheter aortic valve; (c) Paravalvular leak orifice positions; and (d) Top view of the simulation domain..... 50

Figure 4-2: Velocity waveform used as inlet boundary condition for the numerical simulations based on CMR measurements of Hayek et al. 2014 54

Figure 4-3: Different 2D and 3D views (top, right, left and a horizontal cross-section) of velocity magnitude iso-surfaces at three instants $t=0.358 \text{ s}$, $t= 0.590 \text{ s}$ and $t= 0.858 \text{ s}$; A-A) 3D left-side view of velocity magnitude iso-surfaces; B-B) 3D right-side view of velocity magnitude iso-surfaces; C-C) 3D velocity magnitude contours and their projections on the cross section just below the stent. 55

Figure 4-4: Two cross-sectional views of velocity magnitude and stream lines at three instants $t=0.358 \text{ s}$, $t= 0.590 \text{ s}$ and $t= 0.858 \text{ s}$; E-E) 2D view of velocity magnitude contours on a plane crossing both orifices of 20 mm^2 and 4 mm^2 with symmetrical view of two leaflets; F-F) 2D view of velocity magnitude contours on a plane crossing both orifices of 4 mm^2 and 1 mm^2 with symmetrical view of two leaflets..... 57

Figure 4-5: Oscillatory wall shear stress (OSI) on two different cross-sections in the LVOT. Section G-G is located just upstream of the valve stent and section H-H is located 1 cm below the valve stent..... 58

Figure 4-6: (a) Aortic valve leaflets (aortic side) top and isometric view of wall shear stress contours at $t = 0.358$ s; (b) Aortic valve leaflets (left ventricle side) top and isometric view of wall shear stress contours at $t = 0.358$ s.....	59
Figure 4-7: Schematic representation of the difference between (a) Native aortic valve regurgitation and (b) Paravalvular leak post transcatheter aortic valve replacement.	62
Figure 4-8: Evolution of the secondary flow during diastole cycle at 6 instants. A-A) Section right below the valve stent in left ventricular side; B-B) Section 1 cm below the valve stent; C-C) Section 3 cm below the valve stent	64
Figure 4-9: Lambda-2 Evolution during Diastole.....	65
Figure B-1: Computational domain with extended outflow tract.....	84
Figure B-2: Domain mesh with extra care for boundaries, wall and sensitive areas.....	85

LIST OF TABLES

Table 1-1: PVL evaluation criteria by The Valve Academic Research Consortium (VARC) published the VARCII.....	21
Table 3-1: Summary of the cardiovascular parameters used to simulate all cases.....	37
Table 3-2: Differences in left ventricle stroke work for different configurations pre and post transcatheter aortic valve replacement. AS: aortic stenosis; TAV: transcatheter aortic valve; EOA: effective orifice area. The values in the table represent the performance index as computed by (Eq. 7).....	42
Table 4-1: Calculation of discretization errors for the simulation at two regions: A and B. σ (wall shear stress), σ_{ext} (the extrapolated wall shear stress value), e_a (approximate relative error), e_{ext} (extrapolated relative error) and GCI_{fine} (fine-grid convergence index).....	52
Table C-1: Vortex identification, Lambda-2 criterion.....	87

SYMBOLS

a	Acceleration gradient (s^{-2})
A	Area (m^2)
C	Compliance (ml/mmHg)
E	Elastance (mmHg/ml)
\emptyset	Wall shear stress (Pa)
e	Relative error (%)
E_LCo	Valvular energy loss coefficient (m^2)
GCI_{fine}	Fine-grid convergence index
L	Inductance (mmHg.s ² /ml)
λ	Lambda, eigenvalue
μ	Dynamic viscosity (Pa.s)
Ω	Spin tensor (s^{-1})
P	Pressure (Pa)
Q	Flow rate (L/min)
R	Resistance (mmHg.s/ml)
ρ	Density (kg/m^3)
Re	Reynolds number
R_f	Regurgitation fraction (%)
V	Velocity (m/s)
V	Volume (m^3)
t	Time (s)

τ	Total instantaneous shear stress (Pa)
y^+	Dimensionless wall distance
S	Strain rate tensor (s^{-1})

ABBREVIATIONS

AS	Aortic stenosis
AVR	Aortic valve replacement
BHV	Bioprosthetic heart valve
CFD	Computational fluid dynamics
CM	Computational mechanics
D	Dimensional
EOA	Effective orifice area
FEM	Finite elements method
FSI	Fluid solid interaction
LV	Left ventricle
LVOT	Left ventricle out tract
LVSW	Left ventricle stroke work
MHV	Mechanical heart valve
OSI	Oscillatory shear index
PAR	Paravalvular aortic regurgitation
PHV	Prosthetic heart valve
PVL	Paravalvular leak
PPM	Prosthesis patient mismatch
REOA	Regurgitation effective orifice area
SAVR	Surgical aortic valve replacement
SST	Shear stress transport
SV	Stroke volume

SW	Stroke work
TAV	Transcatheter aortic valve
TAVR	Transcatheter aortic valve replacement
THV	Transcatheter heart valve
WSS	Wall shear stress

CHAPTER 1: Introduction

1.1. Overview

The cardiovascular system, also called the circulatory system, is an organ system that permits blood to circulate and provides the body with its oxygen and nutrition demands. It also assists in the removal of metabolic wastes. The human cardiovascular system consists of the heart as a pump, blood vessels and approximately five liters of blood. The top of the heart, known as the heart's base, connects to the great blood vessels of the body, including the aorta.

The aorta is the largest vessel in the body which begins at the top of the left ventricle, the heart's muscular pumping chamber. The heart pumps the blood from the left ventricle into the aorta through the aortic valve. The function of the aortic valve is to open and close with each heartbeat to allow a one-way flow of blood. This valve is known as the most important valve of the heart and the most commonly affected by valvular heart disease requiring heart valve replacement (Iung et al., 2005, Williams et al., 2010).

There are two primary valvular heart disease processes that can affect the aortic valve: aortic insufficiency/aortic regurgitation and aortic stenosis (AS). AS is now the most common valvular heart disease in the western world (Manning, 2013). Research shows that without treatment, half of the people with severe AS symptoms die within an average of 2 years (Otto, 2000).

Medical treatment for severe symptomatic AS is not effective, and replacing the heart valve is considered as the only effective treatment (Bonow et al., 2006). For patients with severe symptomatic AS who are suitable candidates for open-heart surgery, surgical aortic valve replacement (SAVR) is a gold standard treatment (Bonow et al., 2006). However, it has been shown in practice, SAVR is denied in around 33% of elderly candidates (Iung et al., 2005). To

meet the medical needs of these patients who have been deemed inoperable or high-risk for traditional SAVR, transcatheter aortic valve replacement (TAVR) has emerged as a new technology over the past decade and is now being put into clinical practice. This technology has had significant impacts throughout the health care field with the creation of a new biotechnology industry around transcatheter valves and the creation of multidisciplinary “heart teams”; clinicians and engineers. TAVR, however, as a new technology is still associated with some limitations and complications.

This chapter will first provide an overview of the human body circulation system. Secondly, the anatomy and physiology of the heart valves, with emphasis on the aortic valve, are described. Then, aortic valve diseases, in particular, aortic stenosis are explained; to identify the necessity and prevalence of aortic valve replacement (AVR). It is followed by presenting and comparing available AVR methods: SAVR and TAVR, procedures, devices, complications and outcomes. Then, aortic paravalvular regurgitation (PAR) as a major current complication of TAVR is introduced and overviewed in detail. Finally, the objective of this thesis and proposed studies and methodologies are presented.

1.2. Human Body Circulatory System

The circulatory system (Figure 1-1) is powered by the heart, a four-chambered (upper chambers: left and right atria, lower chambers: left and right ventricles) muscular organ that acts as a pump. In the human body, this system consists of two connected subsystems; the systemic circulation and the pulmonary circulation.

In the systemic circulation, the left ventricle pumps oxygenated blood into the aorta. The blood travels from the aorta to arteries and the capillary network, as well as coronary arteries.

There, the blood releases oxygen and takes on carbon dioxide and wastes. The deoxygenated blood is then collected in veins and travels to the right atrium and into the right ventricle.

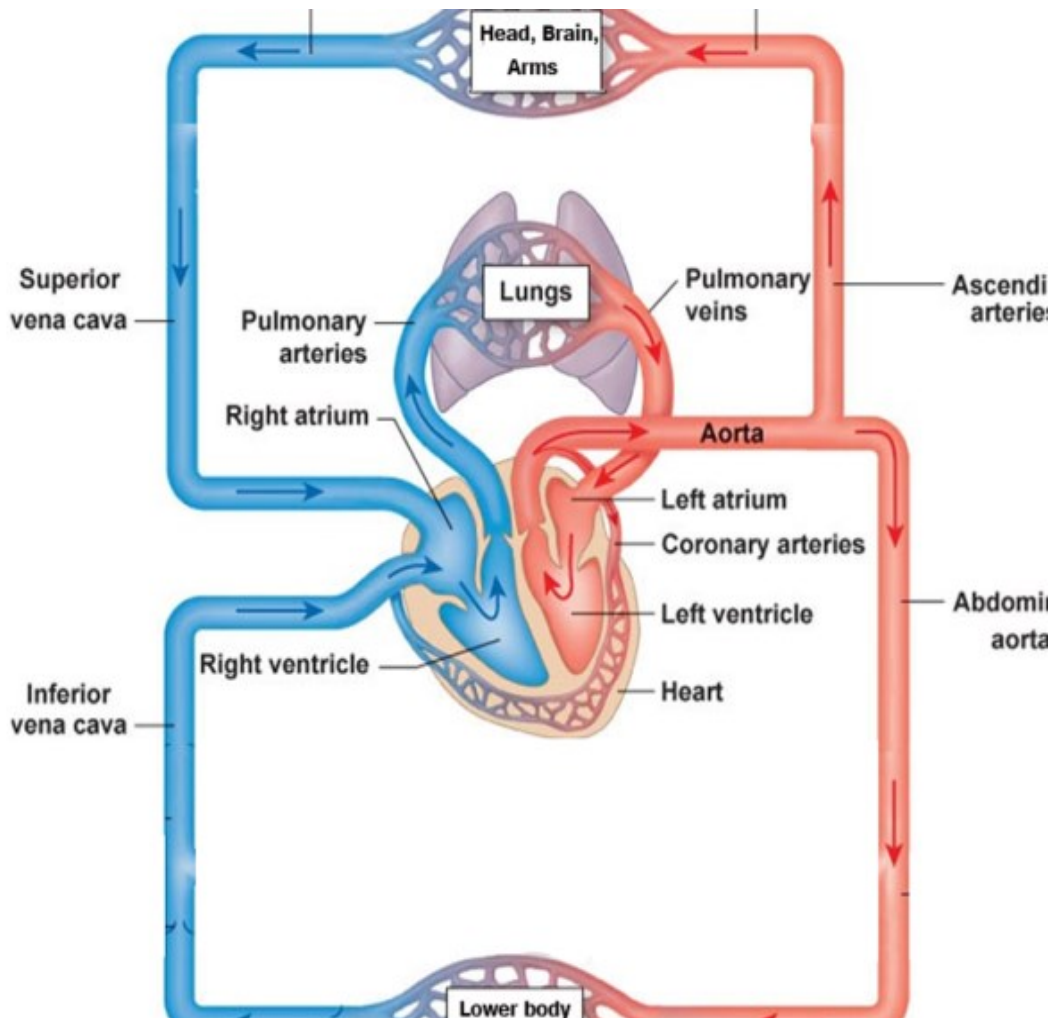


Figure 1-1; Humans circulatory system (Adopted from 2009, Pearson Education Inc.)

In the pulmonary circulation: the right ventricle pumps deoxygenated blood into the pulmonary artery, which branches off into smaller arteries and capillaries in the lung. There, the carbon dioxide is released from the blood and oxygen enters the bloodstream. Then, the oxygenated blood travels through the pulmonary vein and the left atrium into the left ventricle.

The next heart beat starts a new cardiac cycle of systematic circulation. Each cardiac cycle can be divided into two main phase (Figure 1-2): diastole and systole. Diastole represents the period of time when the ventricles are relaxed (no contract). Systole represents the time when the ventricles contract, and eject blood to the system.

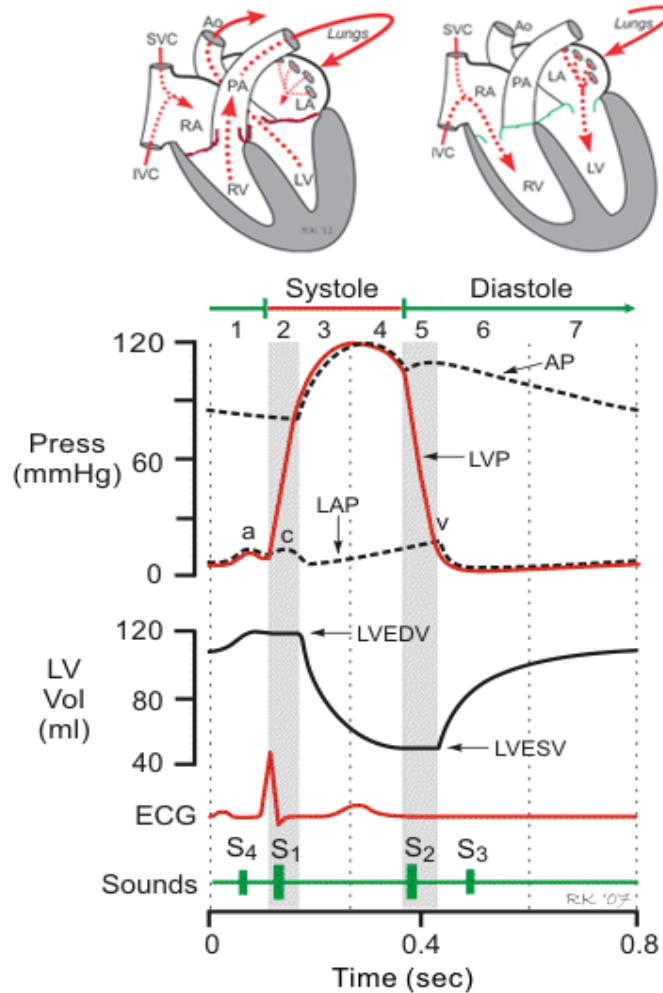


Figure 1-2: Complete cardiac cycle (Richard E. Klabunde, 2007)

1.3. Heart Valves

Cardiac valves are structures that work like one-way doors. They let blood flow from one chamber or vessel to another, and then close to prevent the blood from regurgitating backward. The

normal human heart contains four cardiac valves that regulate blood flow into and out of the heart; aortic valve, pulmonary valve, mitral valve and tricuspid valve (Figure 1-3).

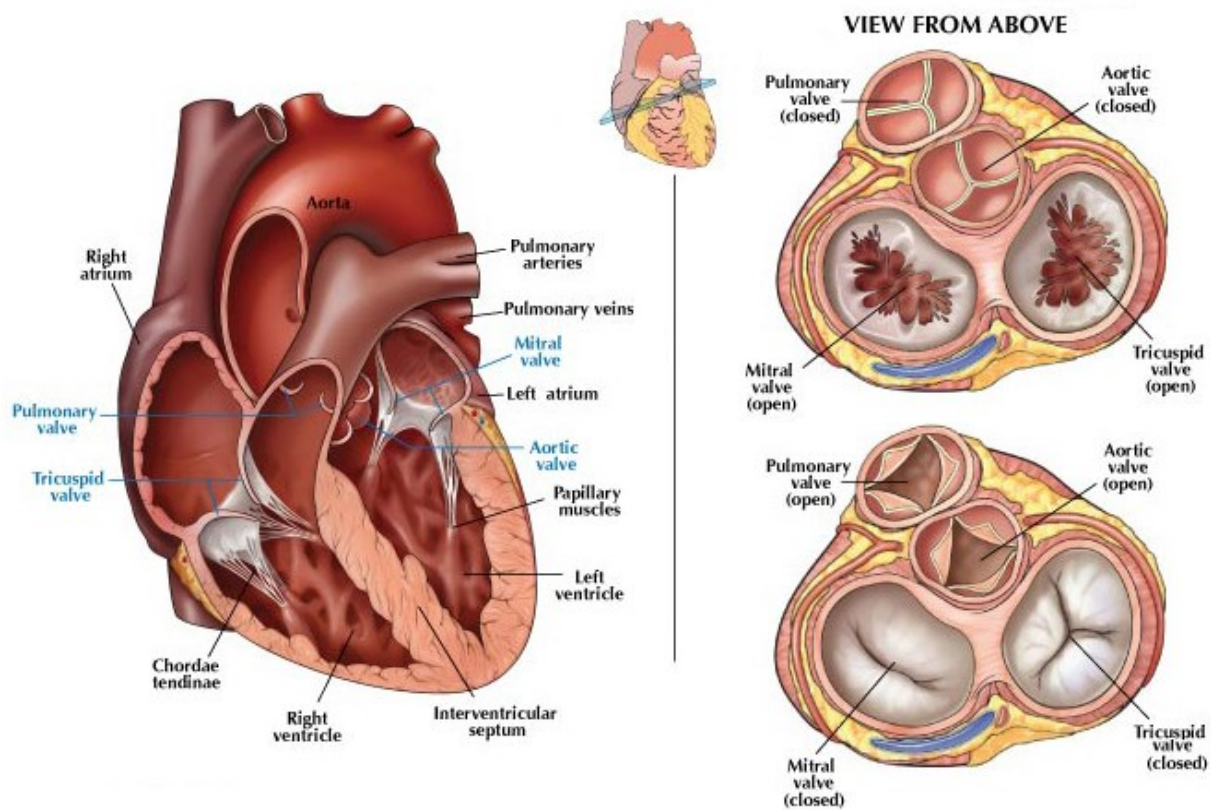


Figure 1-3: Anatomy of the heart valves(Tips, 2013)

1.4. Aortic Valve

The aortic valve (Figure 1-4), the most important valve of the heart (Williams et al., 2010), is located at the left ventricle outflow tract where the aorta begins. As a centerpiece of the heart, it approximately affects many other important cardiac structures.

The aortic valve main function is to prevent blood regurgitation from the aorta into the left ventricle during diastole and to allow the appropriate flow of blood, cardiac output, from the left ventricle into the aorta during systole.

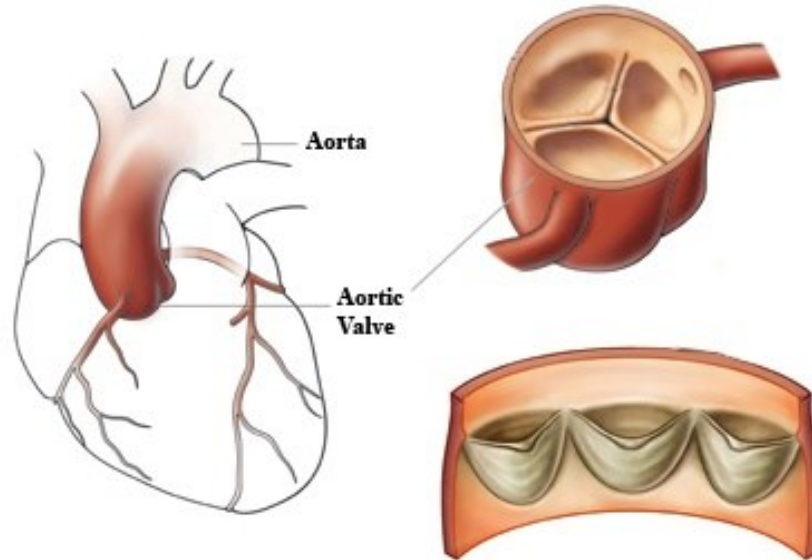


Figure 1-4: Aortic valve and heart skeleton, obtained from (Robvalve, 2014)

Figure (1-5) shows the detailed anatomy of the aortic valve. It consists of three important parts: Annulus, Cusps and Commissures.

- **Annulus:** The aortic valve annulus so called aortic ring (Figure 1-5) is a crown shaped structure at the level of the junction of the aortic valve and the ventricular septum which provides support to the aortic valve complex. (Anderson, 2000; Misfeld and Sievers, 2007) .

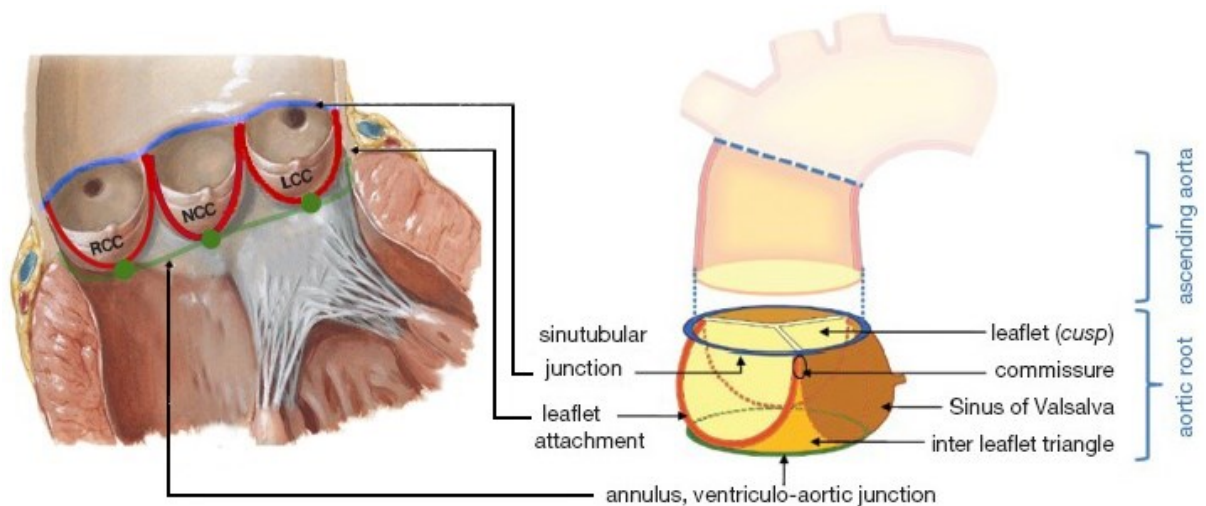


Figure 1-5: Anatomy of the aortic valve (Kasel et al., 2013; Sievers and Schmidtke, 2007)

- **Cusps:** There are three half-moon shaped aortic valve cusps/ leaflets (Figure 1-5); Left coronary cusp (LCC), right coronary cusp (RCC), and posterior or non-coronary cusp (NCC). (Benjamin, 2013).

- **Commissures:** Each cusp is attached to the wall of the aorta by the outward edges of its semicircular border at the level of sinotubular junction (functional level of the aortic valve orifice). The small spaces between each cusp's attachment points are called the aortic valve commissures (see figure 1-5).

1.5. Aortic Valve Stenosis

Aortic stenosis (AS) refers to a heart disease which is usually defined by restricted opening of the aortic valve leaflets during systole. The stenotic aortic valve cannot open fully which causes a partial restriction of blood flow from the left ventricle into the aorta.

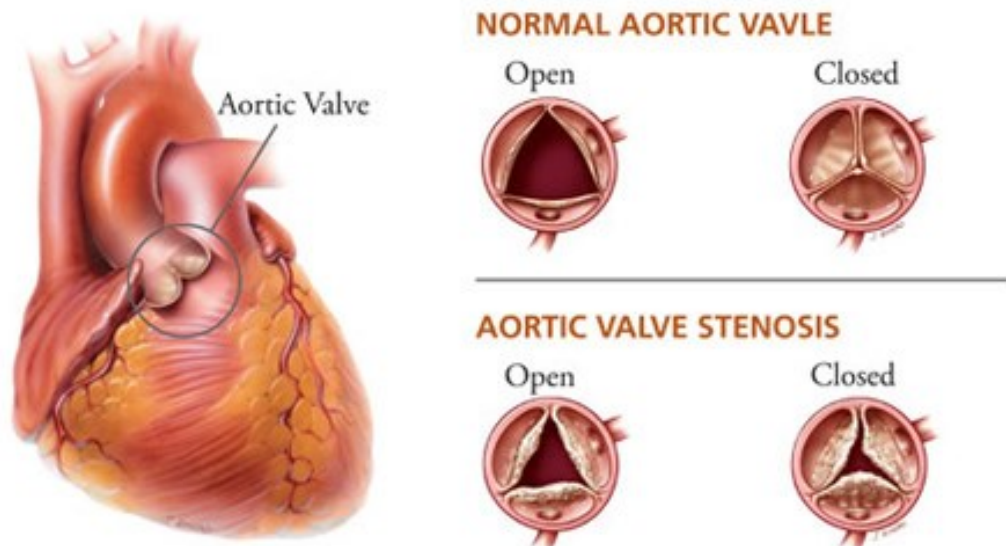


Figure 1-6: Stenotic aortic valve vs. normal aortic valve (Intermountain Heart Institute, 2015)

AS is now the most common valvular heart disease in the western countries (Manning, 2013). The presence of the significant AS increases the left ventricle pressure and cardiac workload which causes hypertrophy and could lead in sudden death and heart failure in case of severe AS (Nishimura, 2002).

AS may exist from birth (congenital), but most often it develops later in life. It mainly occurs due to the accumulation of calcium deposits (calcification) during the time that narrow the valve. Calcification of the valve mostly affects older people and could happen sooner in people who are born with abnormal aortic or bicuspid valves. It is estimated that AS occurs in about 25% of people over 65 years of age (Benjamin, 2013). Another cause is rheumatic fever. This condition can develop after strep throat or scarlet fever which is becoming rarer in the United States.

As the aortic valve gets stenosed and narrowed, the left ventricle has to work harder to pump blood throughout the valve. To do this extra work, the muscles in the ventricle walls become thicker, which can lead to chest pain. As the pressure continues to rise, blood may back up into the lungs. Severe aortic stenosis is really life threatening, and can limit the amount of blood that reaches the brain and the whole body.

Treatments for aortic stenosis depend on how far the disease has progressed. Currently, replacing the aortic valve is considered as the only effective treatment for severe AS (Edwards Lifesciences Corporation, 2013, Bonow et al., 2006).

1.6. Aortic Valve Replacement

Aortic valve replacement (AVR) has been the standard of care for patients with symptomatic severe aortic stenosis for several decades (Bonow et al., 2006; Manning, 2013).

Currently, there are two AVR approaches; surgical aortic valve replacement (SAVR), and minimally invasive transcatheter (Percutaneous) aortic valve replacement (TAVR).

1.6.1. Surgical Aortic Valve Replacement (SAVR)

Surgical aortic valve replacement (SAVR) through open-heart surgery is a common treatment for severe aortic stenosis on patients who are suitable candidates for surgery (Bonow et al., 2006). It consists of a surgical replacement of the native calcified aortic valve with a prosthesis heart valve (mechanical, bio-prosthesis, homograft tissue and Ross procedure) (Manning, 2013).

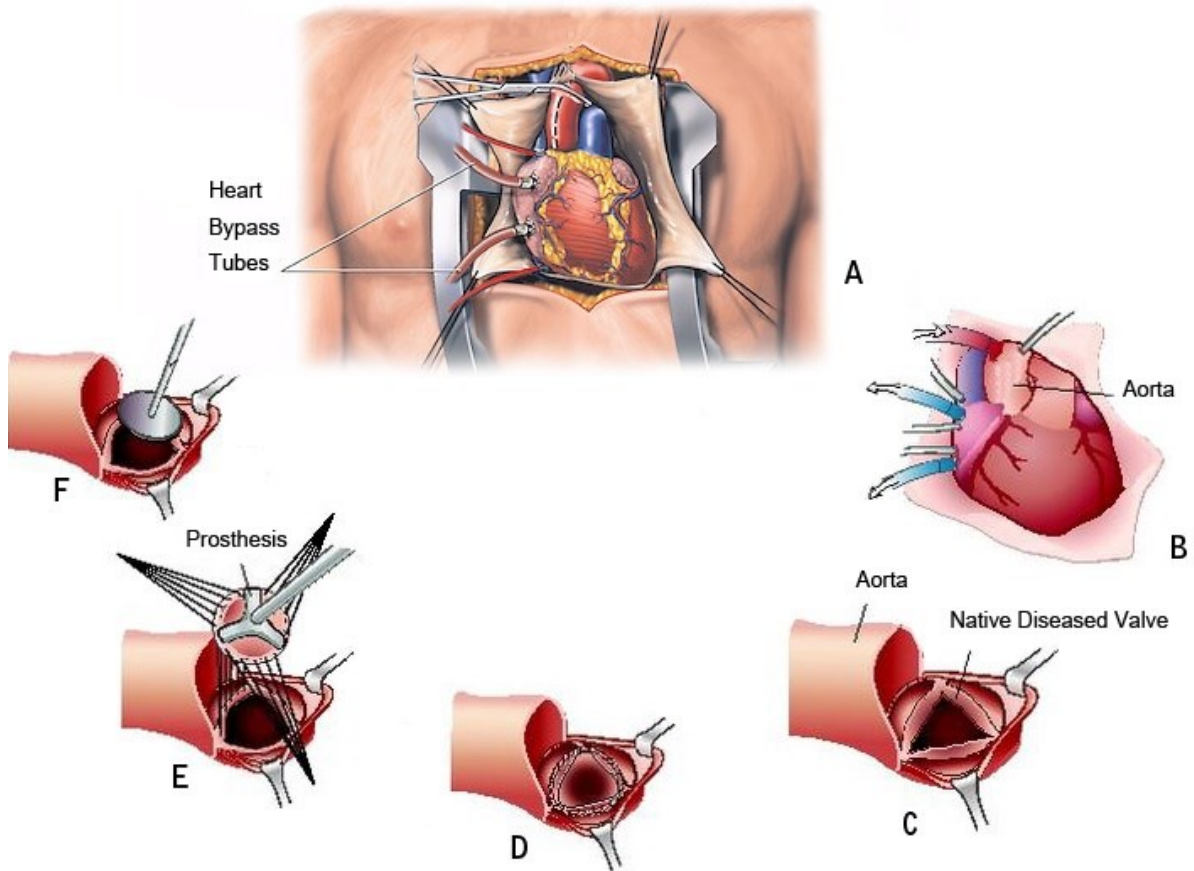


Figure 1-7: Surgical aortic valve replacement (SAVR) procedure

1.6.1.1. Procedure

SAVR is most frequently done through a median sternotomy (Figure 1-7), meaning that the chest is surgically separated. Once the chest has been opened, the patient is put on a cardiopulmonary bypass machine (heart-lung machine). The surgeon replaces the native malfunction aortic valve with an artificial heart valve. After SAVR, the patient will frequently stay in an intensive care unit for 12–36 hours, and is often able to go home after this, in about four days.

1.6.1.2. Prosthetic Heart Valves

Prosthetic heart valves are devices that implanted in the heart of a patient through the open heart surgery. Currently, there are three types of heart valves; mechanical heart valves, tissue/biological heart valves and tissue engineered heart valves. This notes provides a quick overview on characteristics and comparison of the available prosthetic heart valves.

I. Mechanical Heart Valves: Mechanical heart valves (MHV) are prosthetic valves, which are designed to replicate the functions of the natural human heart valves. MHVs are classified into three categories: caged-ball, tilting-disk and (Figure 1-8).

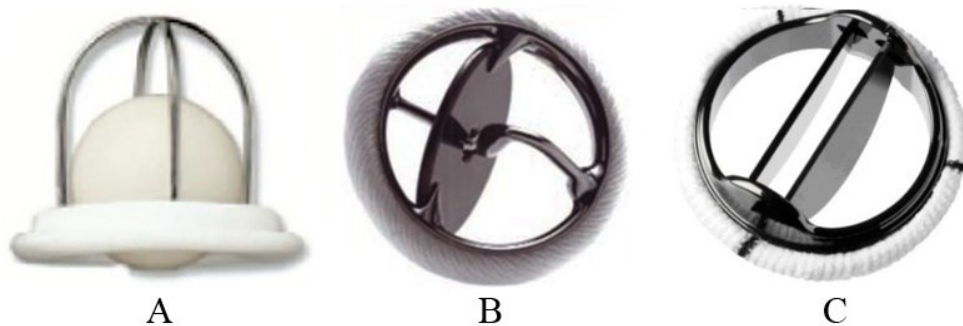


Figure 1-8: Different types of mechanical heart valves: a) caged-ball valve; b) mono-leaflet tilting valve; c) bileaflet valve (Lori et al., 2014; Symersky et al., 2012)

Most of the observational studies on MHVs have shown excellent long term results with no difference in durability between types of prosthesis. MHVs are considered durable and mostly lasts for 20-30 years. However, their main weakness is that all MHVs have an absolute lifelong requirement for anticoagulant treatment to avoid red blood cell damage, clotting and thrombus formation. (Bloomfield, 2002; Pibarot and Dumesnil, 2009).

II. Biological/ Tissue Heart Valves: The requirement for anticoagulant treatment in mechanical heart valve could be avoided by a valve replacement with suitable biological material. Therefore, biological (tissue) heart valves are designed not only to function like natural heart valves ,but also to mimic the anatomy of the native valve and avoid the potential risks of a long term anticoagulation therapy. Currently, tissue valves are the most used heart valves in US and EU.

Depending on where and how the tissues are harvested, biological heart valves categorized into three main groups: autograft valves (replacing by patient's own pulmonary valve), homograft valves (replacing by heart valves of brain dead human organ donor) and xenograft valves (harvested from pig or cow heart valves) (Bloomfield, 2002).

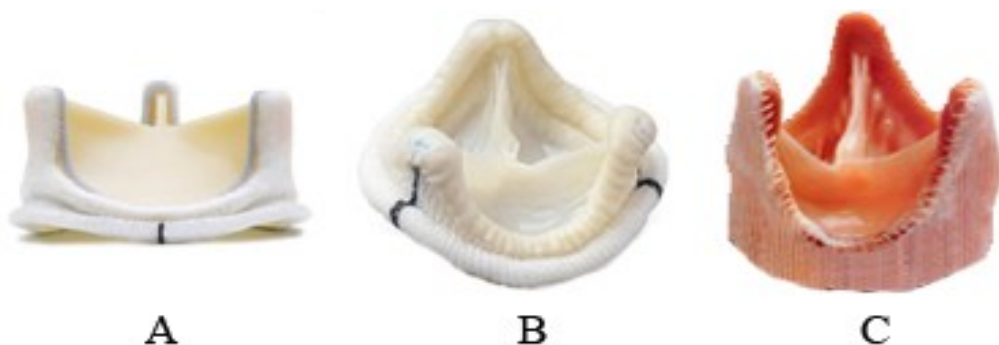
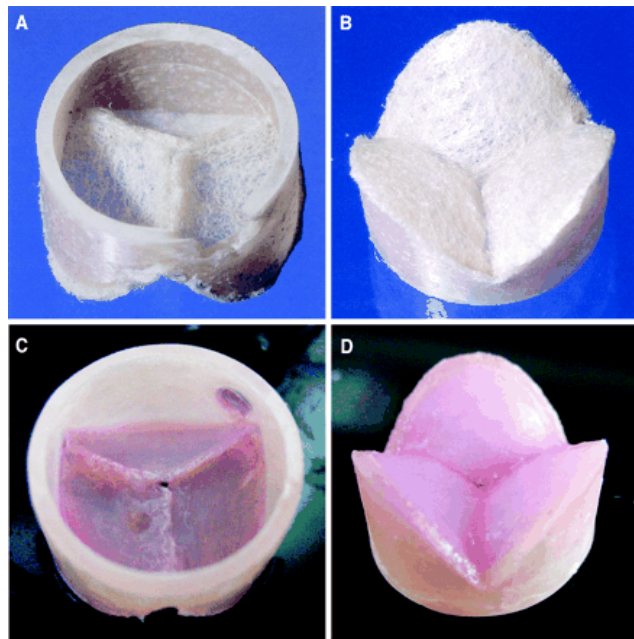


Figure 1-9 : Some types of biological heart valves
a) *Stented pericardial bovine bioprosthesis, Edwards. PREMOUNT magna, b) Stented porcine aortic valve bioprosthesis, Biocore, c) Stentless bioprosthesis, TORONTO SPV*

A major advantage of bioprosthetic valves is the low rate of thromboembolism (1.6 % per patient year). The risk of anticoagulation-related bleeding is also significantly lower. However, several studies have identified that bioprosthesis have limited lifespan as some patients require reoperation in the fourth or fifth postoperative year (Wan and Sarvasti, 2005; Pibarot and Dumesnil, 2009).

III. Tissue Engineered Heart Valves: *Tissue* engineered heart valves (TEHVs) are new, emerging alternative which offer the potential SAVR with a ‘living’ valve that resembles the shape and function of the native valve. TEHVs would be able to grow, repair and remodel as a native valve does (Rippel et al., 2012; Vesely, 2005). Although there is still a long way to go (Neuenschwander and Hoerstrup, 2004), tissue engineered heart valves give new hopes for less invasive procedures with the use of natural-like devices, which would decrease the risk of complications and improve valve performance (Rippel et al., 2012).



*Figure 1-10: Stented trileaflet heart valve scaffold (Mol et al., 2006)
(a) View from aortic side, (b) view from ventricular side, (c, d) After 4 weeks of culturing*

1.6.1.3. SAVR Outcome and Complications

SAVR is both recommended by ACC/AHA and the European Society of Cardiology as a standard of care, and the outcomes for none-high risk suitable surgery candidates is. SAVR decreases mortality, reduces symptoms, and improves patient quality of life (Clark et al., 2012). However, like all surgeries and treatments, there are some risks and complications associated with it.

In addition, several studies have reported that prosthesis patient mismatch (PPM) is frequent (20% to 70%) and has a negative impact on short- and long-term outcomes after SAVR for aortic stenosis (AS) (Pibarot et al., 2014).

Furthermore, even though SAVR improves symptoms and survival, observational studies have identified various subgroups of patients who are at increased risk for operative complications or death. In such patients (33% of elderly candidates) who are deemed inoperable or high risk for SAVR a less invasive treatment may be a suitable alternative (Clark et al., 2012; Jung et al., 2005; Svensson et al., 2011).

1.6.2. Transcatheter Aortic Valve Replacement (TAVR)

Transcatheter aortic valve replacement (TAVR) or transcatheter aortic valve implantation (TAVI) is a fairly recent minimally invasive procedure, which is approved by the FDA as the standard of care for extremely high risk or inoperable patients. It is an authorized alternative to surgery for selected high-risk but operable patients with symptomatic AS (American Heart Association, 2014; Genereux et al., 2013). There have already been over 50,000 implants in over 40 countries since the first TAV was implanted at 2002 (Faxon, 2011; Webb and Wood, 2012a).

1.6.2.1. TAVR Procedure

TAVR repairs the valve without removing the native, damaged and calcified valve. Instead, it expands a replacement valve into the aortic native valve location. Through TAVR procedure the transcatheter valve is delivered via a catheter to its place (Edwards Lifesciences Corporation, 2014). In this procedure (Figure 1-11), a valve with a tiny balloon at the end is sent into its place. Then the balloon is inflated to open the native diseased valve and deflated. In the next step, the balloon is expanded again to open up the transcatheter valve, deflated and removed. TAVs delivery and positioning may be really challenging, and are not without complications (Fishbein et al., 2013). TAVR may be performed using three different approaches, depending on which one provides the best and safest way to access the valve: transfemoral, transapical and transaortic.

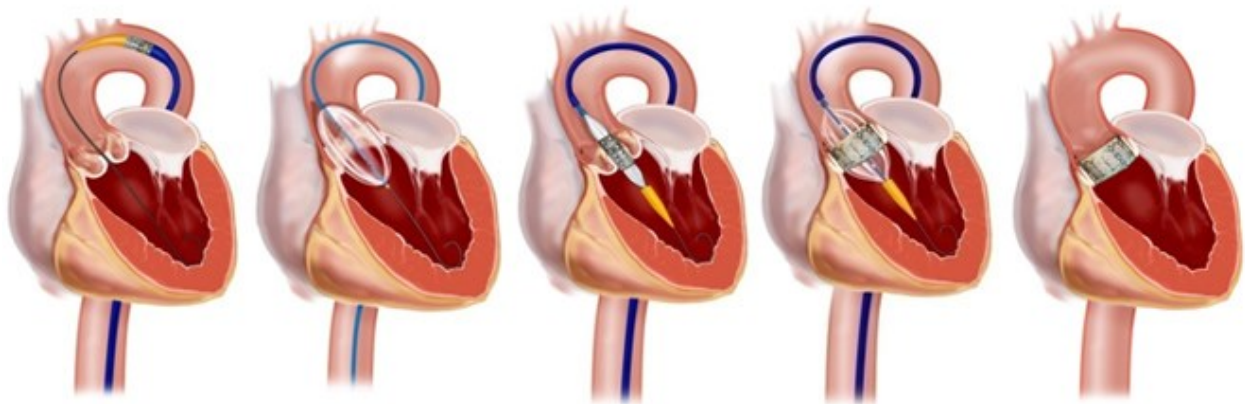


Figure 1-11 Transcatheter aortic valve replacement procedure (TAVR)(Center, 2013)

1.6.2.2. Transcatheter Heart Valves

Transcatheter heart valves (THVs) or percutaneous heart valves are a new technology of heart valves which represent a less invasive way for treating heart valve disease. THVs designed to be delivered via a catheter through the body's cardiovascular system (TAVR procedure), thus eliminating the need of open surgery. Currently, two THV devices are widely used: Edwards

SAPIEN Transcatheter Heart Valve (Figure 1-12-a), Medtronic CoreValve™ (Figure 1-12-b)
 (Généreux et al., 2015).

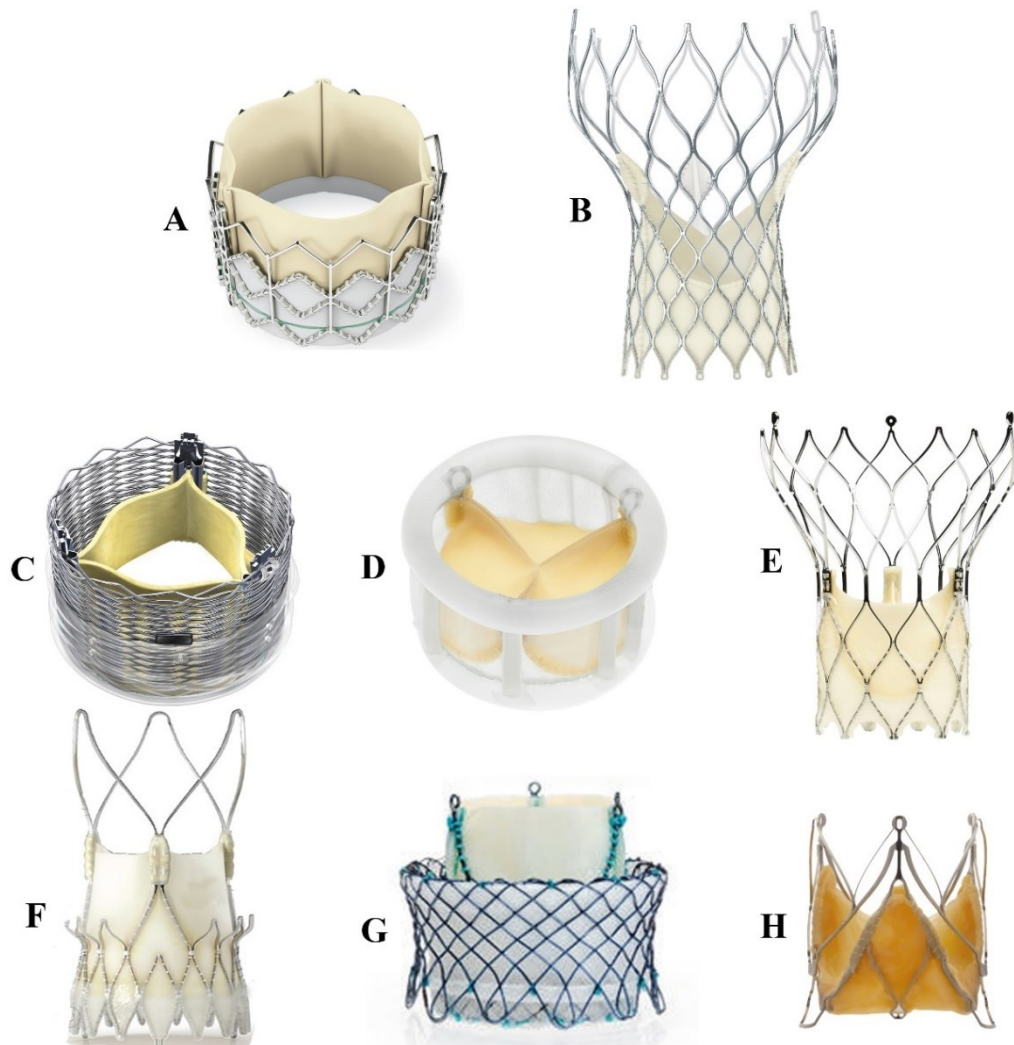


Figure 1-12: different type of transcatheter heart valves
 a) SAPIEN (Edwards Lifesciences, Irvine, CA, USA), b) CoreValve™ (Medtronic, Minneapolis, MN, USA), c) Lotus valve (Boston Scientific Inc., Natick, Massachusetts), d) Direct Flow valve (Direct Flow Medical Inc., Santa Rosa, California), e) Acurate (Symetis Inc., Ecublens, Switzerland), f) Portico (St. Jude Medical Inc., St. Paul, Minnesota), g) HLT (Bracco Inc., Princeton, New Jersey), h) JenaClip (JenaValve Inc., Munich, Germany)

Edwards SAPIEN transcatheter heart valve (Edwards Lifesciences, Irvine, CA, USA), utilizes a balloon-expandable system. It has a cobalt-chromium alloy frame with a bovine pericardium tri-leaflet construction. The inflow of the frame is covered with fabric to provide an

annular seal. This valve is available in three generations: SAPIEN, SAPIEN XT and SAPIEN 3 in 23 mm, 26 mm and 29 mm valve sizes.

Medtronic CoreValve™ (Medtronic, Minneapolis, MN, USA) consists of a tri-leaflet bioprosthetic porcine pericardial tissue valve, which is mounted in a self-expanding stent frame, a nickel-titanium alloy that is malleable at low temperature, but relatively rigid at body temperature. It is available in 26mm, and 29mm prosthesis (Abdel-Wahab et al., 2011).

Currently, only limited nonrandomized studies are available which compared these two devices. In 2014, Iqbal and Serruys published a review study and stated that “there is a device-specific complications between SAPIEN and CoreValve, but no difference in clinical outcomes”. Despite the post-TAVR results show that coronary obstruction may be more frequent with SAPIEN, and paravalvular regurgitation (PAR) and atrioventricular block requiring pacemaker implantation is more common with CoreValve, the patients treated with the CoreValve and the SAPIEN have been shown to have similar short- and long- term outcomes (Abdel-Wahab et al., 2014; Eltchaninoff et al., 2011; Moat et al., 2011; Webb and Wood, 2012)

There are also a number of newer THVs in early clinical evaluation. In general these valves incorporate features, which reduce delivery catheter diameter, improve ease of positioning or removal, and provide better sealing mechanisms to reduce paravalvular leak. For the most part, these next generation of valves are self-expandable (Webb and Wood, 2012a).

- Self-expanding Lotus valve (Boston Scientific Inc., Natick, Massachusetts) (Figure1-12-c)
- Self-expanding Direct Flow valve (Direct Flow Medical Inc., Santa Rosa, California) (Figure1-12-d)
- Self-expanding Acurate (Symetis Inc., Ecublens, Switzerland) (Figure1-12-e)
- Portico (St. Jude Medical Inc., St. Paul, Minnesota) (Figure1-12-f)

- HLT (Bracco Inc., Princeton, New Jersey) (Figure1-12-g)
- JenaClip (JenaValve Inc., Munich, Germany) (Figure1-12-h)

Although these newer valves offer many desirable features, experiences are limited. Therefore, clinical outcomes with the newer generations need to be evaluated.

1.6.2.3. TAVR Outcomes and Complications

TAVR procedure is not without risks; however it is the only available treatment for high risk, inoperable patients with symptomatic aortic stenosis (Généreux et al., 2013), while also providing the added value of a faster patient recovery in most cases (American Heart Association, 2014).

Experience with TAVR has increased significantly over the past several years which addressed TAVR procedure, outcomes and its complications. Although the trend shows that the clinical outcomes of TAVR have steadily improved (Webb and Wood, 2012a), TAVR is still associated with some predictable and unanticipated procedural and post- procedural complications due to the complexity of the procedure, as well as the morbidity of the patients being treated (Fishbein et al., 2013; Holmes et al., 2012), such as:

- Risk factors related to the aortic valve pathology (paravalvular leak, aortic rupture, LV hypertrophy, subaortic stenosis)
- Vascular complications
- Renal complications
- Coronary artery problems
- Mitral valve complications
- Stroke

Many research groups have established systematic reviews on TAVR short-term outcomes in comparison to SAVR or solely ; no differences in 30-day and 1-year mortality, were found among more than 8000 patients in 29 studies between the TAVR and SAVR (Kodali et al., 2012; Tang et al., 2013). However, paravalvular leak (PVL) was more significant after TAVR, and associated with an increase in late mortality (Mohamed Abdel-Wahab et al., 2011).

The outcome of TAVR in high-risk patients have also been studied in single-arm and randomized controlled studies (Fishbein et al., 2013). In the Unites States, PARTNER registered study (Craig R. et al., 2011; Leon et al., 2010; Makkar et al., 2012) demonstrated that TAVR maintains a sustained superiority over medical treatment in inoperable patients with symptomatic severe AS, significantly reduces the rates of death and hospitalization, decreases symptoms and improves in valve hemodynamics. This study also states that for high-risk patients, there is an equivalent outcomes between TAVR and SAVR. However, elevated 50% mortality in 3-year among inoperable patients makes the long-term efficacy of this therapy questionable. The stroke and PVL remain a concern, as well as the lack of benefit of TAVR in extremely high-risk patients (Tang et al., 2013).

1.7. Paravalvular Aortic Leak Following TAVR

As previously stated (Section 1.6.2.3), paravalvular aortic leak (PVL) or regurgitation (PAR) is one the major current complication of TAVR (Dvir et al., 2013). PVL is known to be associated with an increase in late mortality and affect the outcomes of TAVR (Mohamed Abdel-Wahab et al., 2011). This does not mean that mild PVL is uncommon after SAVR, but studies have shown that PVL after SAVR do not have significant impact on short-term and long-term clinical outcomes (Rallidis et al., 1999). FRANCE 2 (Van Belle et al., 2014), European registered

study on 3195 patients from 34 countries reported that the presence of more than mild PVL is the most powerful predictor for 1 year mortality. Incidence of PVL following TAVR, including small non-significant jets, is estimated to be as high as 48%-85% in different studies. (Gotzmann et al., 2012; Lerakis et al., 2013; Smolka and Wojakowski, 2010).

1.7.1. Definition and Causes

PVL refers to blood flowing back, during left ventricle filling, through a channel between the structure of the implanted valve and native valve tissue (as a result of an incomplete circumferential apposition of the prosthesis with the annulus) (Sinning et al., 2013). The majority of PVL orifices are crescent, oval or roundish-shaped and their track can be parallel, perpendicular or serpiginous.

Significant PVL or annular rupture is usually due to prosthetic under sizing or oversizing caused by discordance in the orthogonal diameters of oval-shaped annuli with the circular prosthesis (John et al., 2010). Mal-positioning of the valve or displacement of the valve may also cause PVL (Buellesfeld and Grube, 2012; John et al., 2010). Another risk factor for PVL is a functional bicuspid aortic valve.

1.7.2. Presentations and Symptoms

Clinically significant acute PVL is characterized by a considerable diastolic backflow into the LV leading to acute volume overload, which leads to LV pressure overload, followed by an increase in the LV end-diastolic volume and cardiac output.

In acute severe PVL, the LV is unable to increase the end-diastolic volume effectively. As the LV fails to increase the total stroke volume, the forward stroke volume and systolic arterial pressure decrease (Azadani et al., 2009; Gotzmann et al., 2012).

Therefore, Significant PVL may lead to fatal cardiogenic shock, heart failure (HF), hemolytic anemia and infectious endocarditis. Hemolysis can be severe enough to precipitate symptoms of anemia (Pate et al., 2006; Safi et al., 2000; Smolka & Wojakowski, 2010).

1.7.3. Assessments and Classifications

The severity of PVL should be assessed by the following information (Smolka and Wojakowski, 2010):

- Shape and orientation of the jet
- Number of jets
- Maximum velocity
- Presence of the distal flow reversal
- Pulmonary pressures

The most important diagnostic modality which gives the above information is imaging, such as:

- Angiographic assessment
- Echocardiography assessment [transthoracic echocardiography (TTE), transesophageal echocardiography (TEE)]
- Cardiac Magnetic resonance (CMR)
- Multi-slice computed tomography (MSCT)
- Intraprocedural imaging [Intravascular ultrasound (IVUS), Aortography]

While all above multiple modalities have been used to characterize PVL, echocardiography remains the least costly and most widely available. Currently, echocardiography should be the first step in a comprehensive and integrative evaluation of the post-TAVR patient. If multiple echocardiographic parameters confirm that PVL is severe, CMR would be advocated to more accurate quantitation of regurgitant fraction (Hayek, 2014). It is important to realize that

quantification of PVL after TAVR still remains challenging (Lerakis et al., 2013; Zoghbi et al., 2009).

PVL severity is not only of prognostic value but it may as well lead to therapeutic intervention. Therefore, it is essential to accurately characterize and categorize the severity of PVL, given that the patients undergoing TAVR are typically high risk. The Valve Academic Research Consortium (VARC) published the VARCII criteria (Table 1-1) for hemodynamic severity assessment of AR and/or PVL after TAVR. VARCII classifies PVL severity into three levels; mild, moderate and severe. However, the body of evidence supporting these criteria for the assessment of PVL are limited and requires further validation (Généreux et al., 2013; Kappetein et al., 2012).

In addition, the current guidelines adopted by VARC-2 are arbitrary, derived from the evaluation of aortic regurgitation in native valves, with certain adaptations emphasizing the description of jet anatomy (Kappetein et al., 2012; Zoghbi et al., 2003).

Table 1-1: PVL evaluation criteria by The Valve Academic Research Consortium (VARC) published the VARCII

	Prosthesis-Patient Mismatch (PPM)		
	Insignificant	Moderate	Severe
Indexed effective orifice area [†] (cm ² /m ²)	>0.85 cm ² /m ²	0.85–0.65 cm ² /m ²	<0.65 cm ² /m ²
Indexed effective orifice area [#] (cm ² /m ²)	>0.70 cm ² /m ²	0.90–0.60 cm ² /m ²	<0.60 cm ² /m ²
	Prosthetic Aortic Valve Regurgitation		
	Mild	Moderate	Severe
Semi-quantitative parameters			
Diastolic flow reversal in the descending aorta—PW	Absent or brief early diastolic	Intermediate	Prominent, holodiastolic
Circumferential extent of prosthetic valve paravalvular regurgitation (%)**	<10%	10–29%	≥30%
Quantitative parameters[‡]			
Regurgitant volume (mL/beat)	<30 ml	30–59 ml	≥60 ml
Regurgitant fraction (%)	<30%	30–49%	≥50%
EROA (cm ²)	0.10 cm ²	0.10–0.29 cm ²	≥0.30 cm ²

1.8. Objective and Outline of This Study

The specific aim of the present study is to develop a numerical and computational model to investigate: 1) The flow dynamics patterns induced in the presence of PVL; 2) The variations in left ventricular performance following TAVR in the presence of different severities of paravalvular leak.

The results will be useful in understating the presence of PVL post TAVR and evaluating important parameters that cannot or are difficult to obtain in vivo (e.g. wall shear stress, oscillatory wall shear stress, LV stroke work). This work will also help the process of choosing the appropriate THV valve for TAVR procedure, based on comparing the pre and post TAVR different scenarios.

In reference to the defined objectives, in this research, two separate models are employed: First, the concept of mathematical lumped parameter model is used to model the simplified circulatory system in presence of paravalvular leak and evaluate the variation of the left ventricle stroke work under several pre-TAVR and post-TAVR (combinations of aortic valve stenosis and aortic valve regurgitation/PVL).

Second, three-dimensional (3D) computational fluid dynamic simulations are performed in order to investigate the effect of paravalvular leak on the diastolic flow-field characteristics following transcatheter aortic valve TAVR.

CHAPTER 2: Literature Review

2.1. Introduction

The cardiovascular system has always been of interest to engineers and scientists. Researchers have been studying its characteristics by using experimental, mathematical or computational methods. Several mathematical and numerical models of the cardiovascular system have been introduced since 1959, when Grodins published the first global mathematical model of cardiac and blood vessel hemodynamics (Paeme et al., 2011). Models vary significantly in complexity and objectives, ranging from a simple zero-dimensional model (Westerhof et al., 2009), to a very complex network of representations of the vascular tree (Shim et al., 2008), three-dimensional finite element (FEM) models (Kerckhoffs et al., 2007; Pham and Vincent, 2001), computational fluid dynamic (CFD) models (Schenkel et al., 2009) or even coupled (FSI) models (Sermesant et al., 2006). Each model serves different uses, but they all share the common goal of understanding cardiovascular function and provide us with the following considerable benefits:

- Engineering studies are non-invasive
- They could be performed in less time and at a lower cost
- They could provide us with some data and information that are difficult/impossible to measure in-vivo.

The importance of engineering studies are not less than Trial or PARTNER studies in this area and they have several applications. First, they could provide additional information to support medical decisions. Fast and accurate models could also be used in combination with medical imaging and other diagnostic techniques in a clinical setting to provide real-time information to advance patient care. Second, these studies would help the cardiovascular equipment and tool developers, by validating and predicting the performance of the device, to improve the product design and

decrease the cost of production. The long term goal of these engineering studies is to set up a system of techniques and tools, which could be of help for clinical practice.

In this work, due to the importance and prevalence of the aortic paravalvular leak (PVL) following transcatheter aortic valve replacement (TAVR) (described in Chapter 1), two separate models are employed to investigate the nature of the PVL following TAVR: 1) a zero-dimensional mathematical lumped parameter model and 2) a three-dimensional computational fluid dynamic (CFD) model.

2.2. Numerical Lumped Parameter Modeling

A lumped parameter model is a mathematical model which simplifies the description of the behavior of the distributed physical systems into a topology consisting of discrete entities. Mathematically speaking, the simplification reduces the partial differential equations (PDEs) of the continuous (infinite-dimensional) time and space model of the physical system into ordinary differential equations (ODEs) with a finite number of parameters.

The concept of lumped parameter modeling was first quantitatively formulated and popularized in cardiovascular studies by Otto Frank in 1899. The so called Windkessel model by Otto was a two-element model, which describes the hemodynamics of the arterial system in terms of resistance and compliance. It later extended to three-element and four-element models by adding the characteristic impedance (Westerhof et al., 1971, 1969), and additional inertance (Burattini and Gnudi, 1982), consecutively. However, the lumped model of the arterial system or a part of it cannot be used for wave transmission and wave travel studies as well as blood flow distribution; it serves to simulate the real cardiac circuit, and it is simple and fairly accurate in the approximation of many important parameters of this circuit, such as cardiac output and right ventricular afterloads (Westerhof et al., 2009).

Since then, many scientists have extensively employed similar concepts of lumped parameter modeling in order to evaluate cardiovascular system hemodynamics in different scenarios (Westerhof et al., 2009). In several studies, simple or coupled models (heart-arterial, ventricle-arterial, etc) have been used to do theoretical analysis (Kerckhoffs et al., 2007; Segers et al., 2003, 2002) to predict the contributions of changes in parameters, and to show that the predictions are supported by experimental data. These models have also been employed in modeling pathological conditions, such as pulmonary hypertension (Tanné et al., 2008), aortic stenosis (Garcia and Durand, 1983; Garcia et al., 2005a), aorta coarctation and bicuspid aortic valve (Keshavarz-Motamed et al., 2014b). Several studies have also been reported on the nonlinear models in studies on ventricular assist devices and setups to test artificial valves (Dolan et al., 2006; Geven et al., 2004; Mol et al., 2006).

Despite the fact that lumped parameter modeling application has been widely studied in the cardiovascular area, there is no study which has investigated the effect of PVL on cardiac output or left ventricle stroke workload by implementing the mathematical lumped parameter modeling method.

2.3. Computational Mechanics Modeling

Computational mechanics (CM) modeling is concerned with the use of computational methods to model phenomena governed by the principles of mechanics, which usually involves expressing the natural or engineering system in terms of partial differential equations and solving them by digital computation through discretization. Different specializations within CM, including computational fluid dynamics (CFD), computational structural mechanics (CSM) and fluid-solid

interactions (FSI) have been widely used in the area of cardiovascular research and are capable of modeling really complex scenarios.

Since the 70s, many CM studies have addressed the cardiovascular system in different aspects, starting from very simple two-dimensional symmetric models to realistic three-dimensional dynamic analysis. In this section, a short survey will be given on the different heart valve CM models that have been developed over the years. The review is mainly focused on prosthetic heart valves.

2.3.1. Computational Mechanics Modeling in Heart Valves

One of the first contributions in this field was made in 1972 by Peskin. Peskin succeeded to capture the movement of two flexible solids in a 2D fluid domain using his immersed boundary method (McQueen and Peskin, 1997; Peskin and McQueen, 1989, 1980). Later, Black et al. (1991) was amongst the first to model a 3D geometry of a native aortic heart valve and analyze the stress-strain distribution in the leaflets subject to pressure-load.

Studies dealing with native valve motions have mainly been performed in two major ways: 1) prescribing leaflet movement from experimental data, focused only on the fluid flow (Chandran et al., 1998; Krafczyk et al., 2001, 1998; Vio B et al., 1997); 2) employing the coupled fluid-solid interaction method to include both structural and fluid aspects (Cheng et al., 2004; De Hart et al., 2003; Dumont et al., 2004; Hart et al., 2000; King et al., 1997; Lai et al., 2002; Nicosia et al., 2003; Weinberg and Kaazempur Mofrad, 2007).

2.3.2. Computational Mechanics Modeling in Prosthetic Heart Valves

Over the past five decades a vast number of computational mechanics simulations have been reported in the literature on the structural modeling of prosthetic heart valves (PHVs) and on the computation of the flow dynamics past PHVs. Early studies were more focused on modeling MHVs due to their high availability and the relatively strong materials of the leaflets, which makes them rigid and easier to deal with. Avoiding the complications of FSI analysis, the first studies reported on detailed flow through MHVs with valve leaflets in the fully open position. Tilting disc valves (Kiris et al., 1997; Shim and Chang, 1997) and bi-leaflet valves (Bluestein et al., 2002; Ge et al., 2005; King et al., 1997; Shi et al., 2003) were modeled using this approach. These studies concentrated in regions of high velocity and turbulent shear stresses and also in regions of flow stagnation where activated platelets may cause subsequent embolic problems.

More recently, several studies employing more advanced FSI analysis with moving leaflets for the flow past MHVs have been reported (Borazjani et al., 2008; Dumont et al., 2007, 2005, 2004; Ge et al., 2008; Morbiducci et al., 2009).

Studies also investigated bioprosthesis heart valves (BHVs) including transcatheter heart valves (THVs). Unlike the MHVs, the BHVs leaflet material exhibits a highly non-linear, anisotropic behavior and undergoes large and complex deformations. The flow past the valvular structures results in a complex 3D time-dependent flow and both the solid and fluid dynamics must be accurately resolved.

Early studies mostly reported on theoretical geometries; 2D structures or simplified 3D valve structures with linear material properties (Chandran, 2010). Cataloglu et al. (1977) used linear material assumptions, while Hamid et al. (1985) based their study on a multi-linear model. Huang et al. (1990) employed a 2D model with a total lagrangian approach to solve FEM equations

with large deformations. Christie and Medland (1982) were among the first who developed a 3D model with nonlinear anisotropic material relations. Later, Sanders et al. (1996) modeled a 3D stented bioprosthetic heart valve with nonlinear elastic behavior materials. Using nonlinear material properties was found to be more realistic when compared to experimental and in vivo results (Chandran, 2010).

Considering more recent studies, Kim et al. (2008) carried out a 3D nonlinear dynamic simulation of realistic BHVs' leaflets to investigate the nature of calcification and degradation in BHVs. In another study, Borazjani (2013) developed the first fully-resolved 3D BHV simulation under physiologic conditions without any symmetry assumption, questioning the accuracy of previous symmetrical simulations.

2.3.3. Computational Mechanics Modeling in Transcatheter Aortic Valves

Dwyer et al. (2009b) performed a CFD study on a 3D transcatheter aortic valve, considering its degeneration and hemodynamics due to transcatheter valve (TAV) sclerosis (35% orifice reduction) and stenosis (78% orifice reduction). Their results showed that stenosis led to significant forces on TAV during systole with stress concentrations on the tips of the leaflets. However, diastolic forces on TAV predominated even in presence of significant stenosis. Stenosis also elevates the magnitude of wall shear, reaching values that could be clinically relevant to hemolytic injury and thrombus deposition.

Sun et al. (2010) carried out a FSI simulation of 3D transcatheter valve deployment, addressing the distorted configurations of asymmetrical deployment process of the TAV into a calcified aortic root. Their study indicated that the distorted, elliptical TAVs induced a significant

increase in leaflet peak stresses and strains compared with a nominal circular TAV under the same boundary/loading conditions.

In another study by Sirois et al. (2011), a 3D patient specific simulation of TAV deployment (FE, CFD) was performed. Their CFD model was validated where possible by benchmarking against TAV clinical trial data in the literature. Their analysis of the flow field gave insights on the velocity profile, including coronary artery flow distribution pre- and post-deployment. It was observed that although cardiac output increases and transvalvular pressure decreases following TAV intervention, the amount of coronary artery flow present does not increase proportionally.

Tan et al. (2011) also performed a study on flow patterns before and after TAVI, using combined cardiovascular magnetic resonance imaging (CMR) and CFD. A patient with aortic stenosis was examined using MRI pre- and post-TAVI, and 3D CFD simulations were carried out incorporating MRI-derived patient-specific data. Pre-TAVI velocity profiles demonstrated the highly disturbed turbulent flow and jet impacting the wall of the aortic arch due to the stenosed aortic valve. While, post-TAVI velocity profiles were similar to those in healthy aortas with spatially more uniform WSS and lower turbulence levels, demonstrating the effectiveness of the TAVI procedure in restoring normal aortic flow.

As a step forward in the direction of creating a computational tool able to support TAVI preoperative planning (anticipating surgical operation outcomes), Auricchio et al. (2013) and Morganti et al. (2013) performed FEM studies, modeling TAV deployment process in a few separate patient specific models with native diseased valve in the presence of calcium on the valve leaflets.

2.4. Engineering Studies in Prosthetic Aortic Valve Regurgitation

Some engineering studies have addressed regurgitation and reverse flows through native stenotic or diseased heart valves. Only a few engineering studies have considered to simulate/model the heart valve prosthesis in the presence of regurgitation.

Hsu and Lu (2013) modeled the 3D tilting disk mechanical heart valve in the presence of valve regurgitation with both pulsatile and quasi-steady flow conditions. Their FSI analysis used an immersed moving occluder (rigid tilting prosthetic heart valve) interacting with the flow in an infinite straight duct as a domain during the full heart cycle. Their results also indicated that the steady simulations of the regurgitation is not accurate enough to describe the flow field in comparison to the pulsatile unsteady simulations.

Although to the best of our knowledge there is no computational modeling research which has specifically considered paravalvular leak post-TAVR, a few experimental studies have been conducted to investigate TAV associated with PVL. Azadani et al. (2009) used the left heart experimental setup with implanted TAV in the aortic valve position. A TAV designed to mimic a 23 mm SAPIEN and 3 different sizes (19, 21 and 23 mm) of Carpentier-Edwards bioprostheses. Their objective was to compare the energy loss due to the paravalvular leak in TAVs versus surgically implanted bioprosthesis. Their results suggested that, in the presence of mild PVL, TAV implantation imposes a significantly higher workload on the left ventricle than an equivalently sized surgically implanted bioprosthesis of a similar size.

Scotten and Siegel (2014) conducted an experiment on PVL post-TAVR using a mock TAV device consisting of an Edwards-Perimount model 2800 pericardial surgical valve and adjustable lower panel PVL setting. Their results reported on comparability of thrombogenic potential of TAV to mechanical heart valves.

CHAPTER 3: On the Determination of the Performance of Transcatheter Aortic Valve Implantation: Mathematical Modeling and Clinical Implications

Article 1

A. Saeedi^{1*}, A. Djebbari^{2*}, Z. Keshavarz-Motamed^{1,3,4}, P. Pibarot⁴, N. Dahdah⁵, L. Kadem¹

(* Contributed equality)

1. Mechanical and Industrial Engineering Department, Concordia University, Montréal, Québec, Canada.
2. University of Tlemcen, Tlemcen, Algeria.
3. Institute for Medical Engineering and Science, Massachusetts Institute of Technology, Boston, Massachusetts, USA.
4. Department of Medicine, Laval University, Québec, Québec, Canada
5. Division of Cardiology, Sainte-Justine Hospital, University of Montreal, Montréal, Québec, Canada

Journal of Biomechanics, Submitted, June 2015

Abstract

Transcatheter aortic valve replacement (TAVR) has recently emerged as a feasible and viable solution for symptomatic patients with severe aortic stenosis who are denied standard aortic valve replacement. TAVR short and medium term results are very promising but appear suboptimal in the presence of paravalvular leak. Using a mathematical model, this study simulates several patient conditions based on valve area and regurgitation severity before and after TAVR.

The objective is to define the conditions that lead to suboptimal results. Pre-TAVR conditions include aortic stenosis effective orifice areas (EOAs) of 0.4, 0.6, 0.8 and 1.0 cm² with concomitant aortic regurgitation severities ranging from trace/mild to moderate-to-severe. For each condition, we simulated the implantation of transcatheter aortic valves with effective orifice

areas of 1.3, 1.6 and 1.9 cm² and similar ranges of paravalvular leak as pre-TAVR aortic regurgitation. The performance of TAVR was evaluated considering the relative change in the computed left ventricle stroke work (LVSW). In a large majority of cases (76%), TAVR significantly reduced LVSW (range: -13±8% to -84±2%). However, in 16% of cases, TAVR did not significantly reduce LVSW and in 9%, TAVR led to an increase in LVSW (range: +16±13% to 84±20%). Most of the conditions where TAVR underperformed corresponded to pre-existing aortic stenosis conditions with only trace/mild aortic regurgitation. In conclusion, patients with aortic stenosis and only trace/mild aortic regurgitation should be considered with care when planning for TAVR because of potential suboptimal performance despite a reduction in transvalvular pressure gradients.

3.1. Introduction

Transcatheter aortic valve replacement (TAVR) has recently emerged as a feasible and viable solution for patients with severe symptomatic aortic stenosis who are denied standard surgical aortic valve replacement because of elevated operative risks (Leon et al., 2010; Smith et al., 2011). TAVR short and medium term results are very promising (Genereux et al., 2013; Ussia et al., 2012). There remain, however, important complications lowering the benefit of TAVR in a certain proportion of patients (Leon et al., 2010; Smith et al., 2011; Kodali et al., 2012). The most important one appears to be post-TAVR paravalvular leak (PVL) (Gilard et al., 2012; Kodali et al., 2012). The prevalence of PVL following TAVR varies between studies and ranges from 7% to 70% for mild PVL and 0% to 24% for more than mild PVL severity (Pibarot et al., 2015). PVL has been shown to be an independent predictor of short-term and long-term mortality following TAVR (Abdel-Wahab et al., 2011; Tamburino et al., 2011; Moat et al., 2011). Suboptimal outcome

following TAVR can even be found in patients with mild to moderate PVL (Athappan et al., 2013; Hayashida et al., 2012). It appears therefore that under certain conditions, the benefit of TAVR in terms of lowering left ventricle (LV) pressure load is balanced/overcome by an increase in volume overload, due to PVL. It remains unclear however what specific combinations of valve EOA and valve regurgitation/PVL before and following TAVR will lead to a significant reduction in LV stroke work. For example, does implanting a transcatheter aortic valve (TAV) with an EOA of 1.60 cm² and mild-to-moderate PVL in a patient with a stenotic valve of 0.60 cm² and only a trace/mild aortic valve regurgitation lead to a significant reduction in LV stroke work? To contribute towards answering this question, we developed a lumped parameter model capable of simulating patient conditions before and after TAVR.

More specifically, the objectives of this study are: 1) To evaluate the variations in LV stroke work under several pre-TAVR and post-TAVR combinations of valve EOAs and valve regurgitation/PVL of various intensities; 2) Introduce an estimate for the variation in LV stroke work that can be easily and routinely measured in patients undergoing TAVR.

3.2. Method

A schematic diagram of the lumped parameter model is presented in Figure (3-1). This model includes four different sub-models. 1) left ventricle model; 2) aortic stenosis (AS) model; 3) aortic regurgitation model; 4) systemic circulation model. In this study, our lumped-parameter model developed and validated by Keshavarz-Motamed et al. (2014, 2011) was modified and further developed to simulate aortic regurgitation and PVL following TAVR.

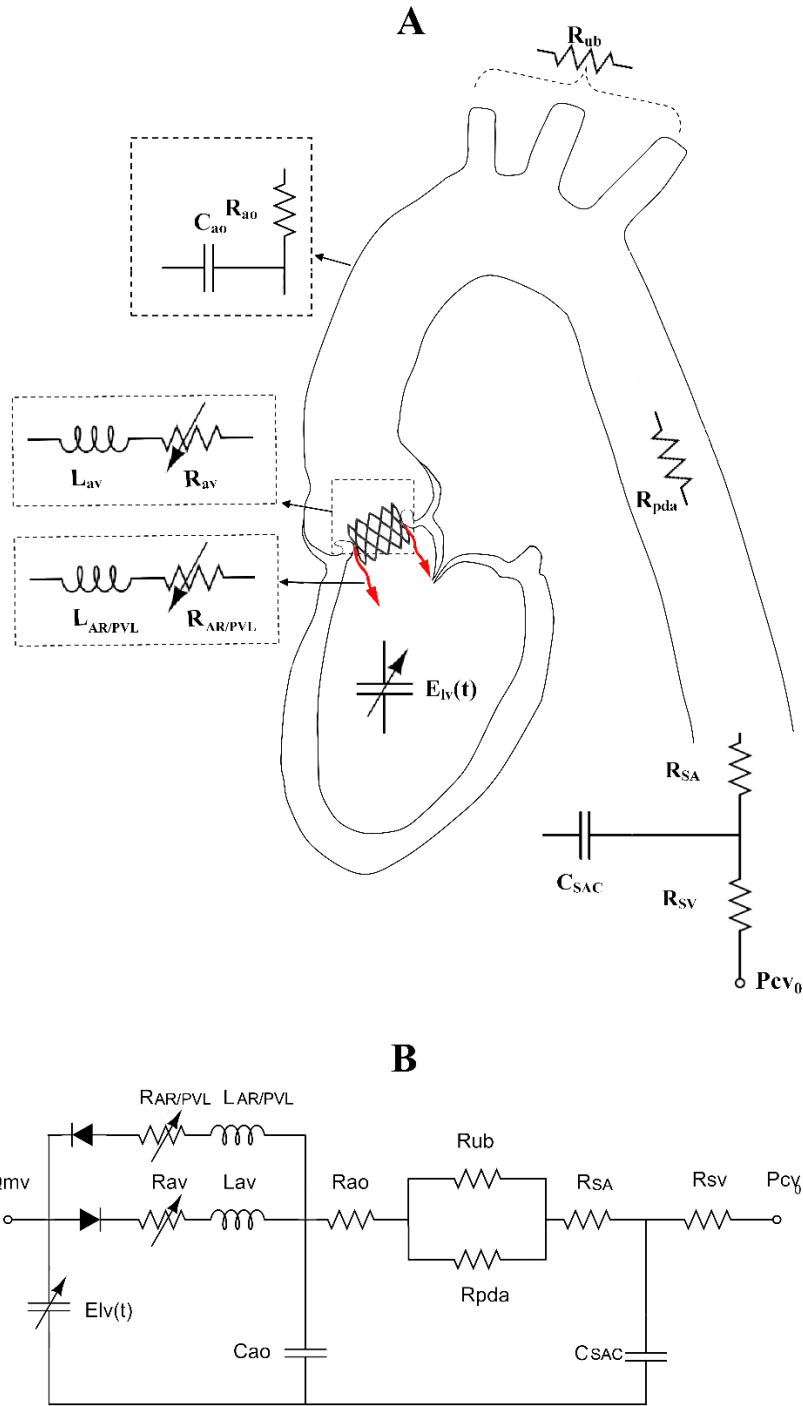


Figure 3-1: Schematic diagrams: a) schematic representation of the lumped parameter model used to simulate aortic stenosis with/without aortic regurgitation and transcatheter aortic valve with/without paravalvular leak; b) electrical representation of the model. $E_{lv}(t)$: normalized time-varying elastance. R_{av} and $R_{AR/PVL}$ represent aortic valve stenosis resistance and aortic valve paravalvular leak or regurgitation resistance, respectively. L_{av} and $L_{AR/PVL}$ represent aortic valve stenosis inductance and aortic valve paravalvular leak or regurgitation inductance, respectively. See Table (3-1) for details.

3.2.1. Heart-Arterial Model

The left ventricle is modeled using the concept of time-varying elastance (Suga et al., 1973):

$$E(t) = \frac{P_{LV}(t)}{V(t) - V_0} \quad (1)$$

Where $P_{LV}(t)$, $V(t)$ and V_0 are the LV pressure, the LV volume and the unloaded volume, respectively. The amplitude of $E(t)$ is normalized with respect to maximal elastance E_{max} , giving $E_N(t_N) = E(t)/E_{max}$. Time is also normalized with respect to the time to attain peak elastance, T_{Emax} ($t_N = t/T_{Emax}$). It has been shown that normalized time-varying elastance curves $E_N(t_N)$ have similar shapes in normal human hearts with various inotropic situations or for diseased human hearts (Senzaki et al., 1996; Suga et al., 1973).

$$E_{max} E_N(t/T_{Emax}) = \frac{P_{LV}(t)}{V(t) - V_0} \quad (2)$$

3.2.2. Aortic Stenosis Model

The following formulation has been used to model instantaneous net pressure gradient across the stenotic aortic valve (TPG_{net}) (Benevento et al., 2015; Garcia et al., 2005b; Keshavarz-Motamed et al., 2014a, 2011):

$$TPG_{net} = \frac{2\pi\rho}{\sqrt{E_L Co}} \frac{\partial Q}{\partial t} + \frac{\rho}{2 E_L Co^2} Q^2 \quad (3)$$

$$E_L Co_{AS} = \frac{(EOA)A}{A - EOA} \quad (4)$$

where $E_L Co$, EOA , A , ρ and Q are the valvular energy loss coefficient, valve effective orifice area, ascending aorta cross sectional area, the fluid density and the transvalvular flow rate, respectively.

3.2.3. Aortic Regurgitation Model

Aortic regurgitation and PVL were modeled following the same approach used for modelling aortic stenosis, except that the pressure difference (AR_TPG_{net}) controlling the regurgitant flow (Q_{AR}) is the difference between aortic pressure and LV pressure during diastole. Furthermore, the EOA used corresponds to a regurgitant orifice area (REOA) and the energy loss coefficient (AR_E_LCo) is computed using the REOA and left ventricle outflow tract (LVOT) area.

$$AR_TPG_{net} = \frac{2\pi\rho}{\sqrt{AR_E_LCo}} \frac{\partial Q_{AR}}{\partial t} + \frac{\rho}{2 AR_E_LCo^2} Q_{AR}^2 \quad (5)$$

$$AR_E_LCo = \frac{(REOA)A_{LVOT}}{A_{LVOT} - REOA} \quad (6)$$

This approach has shown a very good consistency with clinical guidelines (Lancellotti et al., 2010), i.e., the range of REOA corresponds very well to the expected ranges in terms of regurgitant fraction (R_f), the ratio of backward stroke volume to forward stroke volume.

3.2.4. Simulated conditions

LV stroke work was computed under the following conditions:

Pre-TAVR. Four different severe aortic stenosis with valve EOAs of 0.4, 0.6, 0.8 and 1.0 cm² have been tested. These values are consistent with *in vivo* data of patients who underwent TAVR (Ali et al., 2015; Caballero et al., 2015). For each case of severe aortic stenosis different levels of aortic regurgitation have been simulated: Trace/mild (Regurgitant fraction (R_f) < 15%); mild-to-moderate (15% < R_f < 30%); moderate (30% < R_f < 40%) and moderate-to-severe (40% < R_f < 50%). These levels of chronic aortic regurgitation have already been reported in patients with severe aortic stenosis who underwent TAVR (Amat-Santos et al., 2014; Ewe et al., 2015).

The classification used here is consistent with clinical practice guidelines as well (Bonow et al., 2006; Lancellotti et al., 2010; Lerakis et al., 2013; Pibarot et al., 2015; Zoghbi et al., 2009).

Post-TAVR. Three different valve EOAs of 1.30, 1.60 and 1.90 cm² have been tested. These values are consistent within the range of *in vivo* data of patients who underwent TAVR (Clavel et al., 2011). The same levels and classification used for aortic regurgitation were used for PVL following TAVR, which is consistent with the existing literature (Lerakis et al., 2013; Pibarot et al., 2015).

Table 3-1: Summary of the cardiovascular parameters used to simulate all cases.

Description	Abbreviation	Value
Ventricular parameters		
Unstressed volume	V ₀	-15 mL
Maximal elastance	E _{max}	Adjusted for stroke a net stroke volume of 70 mL
Time to maximal elastance	T _{E_{max}}	0.24 s
Aortic valve parameters		
Effective orifice area	EOA	Modified for each case
Regurgitant orifice area	REOA	Modified for each case
Aortic cross-sectional area	A _{ao}	8 cm ²
Systemic circulation parameters		
Aortic systolic pressure	P _s	120 mmHg
Aortic diastolic pressure	P _d	Changes with regurgitant fraction. Baseline value 80 mmHg
Aortic compliance	C _{ao}	0.5 mL/mmHg
Systemic vein resistance	R _{SV}	0.05 mmHg.s.mL ⁻¹
Systemic arteries and veins compliance	C _{SAC}	2 mL/mmHg
Systemic arteries resistance (including arteries, arterioles and capillaries)	R _{SA}	Initial value: 0.8 mmHg.s.mL ⁻¹ Adjusted for an aortic systolic pressure of 120 mmHg
Upper body resistance	R _{ub}	Adjusted to have 15% of total flow rate (McDonald, 1974)
Proximal descending aorta resistance	R _{pda}	0.05 mmHg.s.mL ⁻¹
Output condition		
Central venous pressure	P _{CV0}	4 mmHg
Input condition		
Mitral valve mean flow rate	Q _{mv}	
Other		
Constant blood density		1050 kg/m ³
Heart rate	HR	70 bpm
Duration of cardiac cycle	T	857 ms

Other hemodynamic conditions including heart rate, systolic pressure, baseline diastolic pressure and baseline stroke volume are listed in Table (3-1). Overall, a total of 128 conditions have been tested numerically.

3.2.5. Transcatheter aortic valve replacement performance index (TAVR PI)

In this work, we evaluated the performance of transcatheter aortic valve implantation as the relative variation in LV stroke work before and after TAVR. The first approach uses the $\int P dv$ to compute LV stroke work (the area inside the generated p-v loops):

$$\text{Performance Index (PI)} = 100 \times \frac{LVS_{W_{AS}} - LVS_{W_{TAV}}}{LVS_{W_{AS}}} \quad (7)$$

Where $LVS_{W_{AS}}$ represents LV stroke work developed in the presence of the severe aortic stenosis (before TAVR) and $LVS_{W_{TAV}}$ is LV stroke work developed by the LV after TAVR. Note that the performance index can be negative if TAVR led to an increase in LV stroke work compared to pre-TAVR conditions. For example, a PI of 80% means that TAVR successfully reduced LV work load due to severe AS by 80%. While a PI of -20% means that TAVR led to an increase in LV work load compared to the initial work load induced by the severe AS by 20%.

The second approach, uses the variation of an estimate for LV stroke work. This is because the true value for LV stroke work cannot be determined non-invasively. The estimated LV stroke work is computed as the product of the LV forward stroke volume and peak LV systolic pressure. Peak LV systolic pressure is estimated then as the sum of systolic aortic pressure and mean transvalvular pressure gradient:

$$\text{Estimated Performance Index (PI)} = 100 \times \frac{SV_{AS}(P_s + \overline{TPG}_{AS}) - SV_{TAV}(P_s + \overline{TPG}_{TAV})}{SV_{AS}(P_s + \overline{TPG}_{AS})} \quad (8)$$

Where, SV_{AS} is the forward stroke volume pre-TAVR; \overline{TPG}_{AS} is the mean transvalvular pressure gradient pre-TAVR; SV_{TAV} is the forward stroke volume post-TAVR (that can be different from pre-TAVR conditions depending on the severity of paravalvular leak) and \overline{TPG}_{TAV} is the mean transvalvular pressure gradient post-TAVR. This estimation of peak LV pressure has already been used by our group for the evaluation of valvular-arterial impedance in the context of patients with aortic stenosis and systemic hypertension (Briand et al., 2005).

Computational algorithm. Details of the computational algorithm are presented in appendix A.

3.3. Result

Figure (3-2) shows typical flow and pressure waveforms obtained using our model for three different configurations: 1) aortic stenosis with EOA of 0.8 cm^2 , with no aortic regurgitation ($R_f=0\%$) (Figure 3-2-a); 2) an implanted TAV with an EOA of 1.60 cm^2 and no paravalvular leak ($R_f=0\%$) (Figure 3-2-b); 3) the same implanted TAV with EOA of 1.60 cm^2 but with mild-to-moderate paravalvular leak ($R_f=17\%$) (Figure 3-2-c). Figure (3-2-d) shows the pressure-volume loops resulting from the above cases.

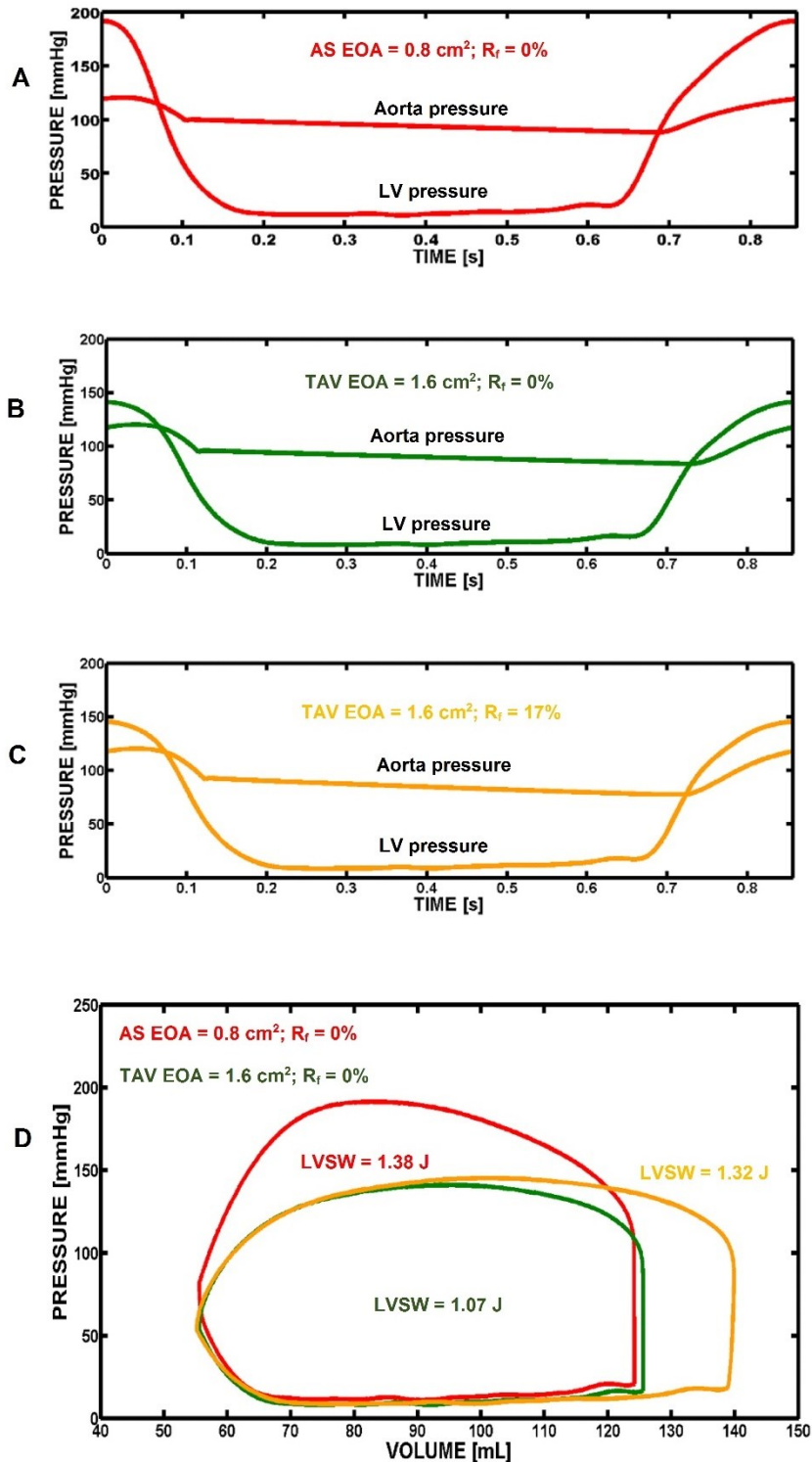


Figure 3-2: Examples of flow, pressure and left ventricle stroke work waveforms obtained using the model for; a) aortic stenosis with EOA of 0.80 cm², with no aortic regurgitation (R_f=0%); b) transcatheter aortic valve with an EOA of 1.60 cm² and no paravalvular leak (R_f=0%); c) transcatheter aortic valve with EOA of 1.60 cm² but with mild-to-moderate paravalvular leak (R_f=17%); d) corresponding pressure-volume loops and left ventricle stroke work (LVSW).

TAV in both cases has successfully led to a reduction in mean transvalvular pressure gradient from 73 mmHg to 18 mmHg (with no PVL) and to 23 mmHg (with moderate-to-severe PVL). However, PVL led to a significant increase in volume overload by an increase in forward stroke volume from 70 mL to 86 mL. As a result, LV stroke work after TAV in the case of mild-to-moderate PVL was not significantly different from LV stroke work prior to TAVR (1.32 vs 1.38 J). The TAV without PVL led to a significantly lower LV stroke volume of 1.07 J. This example illustrates a case where the increase in volume overload, due to PVL, counter balances the beneficial reduction in pressure overload.

Table (3-2) displays the difference in LV stroke work for several possible configurations that can exist prior to TAVR and post TAVR in terms of EOAs and severities of aortic regurgitation or PVL (displayed as a color code). The values in Table (3-2) represent the performance index as computed using equation (7). In the majority of simulated combinations (76%), TAVR led to a significant decrease in LV stroke work ($p < 0.05$). However, in 15% of cases, TAVR did not lead to a significant increase in LV stroke work ($p > 0.05$) and in 9% of cases, LV stroke work following TAVR was significantly higher ($p > 0.05$) than the LV stroke work pre-TAVR. Interestingly, most of the cases where TAVR was not successful in reducing total LV work overload correspond to pre-TAVR conditions with trace/mild or mild-to-moderate chronic aortic regurgitation and post-TAVR conditions with at least mild-to-moderate PVL.

When investigating the performance index (PI) as computed by equation (7), it appears that TAVR can lead a reduction in LV stroke work up to $-84 \pm 2\%$ when a large TAV (EOA = 1.90 cm^2) with no PVL is implanted in a very severe AS (EOA = 0.40 cm^2) with initial concomitant moderate-to-severe aortic valve regurgitation. From another side, TAVR significantly underperforms if a small TAV (EOA = 1.30 cm^2) with moderate-to-severe PVL is implanted in

Table 3-2: Differences in left ventricle stroke work for different configurations pre and post transcatheter aortic valve replacement. The values in the table represent the performance index as computed by (Eq. 7).

		TAV EOA = 1.30 cm ²				TAV EOA = 1.60 cm ²				TAV EOA = 1.90 cm ²			
Regurgitation		Trace/ mild	Mild/ Moderate	Moderate	Moderate / Severe	Trace/ mild	Mild/ Moderate	Moderate	Moderate/ Severe	Trace/ mild	Mild/ Moderate	Moderate	Moderate/ Severe
AS EOA = 0.4 cm ²	Trace/mild	-51±6%	-37±8%	-21±9%	-1±12%	-54±6%	-42±7%	-28±8%	-10±11%	-56±6%	-45±7%	-32±8%	-17±10%
	Mild/ Moderate	-66±5%	-57±7%	-46±8%	-31±10%	-69±5%	-60±6%	-50±7%	-38±9%	-70±5%	-62±6%	-53±7%	-43±8%
	Moderate	-77±3%	-70±4%	-62±5%	-52±6%	-78±3%	-72±4%	-66±4%	-57±5%	-79±3%	-74±4%	-68±4%	-60±5%
	Moderate/ Severe	-82±2%	-77±3%	-71±3%	-63±4%	-83±2%	-79±2%	-73±3%	-67±3%	-84±2%	-80±2%	-75±2%	-69±3%
AS EOA = 0.6 cm ²	Trace/mild	-32±8%	-10±10%	+10±12%	+39±16%	-36±7%	-19±10%	-0±11%	+25±14%	-39±7%	-23±9%	-6±10%	+16±13%
	Mild/ Moderate	-50±6%	-36±8%	-20±10%	+1±12%	-54±6%	-41±8%	-37±9%	-9±11%	-55±6%	-44±7%	-31±8%	-15±10%
	Moderate	-64±5%	-54±6%	-42±7%	-26±9%	-66±4%	-57±5%	-47±6%	-33±8%	-68±4%	-59±5%	-50±6%	-38±7%
	Moderate/ Severe	-74±4%	-66±4%	-57±5%	-46±7%	-75±3%	-69±4%	-61±5%	-51±6%	-76±3%	-70±4%	-63±4%	-55±6%
AS EOA = 0.8 cm ²	Trace/mild	-19±9%	+4±12%	+31±14%	+65±18%	-24±8%	-4±11%	+20±12%	+49±16%	-27±8%	-8±10%	+13±11%	+38±14%
	Mild/ Moderate	-39±7%	-22±9%	-2±11%	+24±14%	-43±7%	-28±9%	-10±10%	+12±13%	-45±6%	-31±8%	-16±9%	-4±12%
	Moderate	-54±5%	-40±7%	-25±7%	-5±10%	-57±5%	-45±6%	-31±7%	-14±9%	-58±4%	-48±6%	-35±6%	-21±8%
	Moderate/ Severe	-66±5%	-56±6%	-45±7%	-30±9%	-68±4%	-59±6%	-49±7%	-37±8%	-69±4%	-61±5%	-53±6%	-42±8%
AS EOA = 1.0 cm ²	Trace/mild	-10±10%	+16±13%	+46±15%	+84±20%	-15±19%	+7±12%	+34±13%	+66±17%	-18±19%	+2±11%	+26±12%	+54±16%
	Mild/ Moderate	-31±8%	-11±10%	+12±12%	+41±15%	-35±7%	-18±9%	+2±10%	+27±14%	-38±7%	-22±9%	-4±10%	+18±12%
	Moderate	-46±6%	-31±7%	-13±8%	+10±11%	-50±5%	-36±10%	-21±7%	-1±10%	-52±5%	-39±6%	-25±7%	-8±9%
	Moderate/ Severe	-59±5%	-47±7%	-34±8%	-16±10%	-62±5%	-51±6%	-39±7%	-24±9%	-63±5%	-54±6%	-43±6%	-30±8%
		LV stroke work following TAVR is significantly lower than LV stroke work before TAVR (p < 0.05)											
		No significant difference between LV stroke work before and following TAVR (p > 0.05)											
		LV stroke work following TAVR is significantly higher than LV stroke work before TAVR (p < 0.05)											

pure borderline severe AS (EOA = 1.00 cm²) and can lead to a performance index, or a relative increase in LV stroke work, of +84±20%.

Figure (3-3) shows the correlation between the computed values of the performance index using equation (7) and the estimated values using equation (8). There was an excellent correlation and concordance between the computed and estimated values (R=0.997, SEE=2.46%).

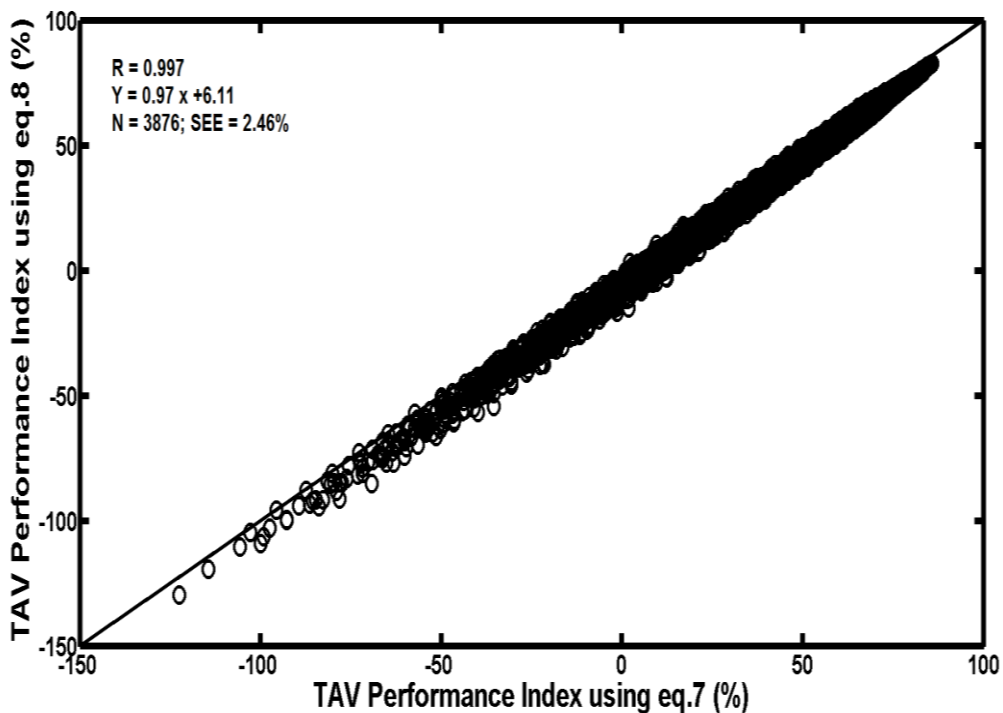


Figure 3-3: Correlation between the Performance Index (PI) computed from (Eq. 7) and estimated using equation (8). SEE: standard error of estimate.

3.4. Discussion

The key findings of this study are: 1) Paravalvular leak following TAVR have a significant negative impact on LV overload mainly when a TAV is implanted in an AS with trace/mild aortic regurgitation; 2) The variation in LV overload following TAVR can be well estimated non-invasively using the TAV performance index.

Since the first in-man implantation of a transcatheter aortic valve by Cribier et al. (2002), TAVR created a paradigm shift in the way severe symptomatic aortic stenosis is treated. Several studies have clearly demonstrated the feasibility and advantages of TAVR in patients with high operative risks who are denied surgical aortic valve replacement (Leon et al., 2010; Smith et al., 2011). TAVR led to immediate short term benefits by lowering transvalvular pressures gradients and an improvement in diastolic function (Clavel et al., 2009; Gonçalves et al., 2011).

However, it has been documented that a proportion of patients did not benefit from TAVR in terms of prognosis or symptoms despite a clear improvement in hemodynamic conditions (increase in valve EOA and decrease in transvalvular pressure gradients) (Buellesfeld et al., 2011; Gotzmann et al., 2011b). This was mainly attributed to the presence of paravalvular leak following TAVR (Gotzmann et al., 2011a, 2011b). Several studies have shown that PVL moderate/severe is an independent predictor of in-hospital death 30 days and 1 year mortality and worsening of LV filling patterns (Abdel-Wahab et al., 2011; Tamburino et al., 2011; Caballero et al., 2015). Some studies have even shown that mild to moderate PVL can lead to limited outcome following TAVR (Athappan et al., 2013; Hayashida et al., 2012). Both anatomical and procedural aspects can lead to PVL, the most significant however, are the circularity of the aortic annulus, the level and location of the calcification of aortic valve leaflets and an inadequate positioning of the TAV (Ali et al., 2015).

The originality of this study is that it does not evaluate PVL and TAVR outcome in terms of LV overload in an absolute frame of reference but relative to pre-TAVR pressure and volume overloads. This allowed the definition of different combinations pre-TAVR *vs.* post-TAVR that theoretically will lead to less favorable outcomes. The results show that critical conditions in terms of LV stroke work occur when PVLs are imposed on a LV that was mainly subjected, pre-TAVR,

to a pressure load (severe AS and trace/mild regurgitation). In fact, when implanted in a pure severe aortic stenosis (trace/mild aortic regurgitation), significant PVL (mild-to-moderate or moderate-to-severe) contribute to an immediate switching from a pressure overload to a volume overload. This can contribute to clarifying the “intriguing association” between mild PVL and mortality (Pibarot et al., 2015). As a consequence, patients with pure aortic stenosis (trace/mild regurgitation) should receive more attention when selecting the TAV to be implanted and implantation procedure in order to minimize PVL.

Evaluation of changes in LV overload using TAV performance index. In this study, we introduced a TAV performance index that represents the relative changes in LV load (including pressure and volume loads) before and after TAVR. Interestingly, equation (7) can be rewritten under another form:

$$\begin{aligned}
 \text{Estimated Performance Index (PI)} &= 100 \times \left\{ 1 - \overbrace{\frac{SV_{TAV}}{SV_{AS}} \times \frac{(P_s + \overline{TPG}_{TAV})}{(P_s + \overline{TPG}_{AS})}}^{\text{LV load ratio}} \right\} \\
 &= 100 \times \left\{ 1 - \overbrace{\frac{(1 - R_{f_{AS}})}{(1 - R_{f_{TAV}})} \times \frac{(P_s + \overline{TPG}_{TAV})}{(P_s + \overline{TPG}_{AS})}}^{\text{LV load ratio}} \right\}
 \end{aligned} \tag{9}$$

Where $R_{f_{AS}}$ and $R_{f_{TAV}}$ represent the regurgitant fraction (before and after TAVR, respectively (see appendix A for details). It appears then that a high TAV performance index is achieved for very small LV stroke work load ratios (ratio between LV load post-TAVR over LV load pre-TAVR). Then, if PVL severity post-TAVR is more significant than the pre-existing regurgitation severity pre-TAVR (volume load ratio > 1) then for TAVR to be beneficial it has to lead to a substantial decrease in pressure load ratio (reduction in mean transvalvular pressure gradient). This explains why a larger number of adverse conditions following TAVR are obtained in this study when a TAV with an EOA of 1.30 cm^2 was implanted in a severe aortic stenosis of

1.00 cm²: the reduction in pressure load ratio was simply not sufficient to counterbalance the increase in volume load ratio due to more than mild PVL. Finally, note that the performance index as defined can also be used with other procedures that may result in aortic regurgitation like balloon valvuloplasty (Cribier et al., 1987) or surgical valve replacement, although aortic regurgitation is now occasionally occurring.

3.5. Limitation

In this work the mathematical modeling did not incorporate potentially unrecoverable myocardial remodeling and contractile dysfunction. This obviously could enter in play in real life situations that need to be accounted for in future studies. Depressed myocardial function may in part profile a lower left ventricular to aortic pressure gradient prior to valve replacement. In such cases, PVL may be deleterious to cardiac work load even in the low grade secondary R_f situations.

On the other hand, beyond the degree of the PVL in terms of effective cardiac output, the interplay between a lower aortic diastolic pressure secondary to the TAVR and the effective coronary artery flow need to be taken into consideration, especially in the elderly patient with coronary artery lesions and atherosclerosis.

3.6. Conclusion

Transcatheter aortic valve replacement is a viable solution for symptomatic patients with severe aortic stenosis who are denied surgical aortic valve replacement because of elevated operative risks. However, the beneficial results might be suboptimal due to the presence of paravalvular leak. This study shows that patients with severe aortic stenosis and trace/mild aortic regurgitation are those that would benefit the least from transcatheter aortic valve replacement with subsequent paravalvular leak, despite a reduction in aortic pressure gradients. This population

should be considered with care when planning for transcatheter aortic valve replacement. Finally, a new non-invasive parameter has been introduced to estimate the performance of transcatheter aortic valve replacement with respect to reducing left ventricle work overload.

CHAPTER 4: Fluid Dynamics of Transcatheter Aortic Valve in the Presence of Paravalvular Leak

Article 2

Azadeh Saeedi¹, Zahra Keshavarz-Motamed^{1, 2, 3}, Georgios Lygouris⁴, Philippe Pibarot²,
Lyes Kadem¹

1. Laboratory of Cardiovascular Fluid Dynamics, Mechanical and Industrial Engineering Department, Concordia University, Montréal, Québec, Canada.
2. Quebec Heart and Lung Institute, Laval University, Québec, Québec, Canada.
3. Institute for Medical Engineering and Science, Massachusetts Institute of Technology, Boston, Massachusetts, USA.
4. Einstein Medical Center, Philadelphia, Pennsylvania, USA

Computer Methods in Biomechanics and Biomedical Engineering Journal, Submitted, May 2015

Abstract

Transcatheter aortic valve replacement has emerged as an alternative option in high surgical risk patients with severe symptomatic aortic stenosis. However, paravalvular leak still represents a significant complication. This study aims at using 3D numerical simulations to investigate the effect of paravalvular leak on diastolic flow-field characteristics following transcatheter aortic valve replacement.

We show that paravalvular leak leads to significant disturbances in blood flow characterized by high speed jets, small and large scale coherent structures and markedly elevated shear stress on both sides of the implanted aortic leaflets. Such unfavorable flow configuration may promote a more rapid degeneration of the transcatheter valve leaflets.

4.1. Introduction

Transcatheter aortic valve replacement (TAVR) has emerged as the preferred therapeutic intervention for inoperable patients with severe symptomatic aortic stenosis and as an alternative option in high surgical risk individuals (Leon et al., 2010; Smith et al., 2011). However, data from multiple registries and trials with different valve designs have shown that TAVR is associated with various complications in approximately one third of cases (Fishbein et al., 2013).

One of the major TAVR related complications is paravalvular leak (PVL) (Dvir et al., 2013). The prevalence of PVL varies among different studies and can range from 7% to 70% for mild PVL and 0% to 24% for more a than moderate PVL (Pibarot et al., 2015). PVL leads to volume overload and increased stroke work of the stiff, non-compliant left ventricle (Bekeredjian and Grayburn, 2005). As a consequence, PVL has been shown to be an independent predictor of short-term and long-term mortality following TAVR (Moat et al. 2011; Tamburino et al. 2011; Abdel-Wahab et al. 2011; Kodali et al. 2012).

Despite its clinical significance, only few studies addressed specifically the hemodynamic effect of PVL after TAVR (Genereux et al. 2013). From a fluid dynamics point of view, different numerical studies have investigated flow through different types of transcatheter valves (Dwyer et al. 2009; Quail and Taylor 2013; Sirois et al. 2011). However, little is known regarding flow patterns induced by PVL following TAVR.

The objective of this numerical study was to investigate the effect of PVL on diastolic flow-field characteristics using 3D numerical simulations. The results of this study will be of interest for transcatheter valve design and for the follow up of patients who have already underwent TAVR.

4.2. Method

4.2.1. Geometrical Model

Figure (4-1) shows the schematic diagram of the model used in this study. The anatomical model includes the left ventricular outflow tract (LVOT), the sinuses of Valsalva, the aortic root and the proximal ascending aorta (Keshavarz-Motamed et al., 2013) (Figure 4-1-a). An Edwards SAPIEN 26 mm transcatheter aortic valve was simulated. It consists of a trileaflet bovine pericardial tissue valve embedded on a stainless steel metallic stent frame and within a tissue skirt (Figure 4-1-b) (Auricchio et al., 2014). See appendix B, figure (B-1) for more details.

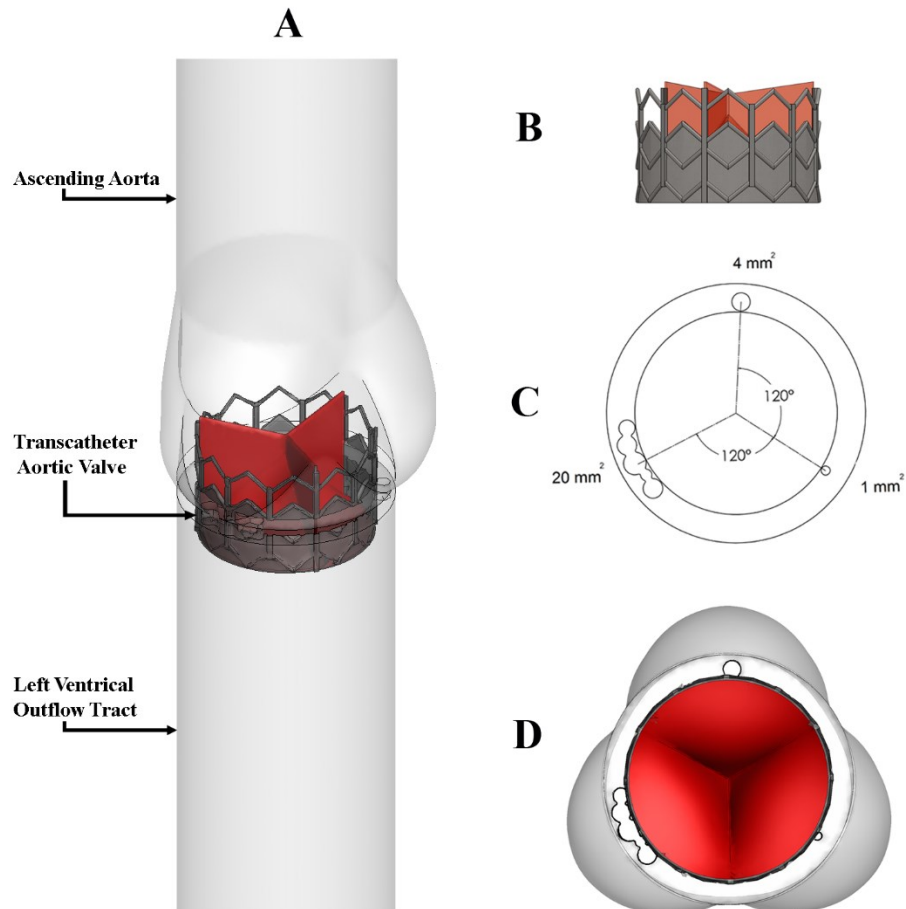


Figure 4-1: Geometry considered for numerical simulations. (a) Simulation domain; (b) Transcatheter aortic valve; (c) Paravalvular leak orifice positions; and (d) Top view of the simulation domain.

PVL was modeled by creating three different orifices at the level of the aortic root (with areas of 1 mm², 4 mm² and 20 mm², respectively) (Fig. 1c and 1d). The size and the shape of the orifices correspond to the smallest, the median and the largest regurgitant orifice areas (ROA) obtained *in vivo* by Hahn et al. (Hahn et al., 2013). Both regular and irregular PVL orifice shapes were considered. All were located in the middle of the cusps (see Fig. 1c), where a high concentration of calcium is usually found in severe aortic stenosis (Sinning et al., 2013).

4.2.2. Numerical Model

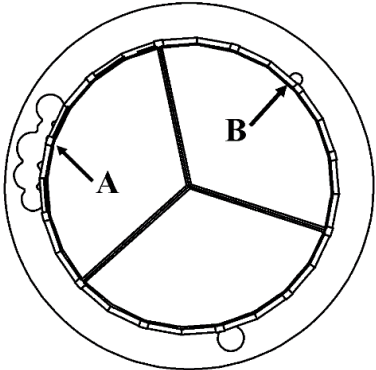
PVL can lead to regions of disturbed flow both upstream and downstream of the transcatheter aortic valve. This in turn generates turbulence during both parts of the cardiac cycle (i.e., $Re > 1000$) (Ryval et al. 2004). The $k-\omega$ -SST model is well adapted to simulate low- Re internal flows ($Re < 10,000$) and was therefore used in our study. This model has also been shown to give a good overall representation of both steady and pulsatile flow and has been validated in blood flow studies where both laminar/transitional and turbulent flow regimes coexist (Ghalichi et al. 1998; Ryval et al. 2004; Keshavarz-Motamed & Kadem 2011; Keshavarz-Motamed et al. 2013).

The model was meshed using tetrahedral elements (Appendix B, figure (B-2)). The grid was also clustered at the valve region and additional care was taken to maintain $y^+ < 1$ for high quality wall treatment by $k-\omega$ -SST model for low- Re flows. Mesh independency was evaluated based on the results of both velocity magnitude and valve wall shear stress (WSS). A total number of 3,794,696 tetrahedral elements were used for the final simulations. The solution marched in time with a time step of 0.001 s to satisfy time independency. The convergence was obtained when all residuals reached a value lower than 10^{-5} . Computations were performed using commercially available computational fluid dynamics software (ANSYS Fluent v14.0).

CFD uncertainty was analyzed considering wall shear stress values as output parameter (Table 4-1) (Celik et al. 2008). The parameters, ϕ , ϕ_{ext} , e_a , e_{ext} and GCI_{fine} represent the wall shear stress, the extrapolated wall shear stress value, the approximate relative error, the extrapolated relative error and the fine-grid convergence index, respectively. For the analysis, WSS was determined at two locations on the valve leaflets close to the smallest and largest regurgitant orifices (see Points A and B in Table 4-1). The computations indicate that the numerical uncertainties on wall shear stress are 2.69% and 5.83%.

Table 4-1: Calculation of discretization errors for the simulation at two regions: A and B. ϕ (wall shear stress), ϕ_{ext} (the extrapolated wall shear stress value), e_a (approximate relative error), e_{ext} (extrapolated relative error) and GCI_{fine} (fine-grid convergence index).

	Point A	Point B
ϕ_1 (Pa)	0.0708179	0.0043424
ϕ_2 (Pa)	0.071053	0.004502
r_{21}	1.4	1.4
ϕ_{ext}^{21} (Pa)	0.071863	0.004606
e_a^{21}	0.33%	3.67%
e_{ext}^{21}	1.45%	5.72%
GCI_{fine}^{21}	2.69%	5.83%



Additionally, to account for the temporal oscillations in wall shear stress the oscillatory shear index (OSI) was computed according to the following equation (Ku et al., 1985):

$$OSI = \frac{1}{2} \left[1 - \frac{\int_0^T \tau dt}{\int_0^T |\tau| dt} \right] \quad (10)$$

Where T and τ are the duration of diastole cycle and total instantaneous wall shear stress, respectively. OSI can reach a maximum value of 0.5 in regions with high oscillating shear stress that are prone to atherosclerosis.

4.2.3. Boundary Conditions and Model Properties

Blood was assumed to be a Newtonian and incompressible fluid with dynamic viscosity of 0.0035 Pa.s and a density of 1050 kg/m³, a valid assumption for flows in large cavities and arteries (Fung 1981; Kuan & Espino 2014; Xenos et al. 2013; Gramigna et al. 2014). The arterial wall was treated as solid and rigid. This can be justified by: (1) patients with severe aortic stenosis who can be candidate for TAVR have reduced arterial compliance (Briand et al., 2005); (2) Jin et al. (2003) showed that rigid wall assumption for the aorta is realistic. Their results showed that the overall behavior for wall shear stress at each point is similar for the rigid and elastic walls with average root mean squared error of 1.23%; (3) Keshavarz-Motamed et al. (2013) performed joint experimental magnetic resonance imaging (MRI) and numerical investigations for different models of the aorta, including normal aorta. There was a good agreement between numerical simulations on rigid aortas and MRI velocity measurements on elastic aortas.

This study focuses on diastole, the filling phase of the left ventricle, during which PVL occurs. Therefore, the aortic valve leaflets were modeled to be rigidly closed. A non-permeable and no-slip boundary condition was applied at the rigid walls. A velocity waveform was imposed at the ascending aorta (Figure 4-2) and an outflow boundary condition was applied at the exit. The diastolic velocity waveform applied at the inlet of the model was obtained from phase contrast magnetic resonance imaging measurements performed by Hayek et al. (2014) in a patient with PVL. This corresponded to maximum diastolic Reynolds numbers of 934 at the inlet and 6300 in the PVL regions. The computed regurgitant fraction was 35%. As a consequence, the simulations

deal with a mild/moderate (grade II) PVL. This PVL grade was frequently observed in patients who underwent TAVR using the SAPIEN valve (30% of patients) or the newest valve design SAPIEN XT valve (42% of patients) (Amat-Santos et al., 2015).

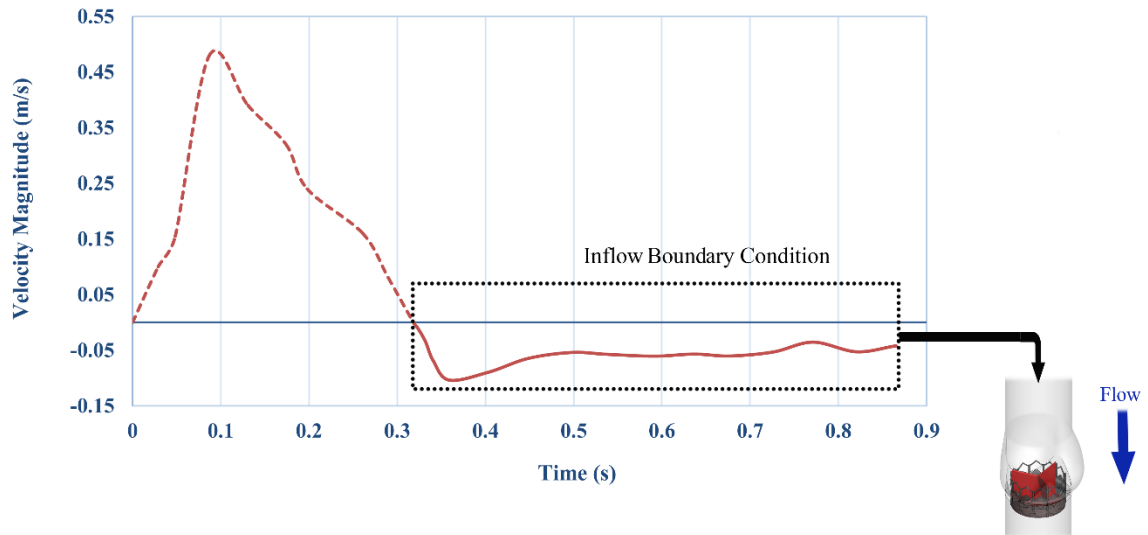


Figure 4-2: Velocity waveform used as inlet boundary condition for the numerical simulations based on CMR measurements of Hayek et al. 2014

4.3. Result

Figure (4-3) displays different 2D and 3D views of multiple iso-surfaces of velocity magnitude in three different instants during diastole: peak diastolic regurgitant flow (0.358 s), mid-diastolic regurgitant flow (0.590 s) and the end diastolic regurgitant flow (0.858 s). Three high speed jets were generated through the regurgitant orifices. The velocity of the jets rapidly increased during early diastole to reach a maximum velocity. At the peak of diastolic regurgitant flow, peak velocities were 4.13 m/s for the 20 mm² orifice, 3.18 m/s for the 4 mm² orifice and 2.33 m/s for the 1 mm² orifice. This is followed by a continuous decrease in orifice jet velocities as a result of the reduction in regurgitant flow during diastole.

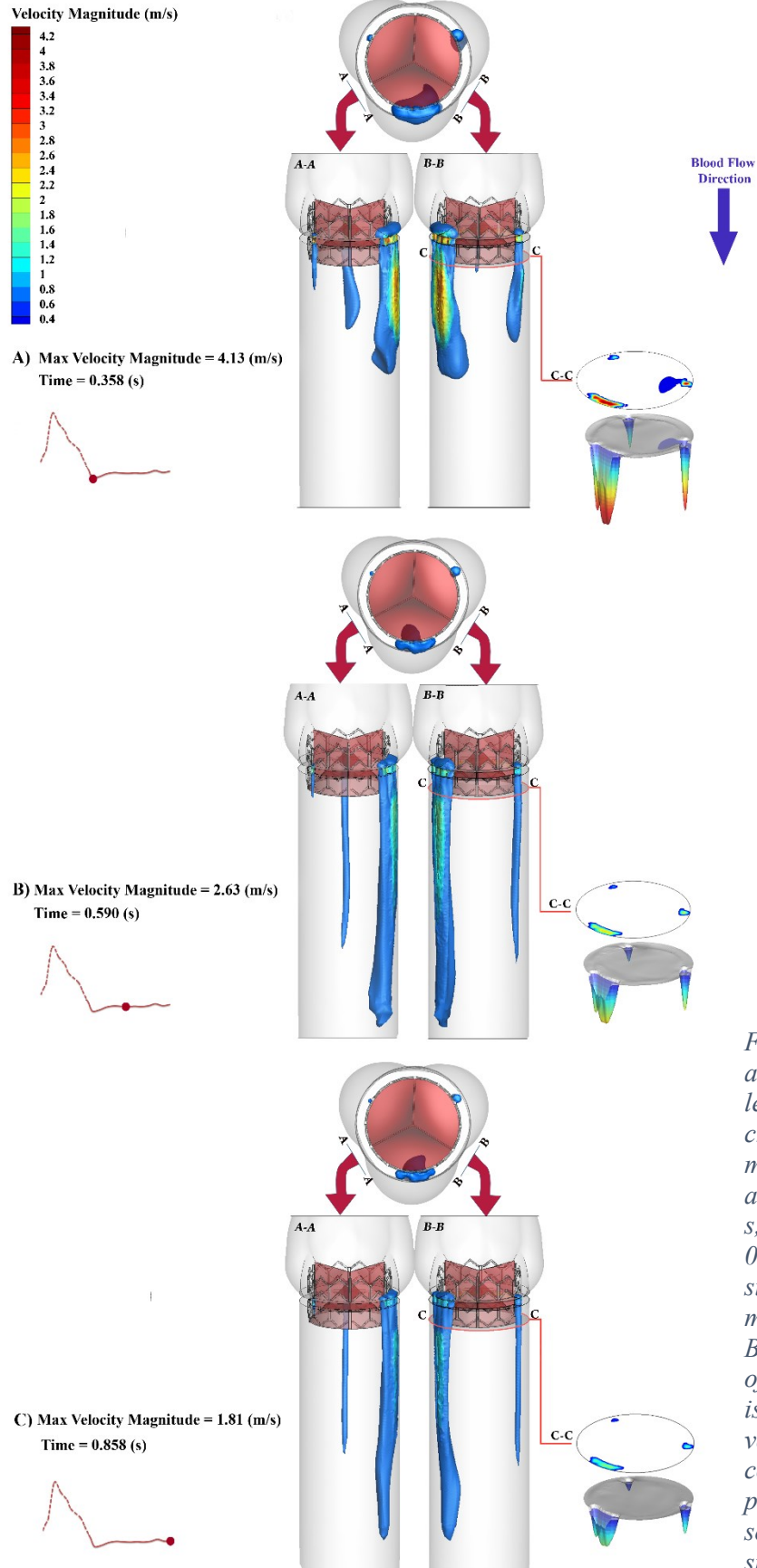


Figure 4-3: Different 2D and 3D views (top, right, left and a horizontal cross-section) of velocity magnitude iso-surfaces at three instants $t=0.358$ s, $t= 0.590$ s and $t= 0.858$ s; A-A) 3D left-side view of velocity magnitude iso-surfaces; B-B) 3D right-side view of velocity magnitude iso-surfaces; C-C) 3D velocity magnitude contours and their projections on the cross section just below the stent.

Figure (4-4) shows velocity magnitude contours and streamlines at two different longitudinal cross sections for the same instants as in Figure (4-3). The presence of three regurgitant orifices leads to an asymmetric flow in the proximal aorta and in the LVOT region. This asymmetry generates coherent structures in the flow field. In the ventricular side, at the peak of regurgitant flow, the high speed jets create large recirculation zones in the LVOT region. These coherent structures are rapidly convected downstream during diastole, leaving just a vortex structure just below the aortic valve leaflets (Panel B, Section EE). By the end of diastole, no major coherent structures are present in the LVOT region. In the proximal aortic side, at the peak of regurgitant flow (Panel A, Section EE), the asymmetry of regurgitant orifice positions leads to vortex shedding from the valve leaflet coaptation region. During the remaining diastole, the shedded vortices are trapped in the valve belly region.

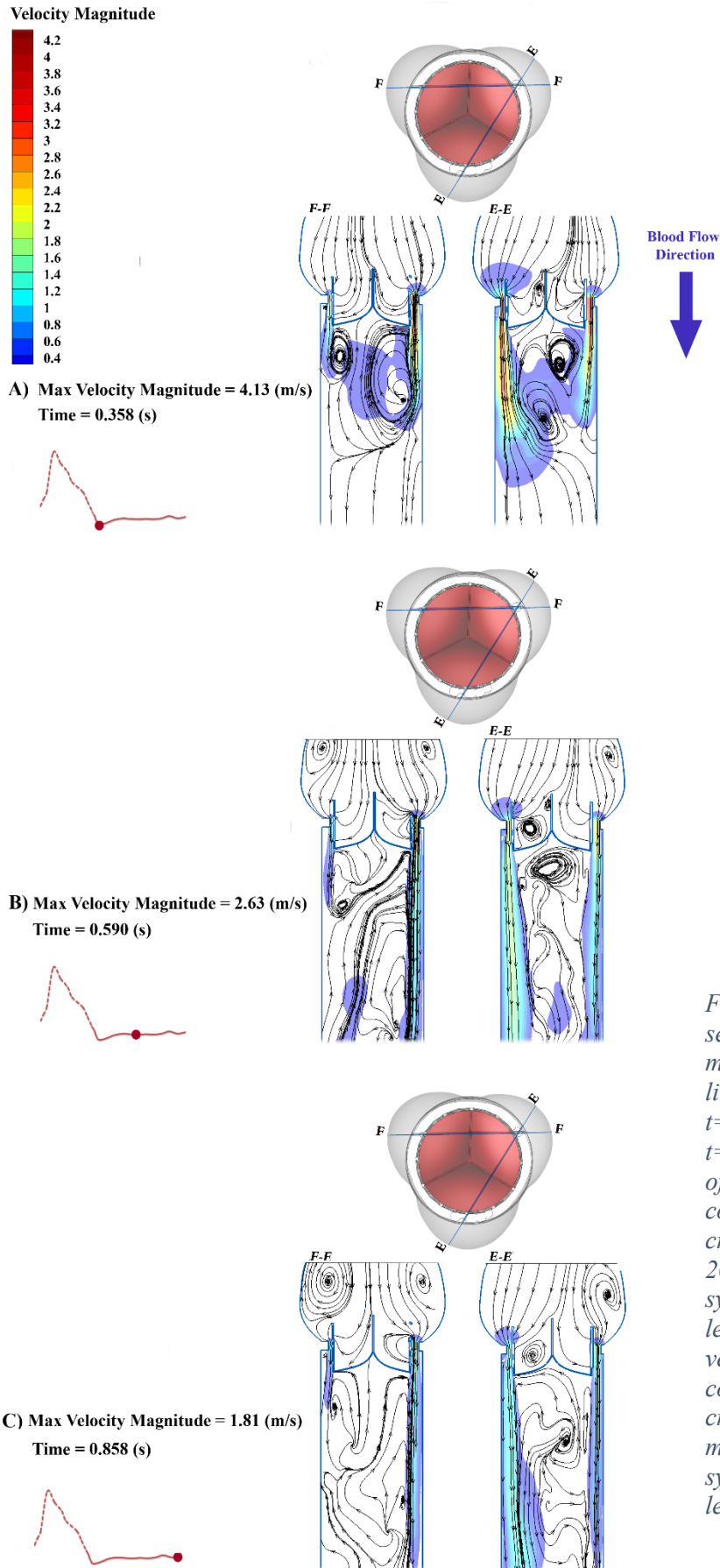


Figure 4-4: Two cross-sectional views of velocity magnitude and stream lines at three instants $t=0.358$ s, $t=0.590$ s and $t=0.858$ s; E-E) 2D view of velocity magnitude contours on a plane crossing both orifices of 20 mm² and 4 mm² with symmetrical view of two leaflets; F-F) 2D view of velocity magnitude contours on a plane crossing both orifices of 4 mm² and 1 mm² with symmetrical view of two leaflets.

Figure (4-5) displays the oscillatory shear index (OSI) at two different cross sections in the LVOT region {section (G-G) and (H-H)}. Section G-G is located just upstream of the valve stent. While section H-H is located 1 cm below the valve stent. Just below the stent, elevated OSI values, close to 0.5, can be found in the regions near the larger orifices (20 mm² and 4 mm²). Further below, OSI values significantly decrease for largest orifices while they increase for the smallest orifice 1 mm².

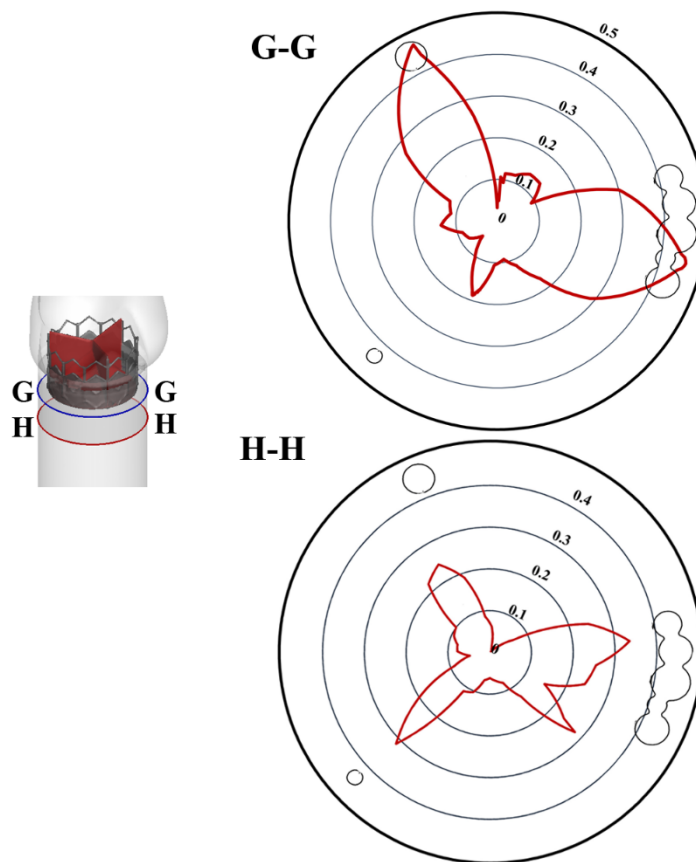


Figure 4-5: Oscillatory wall shear stress (OSI) on two different cross-sections in the LVOT. Section G-G is located just upstream of the valve stent and section H-H is located 1 cm below the valve stent.

Figure (4-6) displays WSS on both sides of the valve leaflets, aortic side (Panel A) and left ventricle side (Panel B) at the peak of the regurgitant flow ($t = 0.358$ s). In the aortic side (Panel

A), it can be observed that the asymmetrical flow caused by PVL leads to elevated WSS, up to 3.05 Pa, around the coaptation area of the leaflets. In addition, high localized WSS exist even on the left ventricular side close to the location of the regurgitant orifices (Panel B). The highest value of WSS (11.05 Pa) is located close to the regurgitant orifice of 4 mm².

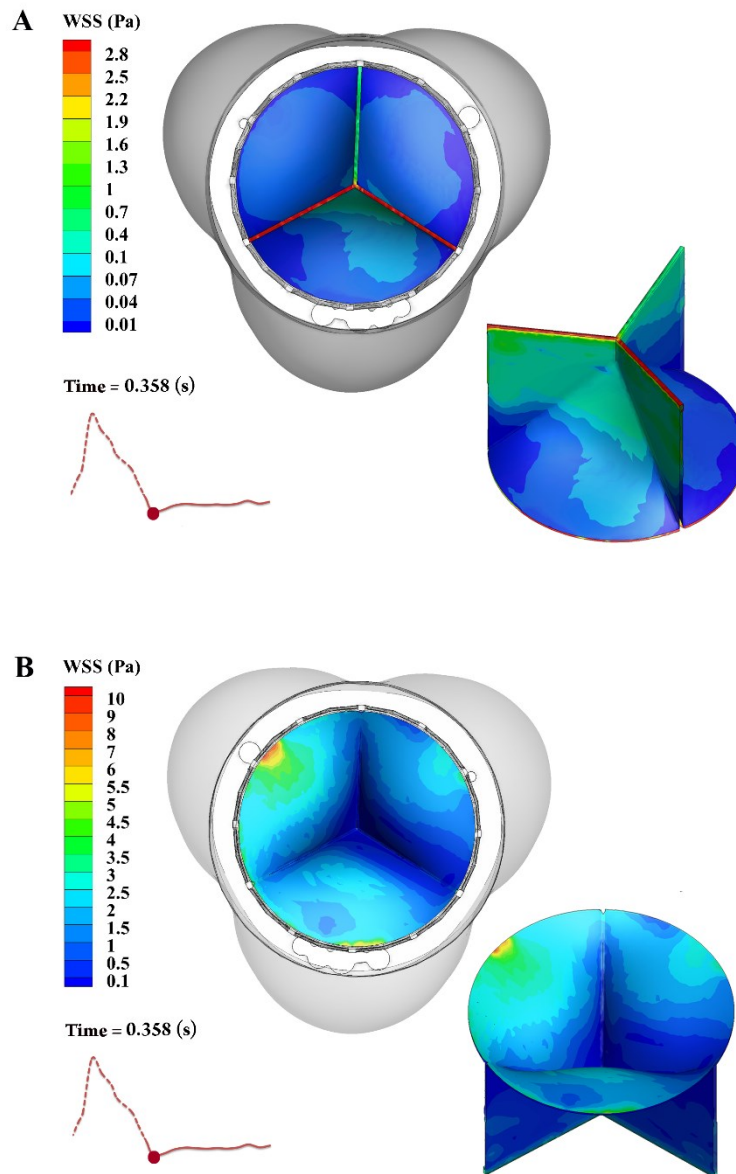


Figure 4-6: (a) Aortic valve leaflets (aortic side) top and isometric view of wall shear stress contours at $t = 0.358$ s; (b) Aortic valve leaflets (left ventricle side) top and isometric view of wall shear stress contours at $t = 0.358$ s.

4.4. Discussion

This study adds significant new knowledge to our understanding of the pathophysiology of paravalvular leak post transcatheter aortic valve replacement. First, paravalvular leak significantly disturbs flow both upstream and downstream of the implanted aortic valve during diastole. Also PVL not only leads to elevated wall shear stress on the aortic side of the valve leaflets, but also on the ventricular side.

Transcatheter aortic valve replacement has been shown to prolong survival in symptomatic patients with severe aortic stenosis who are not eligible for surgical valve replacement and has become the new standard of care. Although, TAVR provides a significant number (33%) of inoperable elderly patients with a life prolonging treatment option (Iung et al., 2005), it is still associated with some complications, with PVL being one of the most significant (Genereux et al., 2013; Haensig et al., 2012; Schultz et al., 2009; Unbehaun et al., 2012). In high risk operative candidates, TAVR and surgical aortic valve replacement (SAVR) have been shown to have similar mortality, reduction in symptoms, and improved valve hemodynamics in the short term post procedure period. PVL however was significantly more prevalent in patients undergoing TAVR than SAVR (6.8% vs. 1.9%). Significant PVL post TAVR is a finding associated with increased long term morbidity and mortality.

From a hemodynamic standpoint, PVL is associated with high speed jets emerging from the ascending aorta towards the LVOT region during diastole. Velocity contours show that high speed jets generated by PVL could reach up to 4.13 m/s for a total effective regurgitant orifice area of 25 mm². This value is consistent with *in vivo* Doppler echocardiographic findings of 4.51 m/s in a patient with a total regurgitant orifice area of 26 mm² (Hayek et al., 2014). According to 2D velocity contours (Figure 4-3), the jets emerging from the regurgitant orifices rapidly diverge

within the LVOT. This represents a significant clinical implication since the evaluation of paravalvular leak can be performed by a delineation of the regurgitant jet vena contracta using 2D transthoracic echocardiographic color Doppler or cardiac magnetic resonance imaging (Goncalves et al. 2012; Hayek et al. 2014). As a consequence, the location of the cross-sectional measurements might lead to significant errors in the determination of the effective regurgitant orifice area.

Our study also demonstrates that paravalvular leak leads to elevated shear stress on the LVOT wall as well as on both sides of the valve leaflets. In the proximal ascending aorta, several recirculation zones are developed around the aortic valve. This unfavorable flow configuration leads to abnormally high shear stress values during diastole. This is an important finding, since it is well documented that changes in shear stress alter the biosynthetic behavior of aortic valve cells and can up-regulate pro-inflammatory markers in aortic valve tissues (Balachandran et al., 2011; Sucosky et al., 2009). Furthermore, several studies have already shown that high mechanical shear stress is a significant determinant of structural deterioration of bioprosthetic valve leaflets (Nobari et al., 2013). As a consequence, PVL in the setting of TAVR might lead to a rapid structural deformation of the transcatheter valve leaflets and subsequently to a reduction in valve durability.

Finally, it is also interesting to note the differences between aortic regurgitation (through valve leaflet commissures) and paravalvular leak following TAVR. Native aortic valve regurgitation is often characterized by somehow a central jet entering the LV cavity and interacting directly with the mitral inflow. The jet may not be deflected towards the LVOT wall and minimally interacts with mitral valve leaflets. On the other hand, paravalvular leak following TAVR is characterized by multiple jets along the LVOT wall (Pibarot et al., 2015). This specific characteristic of paravalvular leak may lead to significant adverse effects on the cardiac structures (Figure 4-6 and 4-7) by: 1) increasing the shear stress on TAV leaflets (leading potentially to

decreased durability); 2) increasing the shear stress in the LVOT area; 3) directly impacting the mitral valve leaflets and potentially generating elevated localized shear stress.

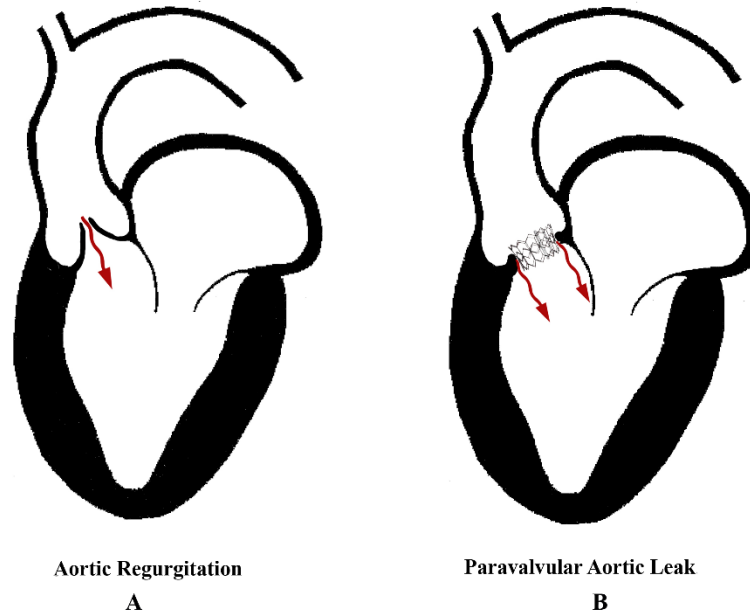


Figure 4-7: Schematic representation of the difference between (a) Native aortic valve regurgitation and (b) Paravalvular leak post transcatheter aortic valve replacement.

4.5. Limitation

In this numerical study, the simulations were performed using a SAPIEN valve. This valve is currently not available anymore in the market, as it has been replaced by two newer generation valves, the SAPIEN XT and the SAPIEN 3. The overall hemodynamic profile of the SAPIEN XT valve is not significantly different from the SAPIEN. Most of the improvements were regarding frame geometry, reduction in metal content, and a lower crimp profile. The prevalence of mild/moderate PVL with SAPIEN XT was still at the same level as the original SAPIEN valve (42% of patients) (Amat-Santos et al., 2015). However, the new SAPIEN 3 including an external cuff at the bottom of the valve stent to prevent PVL is showing very promising results. In a recent

study, Amat-Santos et al. (2015) showed that the prevalence of mild/moderate PVL was significantly reduced (7%) using the SAPIEN 3 valve without negatively impacting transvalvular pressure gradients.

These positive results have however to be considered with caution at the moment because of the small sample size and the absence of an accurate quantitative method for evaluating PVL. Finally, this study does not consider the anatomical shape of the LV cavity below the LVOT region. Further studies are required to investigate the interaction between the PVL and LV filling patterns.

4.6. Conclusion

Paravalvular leak following transcatheter aortic valve replacement leads to significant disturbance in blood flow characteristics both upstream and downstream of the implanted valve. The abnormal flow is characterized by high speed jets, small and large scale coherent structures and markedly elevated shear stress on both sides of the implanted aortic leaflets. Such unfavorable flow configuration may promote a more rapid degeneration of the transcatheter valve leaflets.

4.7. Additional Results and Discussions

In addition to the results which are presented in section (4.3), some results are extracted and presented in this chapter on flow characteristics.

Figure (4-8) represents the evolution of the secondary flow in three different sections below the stent (LV side) at 6 time instants during the diastole cycle.

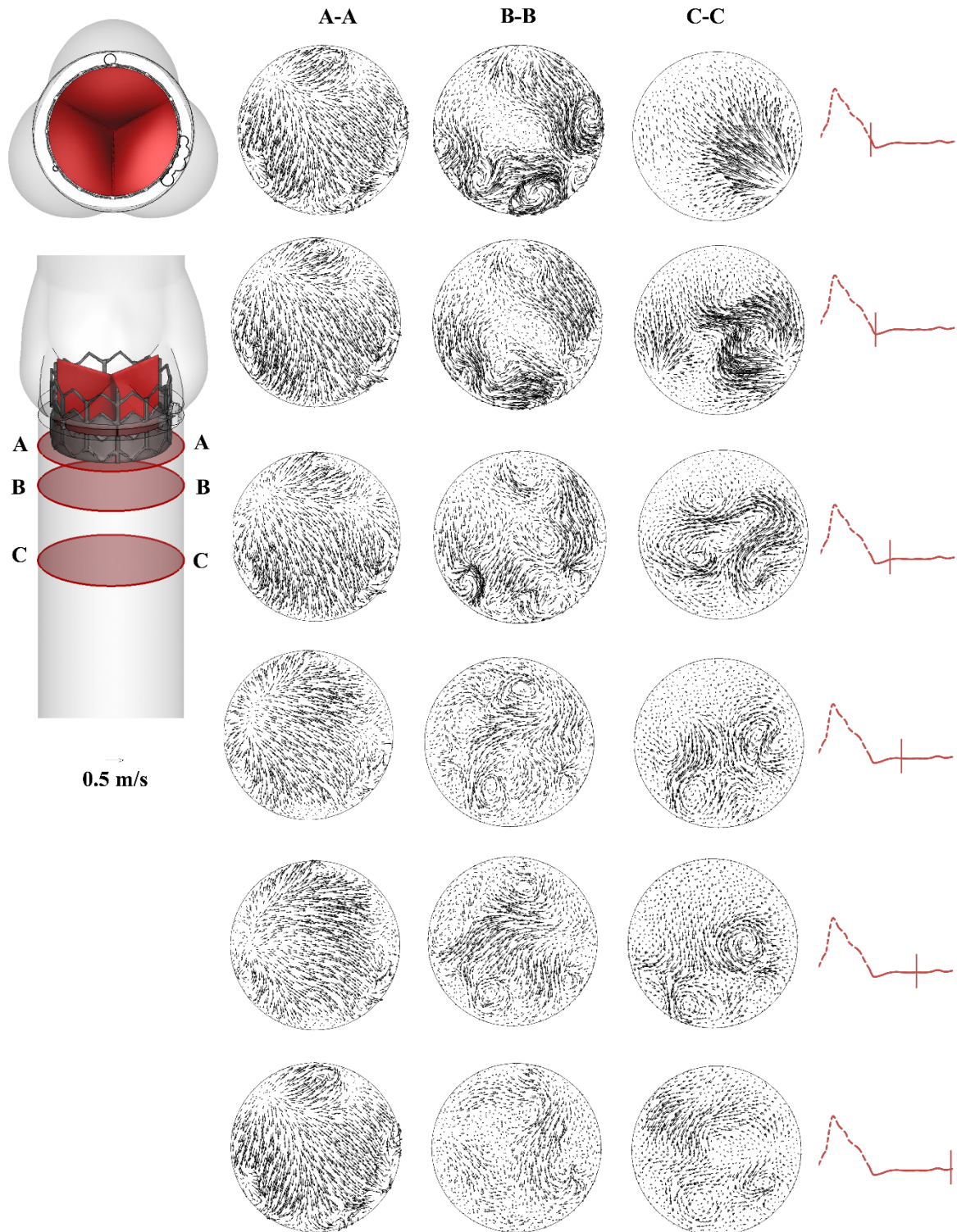


Figure 4-8: Evolution of the secondary flow during diastole cycle at 6 instants. A-A) Section right below the valve stent in left ventricular side; B-B) Section 1 cm below the valve stent; C-C) Section 3 cm below the valve stent

It appeared that as a result of high speed PVL jets, rotating vortices developed in the left ventricular side (highest secondary flow velocity = 1.2 m/s). Abnormal flow conditions persist so close to the left ventricular walls explaining the elevated wall shear stress distribution at the LV inner wall.

Figure (4-9) shows the evolution of the Lambda-2 Criterion. Lambda-2 is a method introduced by Jeong and Hussain (1995) for visualization and extraction of flow vortices (Appendix C).



Figure 4-9: Lambda-2 Evolution during Diastole

As it could be seen from the figure different vortical structures are developed during the diastole and persist till the end of the diastole. . The adverse effect of the small and large scale vortices on blood flow characteristics require further investigation.

CHAPTER 5: Conclusion and Summary

In this study, first a mathematical lumped parameter model which was previously validated by (Keshavarz-Motamed et al., 2011) is used to model several patient conditions with pre-TAVR aortic stenosis and post TAVR paravalvular regurgitation with different level of severities. The performance of TAVR is evaluated considering the relative change in the computed left ventricle stroke work (LVSW). In addition, a new non-invasive parameter (TAVR-PI) is introduced to estimate the efficiency of transcatheter aortic valve replacement in reducing left ventricle work overload. Results show that patients with severe aortic stenosis and trace/mild aortic regurgitation should be considered with care when planning for TAVR due to the potential suboptimal performance of TAVR.

Future studies could also consider the effect of myocardial remodeling and contractile dysfunction due to the presence of the stenosis pre-TAVR, which could increase the risk of post-operative complications and mortality.

Second, a computational fluid dynamic model is performed to study the hemodynamics of the transcatheter aortic valve (TAV) in presence of the paravalvular leak (PVL). A realistic geometry of TAV, and turbulent computational fluid ($k-\omega$ -SST) model are employed and in-vivo boundary condition applied to simulate the PVL during diastole cycle. Results show that PVL following TAVR significantly disturbs blood flow characteristics both upstream and downstream of the TAV. High speed jets, small and large scale coherent structures and drastically elevated shear stress on both sides of the TAV aortic leaflets are seen, which could promote a more rapid deterioration of the transcatheter valve leaflets.

Future studies, could address the 3rd generation of TAVs such as SAPIEN3, since little is known on flow characteristics of these new generation of the valves. Furthermore, future simulations should investigate the interaction between PVL and diastolic inflow and potentially link this to diastolic dysfunction.

REFERENCES

- Abdel-Wahab, M., Comberg, T., Büttner, H.J., El-Mawardy, M., Chatani, K., Gick, M., Geist, V., Richardt, G., Neumann, F.-J., 2014. Aortic regurgitation after transcatheter aortic valve implantation with balloon- and self-expandable prostheses: a pooled analysis from a 2-center experience. *JACC. Cardiovasc. Interv.* 7, 284–92.
- Abdel-Wahab, M., Zahn, R., Horack, M., Gerckens, U., Schuler, G., Sievert, H., Eggebrecht, H., Senges, J., Richardt, G., 2011. Aortic regurgitation after transcatheter aortic valve implantation: incidence and early outcome. Results from the German transcatheter aortic valve interventions registry. *Heart* 97, 899–906.
- Ali, O.F., Schultz, C., Jabbour, A., Rubens, M., Mittal, T., Mohiaddin, R., Davies, S., Di Mario, C., Van der Boon, R., Ahmad, A.S., Amrani, M., Moat, N., De Jaegere, P.P.T., Dalby, M., 2015. Predictors of paravalvular aortic regurgitation following self-expanding Medtronic CoreValve implantation: The role of annulus size, degree of calcification, and balloon size during pre-implantation valvuloplasty and implant depth. *Int. J. Cardiol.* 179, 539–545.
- Amat-Santos, I.J., Dahou, A., Webb, J., Dvir, D., Dumesnil, J.G., Allende, R., Ribeiro, H.B., Urena, M., Paradis, J.-M., DeLarochelière, R., Dumont, E., Bergeron, S., Thompson, C.R., Pasian, S., Bilodeau, S., Leipsic, J., Larose, E., Pibarot, P., Rodés-Cabau, J., 2015. Comparison of hemodynamic performance of the balloon-expandable SAPIEN 3 versus SAPIEN XT transcatheter valve. *Am. J. Cardiol.* 114, 1075–1082.
- American Heart Association, 2014. What is TAVR? [WWW Document]. URL http://www.heart.org/HEARTORG/Conditions/More/HeartValveProblemsandDisease/What-is-TAVR_UCM_450827_Article.jsp
- Anderson, R.H., 2000. Clinical anatomy of the aortic root. *Heart* 84, 670–673.
- Athappan, G., Patvardhan, E., Tuzcu, E.M., Svensson, L.G., Lemos, P. a., Fraccaro, C., Tarantini, G., Sinning, J.M., Nickenig, G., Capodanno, D., Tamburino, C., Latib, A., Colombo, A., Kapadia, S.R., 2013. Incidence, predictors, and outcomes of aortic regurgitation after transcatheter aortic valve replacement: Meta-analysis and systematic review of literature. *J. Am. Coll. Cardiol.* 61, 1585–1595.
- Auricchio, F., Conti, M., Morganti, S., Reali, A., 2014. Simulation of transcatheter aortic valve implantation: a patient-specific finite element approach. *Comput. Methods Biomech. Biomed. Engin.* 17, 1347–57.
- Azadani, A.N., Jaussaud, N., Matthews, P.B., Ge, L., Guy, T.S., Chuter, T. a M., Tseng, E.E., 2009. Energy loss due to paravalvular leak with transcatheter aortic valve implantation. *Ann. Thorac. Surg.* 88, 1857–63.
- Balachandran, K., Sucusky, P., Yoganathan, A.P., 2011. Hemodynamics and mechanobiology of aortic valve inflammation and calcification. *Int. J. Inflamm.* 2011, 263870.

- Bekeredjian, R., Grayburn, P. a, 2005. Valvular heart disease: aortic regurgitation. *Circulation* 112, 125–34.
- Benevento, E., Djebbari, A., Keshavarz-Motamed, Z., Cecere, R., Kadem, L., 2015. Hemodynamic changes following aortic valve bypass: a mathematical approach. *PLoS One* 10, e0123000.
- Benjamin, D.M., 2013. Aortic Valve Anatomy. Medscape.
- Black, M.M., Howard, I.C., Huang, X., Patterson, E.A., 1991. A three-dimensional analysis of a bioprosthetic heart valve. *J. Biomech.* 24, 793–801.
- Bloomfield, P., 2002. Choice of heart valve prosthesis. *Heart* 87, 583–589.
- Bluestein, D., Li, Y.M., Krukenkamp, I.B., 2002. Free emboli formation in the wake of bi-leaflet mechanical heart valves and the effects of implantation techniques. *J. Biomech.* 35, 1533–1540.
- Bonow, R.O., Carabello, B. a, Chatterjee, K., de Leon, A.C., Faxon, D.P., Freed, M.D., Gaasch, W.H., Lytle, B.W., Nishimura, R. a, O’Gara, P.T., O’Rourke, R. a, Otto, C.M., Shah, P.M., Shanewise, J.S., Smith, S.C., Jacobs, A.K., Adams, C.D., Anderson, J.L., Antman, E.M., Fuster, V., Halperin, J.L., Hiratzka, L.F., Hunt, S. a, Lytle, B.W., Nishimura, R., Page, R.L., Riegel, B., 2006. ACC/AHA 2006 guidelines for the management of patients with valvular heart disease: a report of the American College of Cardiology/American Heart Association Task Force on Practice Guidelines. *J. Am. Coll. Cardiol.* 48, e1–148.
- Borazjani, I., 2013a. Immersed voundary-finite element method simulations of bio-prosthetic heart valves. *Comput. Methods Appl. Mech. Eng.* 257, 103–116.
- Borazjani, I., 2013b. Fluid–structure interaction, immersed boundary-finite element method simulations of bio-prosthetic heart valves. *Comput. Methods Appl. Mech. Eng.* 257, 103–116.
- Borazjani, I., Ge, L., Sotiropoulos, F., 2008. Curvilinear immersed boundary method for simulating fluid structure interaction with complex 3D rigid bodies. *J. Comput. Phys.* 227, 7587–7620.
- Briand, M., Dumesnil, J.G., Kadem, L., Tongue, A.G., Rieu, R., Garcia, D., Pibarot, P., 2005. Reduced systemic arterial compliance impacts significantly on left ventricular afterload and function in aortic stenosis: Implications for diagnosis and treatment. *J. Am. Coll. Cardiol.* 46, 291–298.
- Buellesfeld, L., Gerckens, U., Schuler, G., Bonan, R., Kovac, J., Serruys, P.W., Labinaz, M., den Heijer, P., Mullen, M., Tymchak, W., Windecker, S., Mueller, R., Grube, E., 2011. 2-year follow-up of patients undergoing transcatheter aortic valve implantation using a self-expanding valve prosthesis. *J. Am. Coll. Cardiol.* 57, 1650–7.
- Buellesfeld, L., Grube, E., 2012. A permanent solution for a temporary problem: transcatheter valve-in-valve implantation for failed transcatheter aortic valve replacement. *JACC. Cardiovasc. Interv.* 5, 578–81.

- Burattini, R., Gnudi., G., 1982. Computer identification of models for the arterial tree input impedance: comparison between two new simple models and first experimental results. *Med. Biol. Eng. Comput.* 20, 134–144.
- Caballero, L., Saura, D., García-Lara, J., Oliva, M.J., Pinar, E., González-Carrillo, J., García-Navarro, M., Espinosa, M.D., Valdés, M., de la Morena, G., 2015. Influence of aortic regurgitation after TAVI on left ventricular filling pattern. *Eur. J. Clin. Invest.* 45, 18–26.
- Cataloglu, A., Clark, R.E., Gould, P.L., 1977. Stress analysis of aortic valve leaflets with smoothed geometrical data. *J. Biomech.* 10, 153–158.
- Celik , I.B. , Ghia, U., Roache, P.J., Freitas, C.J., others, 2008. Procedure for estimation and reporting of uncertainty due to discretization in CFD applications. *J Fluids Eng.* 130, 1–4.
- Center, T. heart and vascular, 2013. Transfemoral-TAVI-procedure [WWW Document]. URL <http://www.heartvascularcentre.com/treatments/transfemoral-tavi-procedure/attachment/transfemoral-tavi-procedure/>
- Chandran, K., 2010. Role of computational simulations in heart valve dynamics and design of valvular prostheses. *Cardiovasc. Eng. Technol.* 1, 18–38.
- Chandran, K.B., Dexter, E.U., Aluri, S., Richenbacher, W.E., 1998. Negative pressure transients with mechanical heart-valve closure: correlation between in vitro and in vivo results. *Ann. Biomed. Eng.* 26, 546–556.
- Cheng, R., Lai, Y.G., Chandran, K.B., 2004. Three-dimensional fluid-structure interaction simulation of bileaflet mechanical heart valve flow dynamics. *Ann. Biomed. Eng.* 32, 1471–1483.
- Chew, G. G. Patterson, E. A., others, 1999. Simulation of damage in a porcine prosthetic heart valve. *J. Med. Eng. Technol.* 23, 178–189.
- Christie, G.W., Medland, I.C., 1982. A non-linear finite element stress analysis of bioprosthetic heart valves. *Finite Elem. Biomech.* 153–179.
- Clark, M.A., Duhay, F.G., Keyes, M.J., Svensson, L.G., Bonow, R.O., Stockwell, B.T., Cohen, D.J., 2012. Clinical and economic outcomes after surgical aortic valve replacement in Medicare patients 117–126.
- Clavel, M.-A., Rodés-Cabau, J., Dumont, É., Bagur, R., Bergeron, S., De Larocheillère, R., Doyle, D., Larose, E., Dumesnil, J.G., Pibarot, P., 2011. Validation and characterization of transcatheter aortic valve effective orifice area measured by Doppler echocardiography. *JACC. Cardiovasc. Imaging* 4, 1053–62.
- Clavel, M.-A., Webb, J.G., Pibarot, P., Altwegg, L., Dumont, E., Thompson, C., De Larocheillère, R., Doyle, D., Masson, J.-B., Bergeron, S., Bertrand, O.F., Rodés-Cabau, J., 2009. Comparison of the hemodynamic performance of percutaneous and surgical bioprostheses for the treatment of severe aortic stenosis. *J. Am. Coll. Cardiol.* 53, 1883–91.

- Craig R., S., Martin, B.L., Michael, J.M., D. Craig, M., Jeffrey, W.M., Lars, G.S., Murat, T., John, G.W., Gregory, P.F., Raj, R.M., Mathew, W., Todd, D., Samir, K., Vasilis, B., Vinod, H.T., Paul, C., Augusto, D.P., Joseph, E.B., Howard, C.H., Akin, J.J., William, N.A., Duolao, W., Stuart, J.P., 2011. Transcatheter versus surgical aortic-valve replacement in high-risk patients. *N. Engl. J. Med.* 364, 609–619.
- Cribier, A., Eltchaninoff, H., Bash, A., Borenstein, N., Tron, C., Bauer, F., Derumeaux, G., Anselme, F., Laborde, F., Leon, M.B., 2002. Percutaneous transcatheter implantation of an aortic valve prosthesis for calcific aortic stenosis: first human case description. *Circulation* 106, 3006–3008.
- De Hart, J., Baaijens, F.P.T., Peters, G.W.M., Schreurs, P.J.G., 2003. A computational fluid-structure interaction analysis of a fiber-reinforced stentless aortic valve. *J. Biomech.* 36, 699–712.
- Dolan, E., Thijs, L., Li, Y., Atkins, N., McCormack, P., McClory, S., O'Brien, E., Staessen, J. a., Stanton, A. V., 2006. Ambulatory arterial stiffness index as a predictor of cardiovascular mortality in the dublin outcome study. *Hypertension* 47, 365–370.
- Dumont, K., Stijnen, J.M. a, Vierendeels, J., van de Vosse, F.N., Verdonck, P.R., 2004. Validation of a fluid-structure interaction model of a heart valve using the dynamic mesh method in fluent. *Comput. Methods Biomech. Biomed. Engin.* 7, 139–146.
- Dumont, K., Vierendeels, J. a M., Segers, P., Van Nooten, G.J., Verdonck, P.R., 2005. Predicting ATS Open Pivot heart valve performance with computational fluid dynamics. *J. Heart Valve Dis.* 14, 393–399.
- Dumont, K., Vierendeels, J., Kaminsky, R., van Nooten, G., Verdonck, P., Bluestein, D., 2007. Comparison of the hemodynamic and thrombogenic performance of two bileaflet mechanical heart valves using a CFD/FSI model. *J. Biomech. Eng.* 129, 558–565.
- Dvir, D., Barbash, I.M., Ben-Dor, I., Torguson, R., Badr, S., Minha, S., Pendyala, L.K., Loh, J.P., Pichard, A.D., Waksman, R., 2013. Paravalvular regurgitation after transcatheter aortic valve replacement: diagnosis, clinical outcome, preventive and therapeutic strategies. *Cardiovasc. Revasc. Med.* 14, 174–81.
- Dwyer, H. a, Matthews, P.B., Azadani, A., Ge, L., Guy, T.S., Tseng, E.E., 2009a. Migration forces of transcatheter aortic valves in patients with noncalcific aortic insufficiency. *J. Thorac. Cardiovasc. Surg.* 138, 1227–33.
- Dwyer, H. a, Matthews, P.B., Azadani, A., Jaussaud, N., Ge, L., Guy, T.S., Tseng, E.E., 2009b. Computational fluid dynamics simulation of transcatheter aortic valve degeneration. *Interact. Cardiovasc. Thorac. Surg.* 9, 301–308.
- Edwards Lifesciences Corporation, 2013. Treatment options for aortic stenosis [WWW Document]. URL <http://newheartvalve.com/hcp/treatment-options#sthash.IXLYphPb.dpbs>

- Edwards Lifesciences Corporation, 2014. The TAVR procedure [WWW Document]. URL <http://newheartvalve.com/hcp/tavr-overview#sthash.BZluThE9.devn0lVE.dpbs>
- Eltchaninoff, H., Prat, A., Gilard, M., Leguerrier, A., Blanchard, D., Fournial, G., Iung, B., Donzeau-Gouge, P., Tribouilloy, C., Debrux, J.-L., Pavie, A., Gueret, P., 2011. Transcatheter aortic valve implantation: early results of the FRANCE (French Aortic National CoreValve and Edwards) registry. *Eur. Heart J.* 32, 191–7.
- Ewe, S.H., Muratori, M., van der Kley, F., Pepi, M., Delgado, V., Tamborini, G., Fusini, L., de Weger, A., Gripari, P., Bartorelli, A., Bax, J.J., Marsan, N.A., 2015. Effect of aortic regurgitation following transcatheter aortic valve implantation on outcomes. *Am. J. Cardiol.* 115, 664–669.
- Faxon, D.P., 2011. Transcatheter aortic valve implantation: coming of age. *Circulation* 124, e439–40.
- Fishbein, G. a., Schoen, F.J., Fishbein, M.C, 2013. Transcatheter aortic valve implantation: status and challenges. *Cardiovasc. Pathol.* 23, 65–70.
- Frank, O., 1899. The basic shape of the arterial pulse. First treatise: mathematical analysis. 1899. *J. Mol. Cell. Cardiol.* 22, 255–277.
- Fung, Y.C., 1981. Mechanical properties of living tissues, 2nd ed, J Springer. Springer-Verlag New York.
- Gafoor, S., Franke, J., Piayda, K., Lam, S., Bertog, S., Vaskelyte, L., Hofmann, I., Sievert, H., 2014. Paravalvular leak closure after transcatheter aortic valve replacement with a self-expanding prosthesis. *Catheter. Cardiovasc. Interv.* 84, 147–154.
- Garcia, D., Barenbrug, P.J.C., Pibarot, P., Dekker, A.L. a J., van der Veen, F.H., Maessen, J.G., Dumesnil, J.G., Durand, L.-G., 2005a. A ventricular-vascular coupling model in presence of aortic stenosis. *Am. J. Physiol. Heart Circ. Physiol.* 288, H1874–H1884.
- Garcia, D., Durand, L.-G., 1983. Aortic stenosis and systemic hypertension. *Br. Med. J. (Clin. Res. Ed)*. 286, 1960–1961.
- Garcia, D., Pibarot, P., Durand, L.-G., 2005b. Analytical modeling of the instantaneous pressure gradient across the aortic valve. *J. Biomech.* 38, 1303–11.
- Ge, L., Dasi, L.P., Sotiropoulos, F., Yoganathan, A.P., 2008. Characterization of hemodynamic forces induced by mechanical heart valves: Reynolds vs. viscous stresses. *Ann. Biomed. Eng.* 36, 276–297.
- Ge, L., Leo, H.-L., Sotiropoulos, F., Yoganathan, A.P., 2005. Flow in a mechanical bileaflet heart valve at laminar and near-peak systole flow rates: CFD simulations and experiments. *J. Biomech. Eng.* 127, 782–797.

- Genereux, P., Head, S.J., Hahn, R., Daneault, B., Kodali, S., Williams, M.R., others, 2013. Paravalvular leak after transcatheter aortic valve replacement: the new Achilles' heel? a comprehensive review of the literature. *J Am Coll Cardiol* 61, 1125–1136.
- Geven, M.C.F., Bohté, V.N., Aarnoudse, W.H., van den Berg, P.M.J., Rutten, M.C.M., Pijls, N.H.J., van de Vosse, F.N., 2004. A physiologically representative in vitro model of the coronary circulation. *Physiol. Meas.* 25, 891–904.
- Ghalichi, F., Deng, X., Champlain, A. De, Douville, Y., King, M., Guidoin, R., 1998. Low Reynolds number turbulence modeling of blood flow in arterial stenoses. *Biorheology* 35, 281–294.
- Gilard, M., Eltchaninoff, H., Iung, B., Donzeau-Gouge, P., Chevreul, K., Fajadet, J., Leprince, P., Leguerrier, A., Lievre, M., Prat, A., Teiger, E., Lefevre, T., Himbert, D., Tchetché, D., Carrié, D., Albat, B., Cribier, A., Rioufol, G., Sudre, A., Blanchard, D., Collet, F., Santos, P. Dos, Meneveau, N., Tirouvanziam, A., Caussin, C., Guyon, P., Boschhat, J., Le Breton, H., Collart, F., Houel, R., Delpine, S., Souteyrand, G., Favereau, X., Ohlmann, P., Doisy, V., Grollier, G., Gommeaux, A., Claudel, J.-P., Bourlon, F., Bertrand, B., Van Belle, E., Laskar, M., 2012. Registry of transcatheter aortic-valve implantation in high-risk patients. *N. Engl. J. Med.* 366, 1705–1715.
- Gonalves, A., Almeria, C., Marcos-Alberca, P., Feltes, G., Hernández-Antolín, R., Rodríguez, E., Silva Cardoso, J.C., MacAya, C., Zamorano, J.L., 2012. Three-dimensional echocardiography in paravalvular aortic regurgitation assessment after transcatheter aortic valve implantation. *J. Am. Soc. Echocardiogr.* 25, 47–55.
- Gonçalves, A., Marcos-Alberca, P., Almeria, C., Feltes, G., Rodríguez, E., Hernández-Antolín, R.A., Garcia, E., Maroto, L., Fernandez Perez, C., Silva Cardoso, J.C., Macaya, C., Zamorano, J.L., 2011. Acute left ventricle diastolic function improvement after transcatheter aortic valve implantation. *Eur. J. Echocardiogr.* 12, 790–7.
- Gotzmann, M., Bojara, W., Lindstaedt, M., Ewers, A., Bösche, L., Germing, A., Lawo, T., Bechtel, M., Laczkovics, A., Mügge, A., 2011a. One-year results of transcatheter aortic valve implantation in severe symptomatic aortic valve stenosis. *Am. J. Cardiol.* 107, 1687–92.
- Gotzmann, M., Lindstaedt, M., Mügge, A., 2012. From pressure overload to volume overload: Aortic regurgitation after transcatheter aortic valve implantation. *Am. Heart J.* 163, 903–911.
- Gotzmann, M., Pljakic, A., Bojara, W., Lindstaedt, M., Ewers, A., Germing, A., Mügge, A., 2011b. Transcatheter aortic valve implantation in patients with severe symptomatic aortic valve stenosis-predictors of mortality and poor treatment response. *Am. Heart J.* 162, 238–245.e1.
- Gramigna, V., Caruso, M.V., Rossi, M., Serraino, G.F., Renzulli, a., Fragomeni, G., 2014. A numerical analysis of the aortic blood flow pattern during pulsed cardiopulmonary bypass. *Comput. Methods Biomech. Biomed. Engin.* 18, 1574–1581.
- Grodins, B.Y.F.S., 1959. A mathematical synthesis of cardiac and blood vessel hemodynamics. *Q. Rev. Biol.* 34, 93–116.

- Haensig, M., Lehmkuhl, L., Rastan, A.J., Kempfert, J., Mukherjee, C., Gutberlet, M., others, 2012. Aortic valve calcium scoring is a predictor of significant paravalvular aortic insufficiency in transapical-aortic valve implantation. *Eur J Cardiothorac Surg* 41, 1234–1240.
- Hahn, R.T., Khalique, O., Williams, M.R., Koss, E., Paradis, J.-M., Daneault, B., Kirtane, A.J., George, I., Leon, M.B., Kodali, S., 2013. Predicting paravalvular regurgitation following transcatheter valve replacement: utility of a novel method for three-dimensional Echocardiographic measurements of the aortic annulus. *J. Am. Soc. Echocardiogr.* 26, 1043–1052.
- Hamid, M.S., Sabbah, H.N., Stein, P.D., 1985. Finite element evaluation of stresses on closed leaflets of bioprosthetic heart valves with flexible stents. *Finite Elem. Anal. Des.* 1, 213–225.
- Hart, J. De, Peters, G.W.M., Schreurs, P.J.G., Baaijens, F.P.T., 2000. A two-dimensional fluid structure interaction model of the aortic valve 33, 1079–1088.
- Hayashida, K., Lefèvre, T., Chevalier, B., Hovasse, T., Romano, M., Garot, P., Bouvier, E., Farge, A., Donzeau-Gouge, P., Cormier, B., Morice, M.-C., 2012. Impact of post-procedural aortic regurgitation on mortality after transcatheter aortic valve implantation. *JACC. Cardiovasc. Interv.* 5, 1247–56.
- Hayek, S., Sawaya, F., Oshinski, J., Lerakis, S., 2014. Multiparametric assessment of post-transcatheter Aortic valve replacement paravalvular regurgitation grading by transthoracic echocardiography and Cardiac Magnetic Resonance. ” *J. Clin. Exp. Cardiol.* vol. 05, no 05.
- Holmes, D.R., Mack, M.J., Kaul, S., Agnihotri, A., Alexander, K.P., Bailey, S.R., Calhoun, J.H., Carabello, B. a, Desai, M.Y., Edwards, F.H., Francis, G.S., Gardner, T.J., Kappetein, a P., Linderbaum, J. a, Mukherjee, C., Mukherjee, D., Otto, C.M., Ruiz, C.E., Sacco, R.L., Smith, D., Thomas, J.D., 2012. 2012 ACCF/AATS/SCAI/STS expert consensus document on transcatheter aortic valve replacement. *J. Am. Coll. Cardiol.* 59, 1200–54.
- Hsu, U.-K., Lu, P.-J., 2013. Dynamic simulation and hemolysis evaluation of the regurgitant flow over a tilting-disc mechanical heart valve in pulsatile flow. *World J. Mech.* 03, 160–168.
- Huang, X., Black, M.M., Howard, I.C., Patterson, E.A., 1990. A two-dimensional finite element analysis of a bioprosthetic heart valve. *J. Biomech.* 23, 753–762.
- Intermountain Heart Institute, 2015. Aortic valve stenosis [WWW Document]. *Intermt. Med. Cent.* URL <http://intermountainhealthcare.org/hospitals/imed/services/heart-institute/heart-health-a-z/Pages/condition-aortic-valve-stenosis.aspx>
- Iqbal, J., Serruys, P.W., 2014. Comparison of Medtronic CoreValve and Edwards SAPIEN XT for transcatheter aortic valve implantation: the need for an imaging-based personalized approach in device selection. *JACC. Cardiovasc. Interv.* 7, 293–5.
- Iung, B., Cachier, A., Baron, G., Messika-Zeitoun, D., Delahaye, F., Tornos, P., Gohlke-Bärwolf, C., Boersma, E., Ravaud, P., Vahanian, A., 2005. Decision-making in elderly patients with severe aortic stenosis: why are so many denied surgery? *Eur. Heart J.* 26, 2714–20.

- Jeong, J., Hussain, F., 1995. On the identification of a vortex. *J. Fluid Mech.* 285, 69–94.
- Jin, S., Oshinski, J., Giddens, D.P., 2003. Effects of wall motion and compliance on flow patterns in the ascending aorta. *J. Biomech. Eng.* 125, 347–354.
- John, D., Buellesfeld, L., Yuecel, S., Mueller, R., Latsios, G., Beucher, H., Gerckens, U., Grube, E., 2010. Correlation of Device landing zone calcification and acute procedural success in patients undergoing transcatheter aortic valve implantations with the self-expanding CoreValve prosthesis. *JACC. Cardiovasc. Interv.* 3, 233–43.
- Kappetein, a P., Head, S.J., Généreux, P., Piazza, N., van Mieghem, N.M., Blackstone, E.H., Brott, T.G., Cohen, D.J., Cutlip, D.E., van Es, G.-A., Hahn, R.T., Kirtane, A.J., Krucoff, M.W., Kodali, S., Mack, M.J., Mehran, R., Rodés-Cabau, J., Vranckx, P., Webb, J.G., Windecker, S., Serruys, P.W., Leon, M.B., 2012. Updated standardized endpoint definitions for transcatheter aortic valve implantation: the Valve Academic Research Consortium-2 consensus document. *J. Am. Coll. Cardiol.* 60, 1438–54.
- Kasel, A.M., Cassese, S., Bleiziffer, S., Amaki, M., Hahn, R.T., Kastrati, A., Sengupta, P.P., 2013. Standardized Imaging for Aortic Annular Sizing. *JACC Cardiovasc. Imaging* 6, 249–262.
- Kerckhoffs, R.C.P., Neal, M.L., Gu, Q., Bassingthwaighte, J.B., Omens, J.H., McCulloch, A.D., 2007. Coupling of a 3D finite element model of cardiac ventricular mechanics to lumped systems models of the systemic and pulmonic circulation. *Ann. Biomed. Eng.* 35, 1–18.
- Keshavarz-Motamed, Z., Garcia, J., Gaillard, E., Capoulade, R., Le Ven, F., Cloutier, G., Kadem, L., Pibarot, P., 2014a. Non-invasive determination of left ventricular workload in patients with aortic stenosis using magnetic resonance imaging and Doppler echocardiography. *PLoS One* 9, e86793.
- Keshavarz-Motamed, Z., Garcia, J., Gaillard, E., Maftoon, N., Labbio, G., Cloutier, G., Kadem, L., 2014b. Effect of coarctation of the aorta and bicuspid aortic valve on flow dynamics and turbulence in the aorta using particle image velocimetry. *Exp. Fluids* 55, 1696.
- Keshavarz-Motamed, Z., Garcia, J., Kadem, L., 2013. Fluid dynamics of coarctation of the aorta and effect of bicuspid aortic valve. *PLoS One* 8, e72394.
- Keshavarz-Motamed, Z., Garcia, J., Pibarot, P., Larose, E., Kadem, L., 2011. Modeling the impact of concomitant aortic stenosis and coarctation of the aorta on left ventricular workload. *J. Biomech.* 44, 2817–25.
- Keshavarz-Motamed, Z., Kadem, L., 2011. 3D pulsatile flow in a curved tube with coexisting model of aortic stenosis and coarctation of the aorta. *Med. Eng. Phys.* 33, 315–24.
- Keshavarz-Motamed Z, Garcia J, Kadem L. 2011. Mathematical, numerical and experimental study in the human aorta with coexisting models of bicuspid aortic stenosis and coarctation of the aorta, Doctoral thesis, Concordia university, Montreal, QC, Canada

- Kim, H., Lu, J., Sacks, M.S., Chandran, K.B., 2008. Dynamic simulation of bioprosthetic heart valves using a stress resultant shell model. *Ann. Biomed. Eng.* 36, 262–275.
- King, M.J., David, T., Fisher, J., 1997. Three-dimensional study of the effect of two leaflet opening angles on the time-dependent flow through a bileaflet mechanical heart valve. *Med. Eng. Phys.* 19, 235–241.
- Kiris, C., Kwak, D., Rogers, S., Chang, I.-D., 1997. Computational Approach for Probing the Flow Through Artificial Heart Devices. *J. Biomech. Eng.* 119, 452–460.
- Kodali, S.K., Williams, M.R., Smith, C.R., Svensson, L.G., Webb, J.G., Makkar, R.R., Fontana, G.P., Dewey, T.M., Thourani, V.H., Pichard, A.D., Fischbein, M., Szeto, W.Y., Lim, S., Greason, K.L., Teirstein, P.S., Malaisrie, S.C., Douglas, P.S., Hahn, R.T., Whisenant, B., Zajarias, A., Wang, D., Akin, J.J., Anderson, W.N., Leon, M.B., 2012. Two-year outcomes after transcatheter or surgical aortic-valve replacement. *N. Engl. J. Med.* 366, 1686–95.
- Krafczyk, M., Cerrolaza, M., Schulz, M., Rank, E., 1998. Analysis of 3D transient blood flow passing through an artificial aortic valve by Lattice-Boltzmann methods. *J. Biomech.* 31, 453–462.
- Krafczyk, M., Tölke, J., Rank, E., Schulz, M., 2001. Two-dimensional simulation of fluid-structure interaction using lattice-Boltzmann methods. *Comput. Struct.* 79, 2031–2037.
- Ku, D.N., Giddens, D.P., Zarins, C.K., Glagov, S., June, M.A.Y., 1985. Pulsatile Flow and Atherosclerosis in the Human Carotid Bifurcation Positive Correlation between Plaque Location and Low and Oscillating Shear Stress. *Arterioscler. Thromb. Vasc. Biol.*
- Lai, Y.G., Lai, Y.G., Chandran, K.B., Chandran, K.B., Lemmon, J., Lemmon, J., 2002. A numerical simulation of mechanical heart valve closure uid dynamics. *J. Biomech.* 35, 881–892.
- Lancellotti, P., Moura, L., Pierard, L. a., Agricola, E., Popescu, B. a., Tribouilloy, C., Hagendorff, A., Monin, J.L., Badano, L., Zamorano, J.L., Sicari, R., Vahanian, A., Roelandt, J.R.T.C., 2010. European association of echocardiography recommendations for the assessment of valvular regurgitation. Part 2: mitral and tricuspid regurgitation (native valve disease). *Eur. J. Echocardiogr.* 11, 307–332.
- Leon, M.B., Smith, C.R., Mack, M., Miller, D.C., Moses, J.W., Svensson, L.G., others, 2010. Transcatheter aortic-valve implantation for aortic stenosis in patients who cannot undergo surgery. *N Engl J Med* 363, 1597–1607.
- Lerakis, S., Hayek, S.S., Douglas, P.S., 2013. Paravalvular aortic leak after transcatheter aortic valve replacement: current knowledge. *Circulation* 127, 397–407.
- Lori, A., Fletcher, A., Miller Jr., A., 2014. Echocardiographic assessment of prosthetic heart valves. *ScienceDirect* 7, 100–110.
- Makkar, R.R., Fontana, G.P., Jilaihawi, H., Kapadia, S., Pichard, A.D., Douglas, P.S., Thourani, V.H., Babaliaros, V.C., Webb, J.G., Herrmann, H.C., Bavaria, J.E., Kodali, S., Brown, D.L.,

- Bowers, B., Dewey, T.M., Svensson, L.G., Tuzcu, M., Moses, J.W., Williams, M.R., Siegel, R.J., Akin, J.J., Anderson, W.N., Pocock, S., Smith, C.R., Leon, M.B., 2012. Transcatheter aortic-valve replacement for inoperable severe aortic stenosis. *N. Engl. J. Med.* 366, 1696–704.
- Manning, W.J., 2013. Asymptomatic aortic stenosis in the elderly: a clinical review. *JAMA* 310, 1490–7.
- Mcqueen, D.M., Peskin, C.S., 1997. Shared-memory parallel vector implementation of the immersed boundary method for the computation of the blood flow in the beating mammalian heart. *J. Supercomput.* 236, 213–236.
- Misfeld, M., Sievers, H.-H., 2007. Heart valve macro- and microstructure. *Philos. Trans. R. Soc. Lond. B. Biol. Sci.* 362, 1421–36.
- Moat, N.E., Ludman, P., de Belder, M.A., Bridgewater, B., Cunningham, A.D., Young, C.P., others, 2011. Long-term outcomes after transcatheter aortic valve implantation in high-risk patients with severe aortic stenosis. K. TAVI, United Kingdom Transcatheter Aortic Valve Implant. Regist. *J Am Coll Cardiol* 58, 2130–2138.
- Mol, A., Rutten, M.C.M., Driessen, N.J.B., Bouten, C.V.C., Zünd, G., Baaijens, F.P.T., Hoerstrup, S.P., 2006. Autologous human tissue-engineered heart valves: prospects for systemic application. *Circulation* 114, 1152–8.
- Morbiducci, U., Ponzini, R., Nobili, M., Massai, D., Montevicchi, F.M., Bluestein, D., Redaelli, A., 2009. Blood damage safety of prosthetic heart valves. Shear-induced platelet activation and local flow dynamics: A fluid-structure interaction approach. *J. Biomech.* 42, 1952–1960.
- Morganti, S., Auricchio, F., Conti, M., Reali, A., 2013. Patient-specific finite element analysis of transcatheter aortic valve implantation 6–9.
- Murray, M.-I., Geis, N., Pleger, S.T., Kallenbach, K., Katus, H. a., Bekerredjian, R., Chorianopoulos, E., 2015. First Experience With the New Generation Edwards Sapien 3 Aortic Bioprosthesis: Procedural Results and Short Term Outcome. *J. Interv. Cardiol.* 28, 109–116.
- Neuenschwander, S., Hoerstrup, S.P., 2004. Heart valve tissue engineering. *Transpl. Immunol.* 12, 359–65.
- Nicosia, M.A., Cochran, R.P., Einstein, D.R., Rutland, C.J., Kunzelman, K.S., 2003. A coupled fluid-structure finite element model of the aortic valve and root. *J. Heart Valve Dis.* 12, 781–789.
- Nishimura, R. a., 2002. Aortic Valve Disease. *Circulation* 106, 770–772.
- Nobari, S., Mongrain, R., Leask, R., Cartier, R., 2013. The effect of aortic wall and aortic leaflet stiffening on coronary hemodynamic: a fluid-structure interaction study. *Med. Biol. Eng. Comput.* 51, 923–36.

- Otto, C.M., 2000. Timing of aortic valve surgery. *Heart* 211–218.
- Paeme, S., Moorhead, K.T., Chase, J.G., Lambermont, B., Kolh, P., D’orio, V., Pierard, L., Moonen, M., Lancellotti, P., Dauby, P.C., Desai, T., 2011. Mathematical multi-scale model of the cardiovascular system including mitral valve dynamics. Application to ischemic mitral insufficiency. *Biomed. Eng. Online* 10, 86.
- Pate, G.E., Al Zubaidi, A., Chandavimol, M., Thompson, C.R., Munt, B.I., Webb, J.G., 2006. Percutaneous closure of prosthetic paravalvular leaks: case series and review. *Catheter. Cardiovasc. Interv.* 68, 528–33.
- Peskin, C.S., 1972. Flow patterns around heart valves: A numerical method. *J. Comput. Phys.* 10, 252–271.
- Peskin, C.S., McQueen, D.M., 1980. Modeling prosthetic heart valves for numerical analysis of blood flow in the heart. *J. Comput. Phys.* 37, 113–132.
- Peskin, C.S., McQueen, D.M., 1989. A three-dimensional computational method for blood flow in the heart I. Immersed elastic fibers in a viscous incompressible fluid. *J. Comput. Phys.* 81, 372–405.
- Pham, Q., Vincent, F., 2001. A FEM-based deformable model for the 3D segmentation and tracking of the heart in cardiac MRI. *Image Signal ...* 250–254.
- Pibarot, P., Dumesnil, J.G., 2009. Prosthetic heart valves: selection of the optimal prosthesis and long-term management. *Circulation* 119, 1034–48.
- Pibarot, P., Hahn, R.T., Weissman, N.J., Monaghan, M.J., 2015. Assessment of paravalvular regurgitation following TAVR: a proposal of unifying grading scheme. *JACC Cardiovasc. Imaging* 8, 340–360.
- Pibarot, P., Weissman, N.J., Stewart, W.J., Hahn, R.T., Lindman, B.R., McAndrew, T., Kodali, S.K., Mack, M.J., Thourani, V.H., Miller, D.C., Svensson, L.G., Herrmann, H.C., Smith, C.R., Rodés-Cabau, J., Webb, J., Lim, S., Xu, K., Hueter, I., Douglas, P.S., Leon, M.B., 2014. Incidence and sequelae of prosthesis-patient mismatch in transcatheter versus surgical valve replacement in high-risk patients with severe aortic stenosis: a PARTNER trial cohort—a analysis. *J. Am. Coll. Cardiol.* 64, 1323–34.
- Quail, M.A., Taylor, A.M., 2013. Computer modeling to tailor therapy for congenital heart disease. *Curr Cardiol Rep* 15 395.
- Ryval, J., Straatman, A.G., Steinman, A.D., 2004. Two-equation turbulence modeling of pulsatile flow in a stenosed tube. *J Biomech Eng* 126, 625–635.
- Richard E. Klabunde, P., 2007. Cardiovascular physiology concepts [WWW Document]. URL <http://www.cvphysiology.com/Heart Disease/HD002.htm>
- Rippel, R. a, Ghanbari, H., Seifalian, A.M., 2012. Tissue-engineered heart valve: future of cardiac surgery. *World J. Surg.* 36, 1581–91.

- Robvalve, 2014. Anthony's heart valve replacement saga [WWW Document]. URL <https://robovalve.wordpress.com/diagnosis/>
- Sanders, H., Shivakumar, E., Sadeghi, .P.R., 1996. Composite finite element model of a stented bioprosthetic heart valve. In: 1996 MARC 25th Anniversary International Users Conference. Monterey, California USA, pp. 291–302.
- Safi, a. M., Kwan, T., Afflu, E., Al Kamme, A., Saliccioli, L., 2000. Paravalvular regurgitation: a rare complication following valve replacement surgery. *Angiology* 51, 479–487.
- Schenkel, T., Malve, M., Reik, M., Markl, M., Jung, B., Oertel, H., 2009. MRI-based CFD analysis of flow in a human left ventricle: methodology and application to a healthy heart. *Ann. Biomed. Eng.* 37, 503–515. m
- Schultz, C.J., Weustink, A., Piazza, N., Otten, A., Mollet, N., Krestin, G., others, 2009. Geometry and degree of apposition of the CoreValve revalving system with multislice computed tomography after implantation in patients with aortic stenosis. *J Am Coll Cardiol* 54, 911–918.
- Scotten, L.N., Siegel, R., 2014. Thrombogenic potential of transcatheter aortic valve implantation with trivial paravalvular leakage 2.
- Segers, P., Stergiopulos, N., Westerhof, N., 2002. Relation of effective arterial elastance to arterial system properties. *Am. J. Physiol. Heart Circ. Physiol.* 282, H1041–H1046.
- Segers, P., Stergiopulos, N., Westerhof, N., Wouters, P., Kolh, P., Verdonck, P., 2003. Systematic and pulmonary hemodynamics assessed with a lumped-parameter heart-arterial interaction model. *J. Eng. Math.* 47, 185–199.
- Senzaki, H., Chen, C.-H., Kass, D.A., 1996. Single-beat estimation of end-systolic pressure-volume relation in humans: a new method with the potential for noninvasive application. *Circulation* 94, 2497–2506.
- Sermesant, M., Delingette, H., Ayache, N., 2006. An electromechanical model of the heart for image analysis and simulation 25, 612–625.
- Shi, Y., Zhao, Y., Yeo, T.J.H., Hwang, N.H.C., 2003. Numerical simulation of opening process in a bileaflet mechanical heart valve under pulsatile flow condition. *J. Heart Valve Dis.* 12, 245–255.
- Shim, E.-B., Chang, K.-S., 1997. Numerical analysis of three-dimensional Björk–Shiley valvular flow in an aorta. *J. Biomech. Eng.* 119, 45–51.
- Shim, E.B., Jun, H.M., Leem, C.H., Matusuoka, S., Noma, A., 2008. A new integrated method for analyzing heart mechanics using a cell-hemodynamics-autonomic nerve control coupled model of the cardiovascular system. *Prog. Biophys. Mol. Biol.* 96, 44–59.
- Sievers, H.-H., Schmidtke, C., 2007. A classification system for the bicuspid aortic valve from 304 surgical specimens. *J. Thorac. Cardiovasc. Surg.* 133, 1226–33.

- Sinning, J.-M., Vasa-Nicotera, M., Chin, D., Hammerstingl, C., Ghanem, A., Bence, J., Kovac, J., Grube, E., Nickenig, G., Werner, N., 2013. Evaluation and management of paravalvular aortic regurgitation after transcatheter aortic valve replacement. *J. Am. Coll. Cardiol.* 62, 11–20.
- Sirois, E., Wang, Q., Sun, W., 2011. Fluid simulation of a transcatheter aortic valve deployment into a patient-specific aortic root. *Cardiovasc. Eng. Technol.* 2, 186–195.
- Smith, C.R., Leon, M.B., Mack, M.J., Miller, D.C., Moses, J.W., Svensson, L.G., others, 2011. Transcatheter vs. surgical aortic valve replacement in high risk patients with severe aortic stenosis. *N Engl J Med* 364, 2187–2198.
- Smolka, G., Wojakowski, W., 2010. Paravalvular leak – important complication after implantation of prosthetic valve. *E-Journal ESC Counc. Cardiol. Pract.* 9.
- Sucosky, P., Balachandran, K., Elhammali, A., Jo, H., Yoganathan, A.P., 2009. Altered shear stress stimulates upregulation of endothelial VCAM-1 and ICAM-1 in a BMP-4- and TGF dependent pathway. *Arterioscler. Thromb. Vasc. Biol.* 29, 254–260.
- Suga, H., Sagawa, K., Shoukas, 1973. Load independence of the instantaneous pressure-volume ratio of the canine left ventricle and effects of epinephrine and heart rate on the ratio. *Circ. Res.* 32, 314–322.
- Sun, W., Li, K., Sirois, E., 2010. Simulated elliptical bioprosthetic valve deformation: implications for asymmetric transcatheter valve deployment. *J. Biomech.* 43, 3085–90.
- Svensson, L.G., Ph, D., Tuzcu, E.M., Webb, J.G., Fontana, G.P., Makkar, R.R., Williams, M., Dewey, T., Kapadia, S., Babaliaros, V., Thourani, V.H., Corso, P., Pichard, A.D., Bavaria, J.E., Herrmann, H.C., Akin, J.J., Anderson, W.N., Wang, D., 2011. Transcatheter versus surgical aortic-valve replacement in high-risk patients. *new Engl. J.* 2187–2198.
- Symersky, P., Habets, J., Westers, P., de Mol, B. a J.M., Prokop, M., Budde, R.P.J., 2012. Prospective ECG triggering reduces prosthetic heart valve-induced artefacts compared with retrospective ECG gating on 256-slice CT. *Eur. Radiol.* 22, 1271–7.
- Tamburino, C., Capodanno, D., Ramondo, A., Petronio, A.S., Ettori, F., Santoro, G., Klugmann, S., Bedogni, F., Maisano, F., Marzocchi, A., Poli, A., Antoniucci, D., Napodano, M., De Carlo, M., Fiorina, C., Ussia, G.P., 2011. Incidence and predictors of early and late mortality after transcatheter aortic valve implantation in 663 patients with severe aortic stenosis. *Circulation* 123, 299–308.
- Tan, F.P.P., Xu, X.Y., Torii, R., Wood, N.B., Delahunty, N., Mullen, M., Moat, N., Mohiaddin, R., 2011. Comparison of aortic flow patterns before and after transcatheter aortic valve implantation. *Cardiovasc. Eng. Technol.* 3, 123–135.
- Tang, G.H.L., Lansman, S.L., Cohen, M., Spielvogel, D., Cuomo, L., Ahmad, H., Dutta, T., 2013. Transcatheter aortic valve replacement: current developments, ongoing issues, future outlook. *Cardiol. Rev.* 21, 55–76.

- Tanné, D., Kadem, L., Rieu, R., Pibarot, P., 2008. Hemodynamic impact of mitral prosthesis-patient mismatch on pulmonary hypertension: an in silico study. *J. Appl. Physiol.* 105, 1916–1926.
- Tips, P., 2013. Anatomy & physiology of the heart [WWW Document]. URL <http://pharmatips.doyouknow.in/Articles/Human-Anatomy/Anatomy-Physiology-Of-The-Heart.aspx>
- Unbehaun, M.P., Dreysse, S., Drews, T., Kukucka, M., Mladenow, A., others, 2012. Transapical aortic valve implantation: incidence and predictors of paravalvular leakage and transvalvular regurgitation in a series of 358 patients. *J Am Coll Cardiol* 59, 211–221.
- Ussia, G.P., Barbanti, M., Petronio, A.S., Tarantini, G., Ettori, F., Colombo, A., Violini, R., Ramondo, A., Santoro, G., Klugmann, S., Bedogni, F., Maisano, F., Marzocchi, A., Poli, A., De Carlo, M., Napodano, M., Fiorina, C., De Marco, F., Antoniucci, D., de Cillis, E., Capodanno, D., Tamburino, C., 2012. Transcatheter aortic valve implantation: 3-year outcomes of self-expanding Corevalve prosthesis. *Eur. Heart J.* 33, 969–76.
- Vesely, I., 2005. Heart valve tissue engineering. *Circ. Res.* 97, 743–55.
- Vino B, M., H, Q.Y., Paul J., D., Thubrikar, M.J., 1997. Three dimensional coupled fluid-structure simulation of pericardial bioprosthetic aortic valve function. *ASAIO J.* 43.
- Wan, I, Sarvasti, N, B., others, 2005. Choosing a prosthesis heart valve. *Folia Med. Indones.* 41, 491–504.
- Webb, J., Gerosa, G., Lefèvre, T., Leipsic, J., Spence, M., Thomas, M., Thielmann, M., Treede, H., Wendler, O., Walther, T., 2014. Multicenter evaluation of a next-generation balloon-expandable transcatheter aortic valve. *J. Am. Coll. Cardiol.* 64, 2235–2243.
- Webb, J.G., Wood, D. a, 2012a. Current status of transcatheter aortic valve replacement. *J. Am. Coll. Cardiol.* 60, 483–92.
- Weinberg, E.J., Kaazempur Mofrad, M.R., 2007. Transient, three-dimensional, multiscale simulations of the human aortic valve. *Cardiovasc. Eng.* 7, 140–155.
- Wesly, R.L., Vaishnav, R.N., Fuchs, J.C., Patel, D.J., Greenfield, J.C., 1975. Static linear and nonlinear elastic properties of normal and arterialized venous tissue in dog and man. *Circ. Res.* 37, 509–520.
- Westerhof, N., Bosman, F., De Vries, C.J., Noordergraaf, A., 1969. Analog studies of the human systemic arterial tree. *J. Biomech.* 2, 121–143.
- Westerhof, N., Elzinga, G., Sipkema, P., 1971. An artificial arterial system for pumping hearts. *J Appl Physiol* 31, 776–781.
- Westerhof, N., Lankhaar, J.W., Westerhof, B.E., 2009. The arterial windkessel. *Med. Biol. Eng. Comput.* 47, 131–141.

- Williams, J.W., Remy, C., Andrew, W., Glower, D., 2010. Percutaneous heart valve replacement, comparative effectiveness technical briefs, No. 2. Agency for Healthcare Research and Quality (US).
- Woehrle, J., Gonska, B., Rodewald, C., Scharnbeck, D., Seeger, J., Markovic, S., Rottbauer, W., 2015. Transfemoral aortic valve replacement with the repositionable Lotus valve compared with the balloon-expandable Edwards Sapien 3 valve. *J. Am. Coll. Cardiol.* 65, A1820.
- Xenos, M., Karakitsos, D., Labropoulos, N., Tassiopoulos, A., Bilfinger, T. V., Bluestein, D., 2013. Comparative study of flow in right-sided and left-sided aortas: numerical simulations in patient-based models. *Comput. Methods Biomech. Biomed. Engin.* 18, 414–425.
- Yang, T.-H., Webb, J.G., Blanke, P., Dvir, D., Hansson, N.C., Nørgaard, B.L., Thompson, C.R., Thomas, M., Wendler, O., Vahanian, A., Himbert, D., Kodali, S.K., Hahn, R.T., Thourani, V.H., Schymik, G., Precious, B., Berger, A., Wood, D.A., Pibarot, P., Rodés-Cabau, J., Jaber, W.A., Leon, M.B., Walther, T., Leipsic, J., 2015. Incidence and severity of paravalvular aortic regurgitation with multidetector computed tomography nominal area oversizing or undersizing after transcatheter heart valve replacement with the Sapien 3: a comparison with the Sapien XT. *JACC Cardiovasc. Interv.* 8, 462–471.
- Zoghbi, W. a, Chambers, J.B., Dumesnil, J.G., Foster, E., Gottdiener, J.S., Grayburn, P. a, Khandheria, B.K., Levine, R. a, Marx, G.R., Miller, F. a, Nakatani, S., Quiñones, M. a, Rakowski, H., Rodriguez, L.L., Swaminathan, M., Waggoner, A.D., Weissman, N.J., Zabalgoitia, M., 2009. Recommendations for evaluation of prosthetic valves with echocardiography and Doppler ultrasound: a report from the American society of echocardiography's guidelines and standards committee and the task force on prosthetic valves, developed in conjunction. *J. Am. Soc. Echocardiogr.* 22, 975–1014; quiz 1082–4.

APPENDIX A

The lumped model illustrated in figure (3-1) was analyzed numerically by creating and solving a system of ordinary differential equations in Matlab Simscape (MathWorks, Inc). A Fourier series representation of an experimental normalized elastance curve for human adults was used as input to the main program (Senzaki et al., 1996).

Simulations were started at the onset of isovolumetric contraction. The left ventricle volume $V(t)$ was calculated using the left ventricle pressure P_{LV} and elastance values. The P_{LV} used at the beginning of the calculation was the initial value assumed across the variable capacitor and was automatically adjusted later by the system of equations as the solution advances. The left ventricle flow rate subsequently was calculated as the time derivative of the left ventricle volume. A diode with very low on resistance and off conductance was used in the aortic valve to prevent backflow from the valve. The same concept was used for aortic valve regurgitation.

Matlab's "ode23t" trapezoidal rule variable-step solver was used to solve the system of differential equations with an initial time step of 0.1 milliseconds. The convergence residual criterion was set to 10^{-5} and the respective initial voltages and currents of the capacitors and inductors were set to zero.

This algorithm introduced and verified by Keshavarz-Motamed et al. (2011).

APPENDIX B

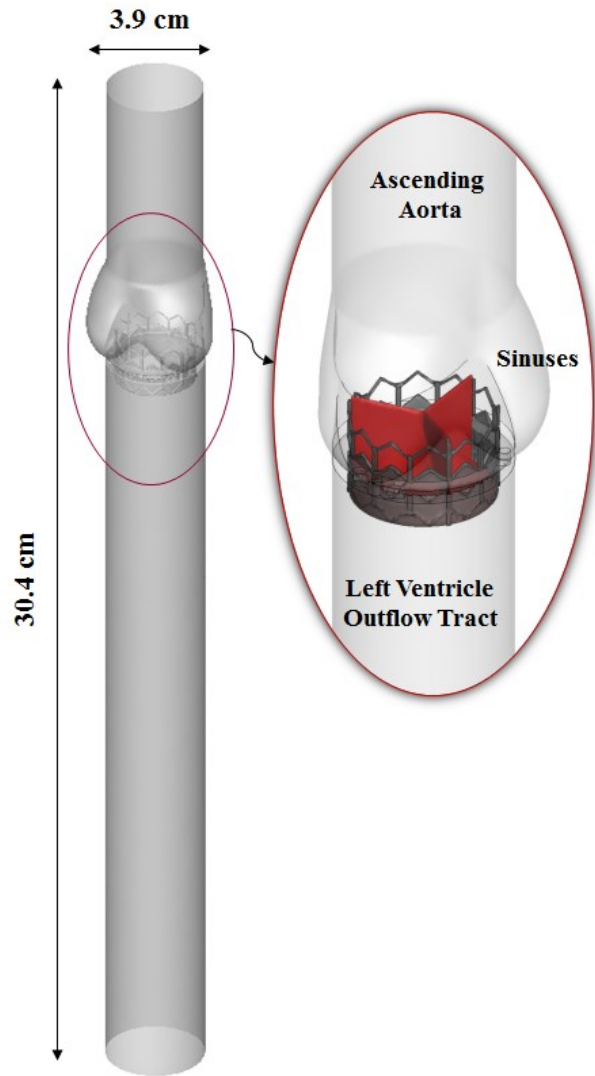


Figure B-1: Computational domain with extended outflow tract

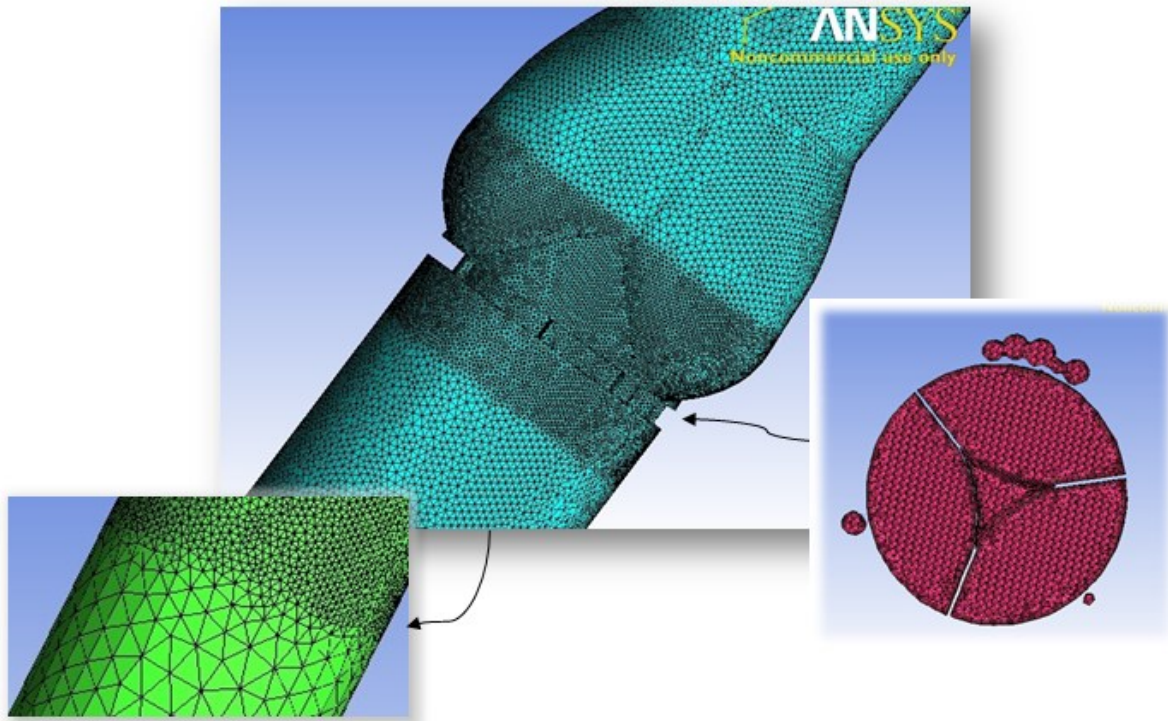


Figure B-2: Domain mesh with extra care for boundaries, walls and sensitive areas

APPENDIX C

In 1995, Jeong and Hussain introduced a new computational method for identifying the vortex regions and cores based on the pressure minimum. Among the different vortex core character definitions, this definition is found to represent the topology and geometry of vortex cores correctly for the large variety of flows. The proposed method known as Lambda-2 criterion is now widely in use by scientists and engineers. This appendix represents a short review on the method and equations.

Pressure minimum itself cannot be used as a general detection criterion for a vortex core due to two effects: (1) unsteady straining, which can create a pressure minimum without a vortical motion, and (2) viscous effects, which can eliminate the pressure minimum in a flow with vertical or swirling motion. However, pressure minimum provides a good starting point for a new definition. Therefore, by discarding the contributions of unsteady irrotational straining and viscosity, we expect to obtain a better indicator for the existence of a vortex.

Taking the gradient of the Navier-Stokes equations, we will have Hessian $(P,_{ij})$ (extrema information):

$$a_{i,j} = -\frac{1}{\rho}P,_{ij} + v u_{ij,kk} \quad (1)$$

Where $a_{i,j}$ is the acceleration gradient (symmetric and antisymmetric), and $(P,_{ij})$ is symmetric:

$$a_{i,j} = \left[\frac{DS_{ij}}{Dt} + \Omega_{ik} \Omega_{kj} + S_{ik} S_{kj} \right] + \left[\frac{D\Omega_{ij}}{Dt} + \Omega_{ik} S_{kj} + S_{ik} \Omega_{kj} \right] \quad (2)$$

The antisymmetric part (second part) is the well-known vorticity transport equation. Considering the symmetric part, we have:

$$\left[\frac{DS_{ij}}{Dt} + \nu S_{ij,kk} + \Omega_{ik} \Omega_{kj} + S_{ik} S_{kj} \right] = -\frac{1}{\rho} P_{,ij} \quad (3)$$

The occurrence of a local pressure minimum in a plane requires two positive eigenvalues of the tensor. Here, as argued above, we will not consider the first two terms in the left-hand side of (3) since the first term represents unsteady irrotational straining and the second term represents viscous effects. Thus, we consider only $\Omega^2 + S^2$ to determine the existence of a local pressure minimum due to vortical motion and define a vortex core as a connected region with two negative eigenvalues of $\Omega^2 + S^2$. Note that since $\Omega^2 + S^2$ is symmetric, it has real eigenvalues only. If λ_1, λ_2 and λ_3 , are the eigenvalues and $\lambda_1 \gg \lambda_2 \gg \lambda_3$ the new definition is equivalent to the requirement that $\lambda_2 < 0$ within the vortex core.

The identification of the vortex is summarized in the table below.

Table C-1: Vortex identification, Lambda-2 criterion

λ_1	λ_2	λ_3	$\sum \lambda_i$	Negative λ_2
+	-	-	-	Vortex core
+	-	-	+	Vortex core
+	+	-	-	Note vortex core
+	+	+	+	Not vortex core